AD_____

Award Number: DAMD17-03-1-0206

TITLE: Molecular Medicine II: Hormone Dependent Cancers

PRINCIPAL INVESTIGATOR: Rudolph M. Navari, M.D., Ph.D.
Kevin T. Vaughan, Ph.D.
Victoria A. Ploplis, Ph.D.
Francis J. Castellino, Ph.D.
Marvin J. Miller
Bradley D. Smith, Ph.D.
Vincent Jo Davisson, Ph.D.
Martin Tenniswood, Ph.D.
Paul Helquist, Ph.D.
Crislyn D'Souza-Schorey
Jeff Schorey
Mary Prorok
Melanie E. DeFord
Alan L. Johnson, Ph.D.
Edward H. Hinchcliffe, Ph.D.

CONTRACTING ORGANIZATION: Notre Dame University
Notre Dame, IN 46556

REPORT DATE: April 2005

20060309 137

TYPE OF REPORT: Annual

PREPARED FOR: U.S. Army Medical Research and Materiel Command
Fort Detrick, Maryland 21702-5012

DISTRIBUTION STATEMENT: Approved for Public Release;
Distribution Unlimited

REPORT DOCUMENTATION PAGE

Form Approved
OMB No. 074-0188

1. AGENCY USE ONLY (Leave blank)	2. REPORT DATE April 2005	3. REPORT TYPE AND DATES COVERED Annual (1 Apr 2004 – 31 Mar 2005)

4. TITLE AND SUBTITLE
Molecular Medicine II: Hormone Dependent Cancers

5. FUNDING NUMBERS
DAMD17-03-1-0206

6. AUTHOR(S)
Rudolph M. Navari, M.D., Ph.D.; Kevin T. Vaughan, Ph.D.;
Victoria A. Ploplis, Ph.D.; Francis J. Castellino, Ph.D.;
Marvin J. Miller; Bradley D. Smith, Ph.D.; Vincent Jo Davisson,
Ph.D.; Martin Tenniswood, Ph.D.; Paul Helquist, Ph.D.;
Crislyn D'Souza-Schorey; Jeff Schorey; Mary Prorok;
Melanie E. DeFord; Alan L. Johnson, Ph.D.; Edward H. Hinchcliffe,
Ph.D.

7. PERFORMING ORGANIZATION NAME(S) AND ADDRESS(ES)
Notre Dame University
Notre Dame, IN 46556

E-Mail: navari.1@nd.edu

8. PERFORMING ORGANIZATION REPORT NUMBER

9. SPONSORING / MONITORING AGENCY NAME(S) AND ADDRESS(ES)

U.S. Army Medical Research and Materiel Command
Fort Detrick, Maryland 21702-5012

10. SPONSORING / MONITORING AGENCY REPORT NUMBER

11. SUPPLEMENTARY NOTES

12a. DISTRIBUTION / AVAILABILITY STATEMENT
Approved for Public Release; Distribution Unlimited

12b. DISTRIBUTION CODE

13. ABSTRACT (Maximum 200 Words)
Abstracts provided in each section.

14. SUBJECT TERMS
Subject terms provided in each section.

15. NUMBER OF PAGES
104

16. PRICE CODE

17. SECURITY CLASSIFICATION OF REPORT	18. SECURITY CLASSIFICATION OF THIS PAGE	19. SECURITY CLASSIFICATION OF ABSTRACT	20. LIMITATION OF ABSTRACT
Unclassified	Unclassified	Unclassified	Unlimited

NSN 7540-01-280-5500

Standard Form 298 (Rev. 2-89)
Prescribed by ANSI Std. Z39-18
298-102

Abstract

Metastatic cancers arise in a variety of epithelial tissues but acquire characteristics of motile cells to invade other tissues. The genetic basis of these transitions is not known, but genetic propensities have been identified for several organ-specific cancers. Mutations in the APC gene (adenomatous polyposis coli) predispose individuals to colon cancer, although the exact mechanisms of colon cancer induction are not clear. One proposed mechanism involves defects in the B-catenin signaling pathways which are activated in patients with a defective APC gene. In this project we are testing the hypothesis that abnormal regulation of the search-capture process is the basis of colon cancer initiation. Task 1 is to compare the distributions of proteins involved in search capture in normal and colon cancer cell lines. Progress on Task 1 includes mapping of dynactin and EB1 distributions in several cell lines. Task 2 is to test the impact of APC mutations on microtubule plus-end tracking. Progress on Task 2 includes live-cell imaging of motors and search-capture proteins in normal and colon cancer lines. Task 3 is to determine if APC and dynactin share common regulatory mechanisms. Progress on Task 3 includes identification of dynactin kinases and analysis of kinases inhibitors on other search-capture proteins.

Subject Terms: regulation, phosphorylation, search-capture, dynactin

Table of Contents

Impact of APC Mutations on Microtubule-Cargo Interactions

Kevin T. Vaughan, Ph.D.
Principal Investigator

BACKGROUND:

Microtubule-based transport represents a major mechanism to deliberately target proteins, organelles and chromosomes to specific destinations. These transport events are particularly important during mitosis when chromosome segregation must be accomplished with a high degree of synchrony and within a narrow window of time. Defects in these processes are now recognized as a major factor in genomic instability. One pathological outcome of genomic instability is the loss of tumor suppressor genes such as APC (adenomatous polyposis coli), ultimately leading to cancer (Fearon and Vogelstein, 1990).

One of the most conceptually challenging aspects of microtubule-based transport is how the chromosomes and microtubules initiate contact with each other. Although scientists originally thought that chromosomes attracted microtubules, a more recent model called the "search-capture model" proposes that microtubules randomly explore space and accidentally encounter chromosomes (Mitchison and Kirschner, 1985). Proteins in specialized structures on the chromosomes called kinetochores capture these microtubules and initiate the recruitment of molecular motor proteins for transport. These "search-capture" events must occur for each chromosome and represent the rate-limiting step in chromosome segregation.

We are particularly interested in these "search-capture" events because components of the cytoplasmic dynein-dynactin pathway appear to be essential for productive interactions between chromosomes and microtubules. Another essential component is the APC gene product which has been recently identified at kinetochores during "search-capture" events {Kaplan, 2001 #3423}(Fodde et al., 2001a). This new insight into APC function suggests that in addition to stimulation of the *Wnt* pathway, APC mutations are likely to disrupt "search-capture" of chromosomes which will contribute to genomic instability (Fodde et al., 2001a; Fodde et al., 2001b). A systematic dissection of APC function during "search-capture" will be required to understand the significance of APC mutations during mitosis.

Detailed analysis of "search-capture" events has been hampered by the limitations of imaging during mitosis. Most cells round up during mitosis and accomplish "search-capture" in a very short period of time. The Vaughan laboratory has recently discovered that the very same "search-capture" process is used during the transport of membranous organelles during interphase (Vaughan et al., 2002). These events are common, occur during interphase when high-resolution imaging can be performed, and are spaced over the majority of the cell cycle. As a result, "search-capture" of membranous organelles represents a superior model system in which to study "search-capture". The recent characterization of proteins at kinetochores and on organelles suggests that the very same class of molecules mediates "search-capture" on these two structures (Coquelle et al., 2002).

Hypothesis: As an essential component of the kinetochore, the APC gene product is thought to play an important role in microtubule capture during mitosis. The defects induced by APC mutations are predicted to reduce the frequency of microtubule capture. Because these events are challenging to visualize during mitosis, we will use microtubule capture of organelles during interphase as a system to study APC. Based on the genomic defects observed in APC-deficient cells, we hypothesize that APC mutations will disrupt microtubule capture by organelles. This will result in defective recruitment of dynactin and cytoplasmic dynein which will inhibit microtubule-based transport.

Impact of APC Mutations on Microtubule-Cargo Interactions

Kevin T. Vaughan, Ph.D.
Principal Investigator

Overview:

The overall goal of this project has been to determine if mutations in microtubule plus-end binding proteins affect the normal search capture process of organelles and chromosomes. We have focused on proteins and genes in which specific mutations are linked to known disease mechanisms and on phosphorylation which has been implicated as the basis of abnormal function for several candidates. We have implemented several search-capture assays to test the consequences of mutant proteins and manipulation of phosphorylation state. Each approach is ultimately designed to reveal the molecular basis of chromosome search-capture and the specific roles of individual proteins.

Progress on Task 1:

Task 1 is focused on the distribution of microtubule plus-end binding proteins and the analysis of plus-end binding protein phosphorylation. The project has struggled with reagents for APC because of the low abundance of APC and the difficulty in transfecting APC expression constructs for imaging purposes. As a result, we have focused our efforts on EB1 because of it intimate linkage to APC (Su et al., 1995) and dynactin because EB1 is thought to bind microtubules via dynactin (Askham et al., 2002).

Recent analysis of a related microtubule plus-end binding protein known as CLIP-170 suggests that the plus-end binding specificity is controlled by mTOR (Choi et al., 2002). MTOR is a serine-threonine kinase known to be involved in sensing nutrient abundance and has been recognized as a mediator of cancer progression (Rao et al., 2004). Based on the similarities between EB1, dynactin and CLIP-170, we tested the impact of mTOR inhibition on microtubule plus-end binding and search capture.

MTOR inhibition was accomplished using the small molecule inhibitor rapamycin (TOR means **T**arget **O**f **R**apamycin). Our first level of analysis was immunofluorescence microscopy of COS-7 cells treated with rapamycin and then processed for imaging of EB1 and dynactin. This assay was selected because phosphorylation of EB1 and dynactin has been implicated in regulation of microtubule binding and microtubule plus-end binding which reflects their roles in search-capture (Vaughan, 2004). Rapamycin treatment had opposite effects on EB1 and dynactin; inhibition of mTOR resulted in enhanced microtubule binding for EB1, but decreased binding of dynactin leading to an enhanced cytoplasmic pool (Fig. 1). The significance of microtubule plus-end specific binding revolves around the dynamics of microtubule binding for search-capture proteins. All know search-capture proteins exhibit dynamic binding in which proteins are recruited to the elongating microtubule plus-end and are then released by phosphorylation after a brief duration of binding. Enhanced microtubule binding reflects inhibition of the specific kinase, whereas decreased microtubule binding suggests enhanced phosphorylation or activation of a specific kinase. The fact that rapamycin treatment lead to enhanced micirotubule binding of EB1 (and therefore APC) suggests that either mTOR of a mTOR-dependent
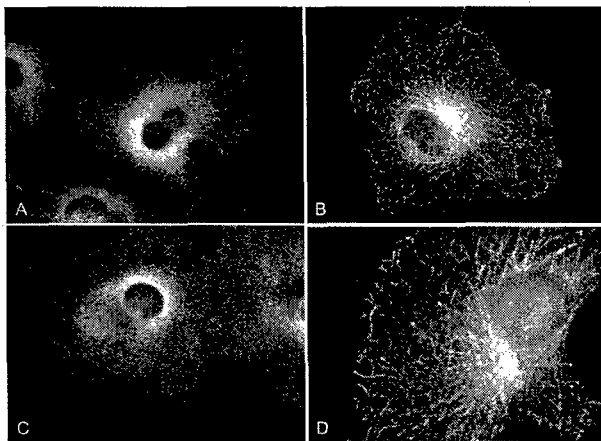
Fig. 1. Rapamycin Treatment Releases Endogenous p150^{Glued} **From and Enhances Binding of Endogenous EB1 Proteins to Microtubules.**
COS-7 cells were treated without (A and B) or with (C and D) of 10 nM rapamycin for 2 hrs. methanol fixed and submitted to IFM using monoclonal antibody against endogenous p150^{Glued} protein (A and C) and with monoclonal antibody against endogenous EB1 (B and D).


Fig. 2. Rapamycin Treatment Induces Opposite Effects on GFP-p150 and GFP-EB1 Binding to Microtubules. Live cell imaging of transfected COS-7 cells with GFP-p150 (1-330) (A) and full length EB1-GFP (B). Cells were treated with 10 nM rapamycin for 2 hrs prior to image acquisition.

kinase is responsible for regulation of the EB1-APC-mediated search capture events. This is the first evidence for identification of an EB1 kinase, and suggests that one target for the mTOR pathway is the search-capture process itself.

In contrast, rapamycin treatment induced release of p150Glued and dynactin from microtubule plus-ends, suggesting that the linkage of dynactin to mTOR is indirect. because release is mediated by phosphorylation (Vaughan et al., 2002), the inhibition of mTOR should lead to enhanced binding if mTOR is a dynactin kinase. The fact that mTOR inhibition leads to release suggests that either mTOR regulates another kinase and that this secondary kinase phosphorylates dyanctin, or mTOR is involved in stimulating a phosphatase and that rapamycin treatment inhibits that phosphatase.

To confirm that the rapamycin effects on EB1 and dynactin are direct, we have prepared and analyzed COS-7 cells transfected with GFP-EB1 and GFP-dynactin for live-cell analysis (Fig. 2). Control cells transfected with GFP-p150Glued displayed normal tip-tracking reflecting dynamic microtubule binding and release. In contrast, GFP-p150Glued-expressing cells treated with rapamycin reveal a large soluble pool of the p150Glued protein and no evidence of microtubule binding.

As a further measure of the specificity of mTOR regulation, we performed 2-D gel analysis of p150Glued and determined the complexity of protein isoforms in COS-7 cells

where only one p150Glued polypeptide is expressed. Western blots of 2-D gels indicate that control cells are dominated by a pair 2-D gel variants reflecting a phosphorylated and dephosphorylated version of the protein. After rapamycin treatment, this pair of spots expands to 4 variants (Fig. 3), reflecting phosphorylation at at least two positions.

Because this regulation appears to play a dominant role in the dynamic binding of microtubule plus-end binding proteins, we have isolated sufficient quantities of p150Glued from rapamycin-treated COS-7 cells for MS/MS mapping of phosphorylation sites (Fig. 4). This mapping is underway and about 50% complete in collaboration with the Harvard University Protein Microchemistry Facility. Progress on Task 1 is 70% complete.

Fig. 3. Rapamycin Increases P150^{Glued} Phosphorylation Complexity. COS-7 cells were grown in absence (A) or presence (B) of 10 nM rapamycin for 2 hrs. Cell extracts were subjected to 2-D gel electrophoresis and western blot. Membranes were probed with monoclonal antibody against p150^{Glued}.

Progress on Task 2:

Task 2 is focused on the impact of APC mutations on the activities of other microtubule plus-end binding proteins. We have now completed the construction of both GFP and mRFP-tagged versions of multiple proteins involved in the search-capture process. Among the constructs we have completed are: 1) green and red versions of α-tubulin, 2) green and red versions of p150Glued, EB1, CLIP-170 and MAP4, 3) GFP-tagged histones, cytoplasmic dynein and E-cadherin.

These constructs are being used to determine the hierarchy of recruitment and binding to microtubule plus-ends, as well as the impact of disease-linked mutations in APC, p150Glued and microtubule motors on the search-capture process. Co-expression of EB1, p150Glued and CLIP-170 reveal a hierarchy in which EB1 binds first to the elongating microtubule plus-end, followed by p150Glued which is followed by CLIP-170. Based on prepvious work, we anticipate that the cytoplasmic dynein motor will be recruited next which will lead to translocation.

Several assays have been used to test the co-dependence of these plus-end binding proteins on each other and other candidates. Depletion of p150^{Glued} using siRNA technology reveals several key features of the search-capture process. First, successful depletion of p150^{Glued} also depletes EB1 from microtubule plus-ends, suggesting that

Fig. 4. P150^{Glued} Samples for Mass Spectrometry. COS-7 cells were grown in presence of 10 nM rapamycin for 2 hrs and cells extract prepared in RIPA buffer (50 mM TRIS pH 8.0, 150 mM NACL and 1% NP 40) followed by centrifugation 12,000 rpm at 10 min in roon temperature. The supernatant was immunoprecipitated with antibody against dynamitin. The band corresponding to p150^{Glued} was excised and submitted to mass spectrometry analysis.

EB1 is dependent on p150^{Glued} for microtubule targeting. Second, CLIP-170, another protein implicated in search-capture, is unaffected by p150^{Glued} depletion, suggesting that CLIP-170 binding microtubule plus-ends independently. Third, depletion of p150^{Glued} also decreases the frequency of search-capture events, suggesting that dynactin is essential for search-capture.

The next approach has been to transfect p150Glued constructs harboring a G59S mutation into the siRNA-treated cells to exchange the GFP-tagged construct for the endogenous p150Glued polypeptide. Whereas rescue with the wild-type protein reconstitutes normal search-capture activity, rescue with the G59S mutant fails to induce normal search-capture and ablates the recruitment of EB1 (and therefore APC) to microtubule plus-ends. Progress on Task 2 is 30% completion.

Fig. 5. Expression of mTOR Constructs Suggests Rapamycin Acts Through mTOR to Regulate P150^{Glued}. COS-7 cells were co-transfected with GFP-p150^{Glued}(1-330) and wild type mTOR construct (A) or kinase dead mTOR (Asn2343-Lys) (B). Consistent with the effect of rapamycin which reduced microtubule binding, expression of wild-type mTOR enhanced microtubule binding. In contrast, expression of the kinase-dead mTOR lead to reduced microtubule binding. C) Graphic representation of GFP-p150^{Glued} distributions in COS-7 cells. Each group represents the average of three coverslips. The distributions of GFP-p150^{Glued} were scored as: tip–specific binding "(ie. *tip-tracking*"), decorated, bundled or cytoplasmic (soluble).

Progress on Task 3:

Task 3 is designed to test if dynactin and APC are regulated in the same way. because of the issues with direct analysis of APC, we have concentrated on EB1 as an indicator of APC function. Based on the ongoing work on mTOR-based signaling, we have generated expression constructs encoding wild-type mTOR, and a version of mTOR with a defective nucleotide binding motif (known as kinase-dead). Analysis of cells transfetced with GFp-p150Glued and wild-type mTOR reveals effects which contrast rapamycin treatment. Wild-type mTOR induces enhanced microtubule binding mimicking the effects of PKA inhibition (Fig. 5). This is consistent with our current hypothesis in which mTOR regulates another enzyme to either inhibit the p150Glued kinase or stimulate the p150Glued phosphatase. Rapamycin treatment, which has the opposite effect, essentially works against mTOR to induce greater p150Glued phosphorylation.

If our hypothesis is correct, transfection of a defective mTOR construct should mimic the rapamycin effect. To test this model, we co-transfected GFP-p150Glued and the kinase-dead mTOR construct and measured microtubule binding and tip-tracking in live-cell assays. As predicted, this mTOR construct induced a release from microtubule binding and an enhanced cytoplasmic pool.

As a reflection of APC behavior, we performed the same assays with EB1 and determined that EB1 behaves differently from p150Glued. EB1 behaves as if mTOR is a direct kinase, and cotransfection of GFP-EB1 and wild-type mTOR induces enhanced

solubility of EB1 into the soluble pool. This is consistent with the phosphorylated version of the protein. In contrast, co-transfection of GFP-p150Glued and kinase-dead mTOR induces enhanced microtubule binding suggesting domination of the dephosphorylated form. Together these studies suggest that p150Glued and EB1/APC are regulated in opposing ways by the mTOR kinase.

Progress on Task 3 is 70%.

Key Research Accomplishments:

- development of live-cell search-capture assay.
- finding that dynactin is an essential component of search-capture.
- development of siRNA approaches for search-capture.
- generation of siRNA/"rescue" constructs.
- identification of mTOR as an EB1 kinase.
- implication of mTOR as an indirect regulator of dynactin.
- analysis of wild-type and kinase-dead mTOR constructs.
- phosphorylation site mapping after rapamycin treatment.
- analysis of EB1 and p150Glued phosphorylation by mTOR by 2-D gel analysis.

Reportable Outcomes:

- SiRNA analysis reveals a connection between EB1 and dynactin
- SiRNA analysis suggests independent regulation by CLIP-170.
- APC mutations alter the phosphorylation kinetics of dynactin.
- EB1 and dynactin are regulated by mTOR kinase, but with opposite outcomes.

Conclusions:

1) We have identified an important role for dynactin, EB1 and CLIP-170 in search-capture.

2) SiRNA analysis suggests that EB1 is dependent on dynactin for binding to microtubules during search-capture, but that CLIP-170 can bind independently.

3) Because APC is now thought to bind microtubules indirectly through EB1, this suggests that dynactin mediates that targeting of APC to cargo such as chromosomes.

4) Live-cell imaging reveals that APC mutations alter the phosphorylation kinetics of search-capture kinases.

5) One of these kinases is mTOR which appears to phosphorylate EB1 directly, but dynactin indirectly.

6) Rapamycin induces phosphorylation of p150Glued, but through an indirect mechanism.

7) This rapamycin-induced phosphorylation is in addition to the PKA-induced phosphorylation observed earlier.

8) A hierarchy of microtubule plus-end binding has been deduced that suggests sequential loading of EB1, p150Glued, CLIP-170 and cytoplasmic dynein.

References:

Askham, J.M., K.T. Vaughan, H.V. Goodson, and E.E. Morrison. 2002. Evidence that an interaction between EB1 and p150(Glued) is required for the formation and maintenance of a radial microtubule array anchored at the centrosome. *Mol Biol Cell*. 13:3627-45.

Choi, J.H., P.G. Bertram, R. Drenan, J. Carvalho, H.H. Zhou, and X.F. Zheng. 2002. The FKBP12-rapamycin-associated protein (FRAP) is a CLIP-170 kinase. *EMBO Rep*. 3:988-94.

Coquelle, F.M., M. Caspi, F.P. Cordelieres, J.P. Dompierre, D.L. Dujardin, C. Koifman, P. Martin, C.C. Hoogenraad, A. Akhmanova, N. Galjart, J.R. De Mey, and O. Reiner. 2002. LIS1, CLIP-170's Key to the Dynein/Dynactin Pathway. *Mol Cell Biol*. 22:3089-3102.

Faulkner, N.E., D.L. Dujardin, C.Y. Tai, K.T. Vaughan, C.B. O'Connell, Y. Wang, and R.B. Vallee. 2000. A role for the lissencephaly gene LIS1 in mitosis and cytoplasmic dynein function. *Nat Cell Biol*. 2:784-791.

Fearon, E.R., and B. Vogelstein. 1990. A genetic model for colorectal tumorigenesis. *Cell*. 61:759-67.

Fodde, R., J. Kuipers, C. Rosenberg, R. Smits, M. Kielman, C. Gaspar, J.H. van Es, C. Breukel, J. Wiegant, R.H. Giles, and H. Clevers. 2001a. Mutations in the APC tumour suppressor gene cause chromosomal instability. *Nat Cell Biol*. 3:433-8.

Fodde, R., R. Smits, and H. Clevers. 2001b. APC, signal transduction and genetic instability in colorectal cancer. *Nature Rev Cancer*. 1:55-67.

Kaplan, K.B., A.A. Burds, J.R. Swedlow, S.S. Bekir, P.K. Sorger, and I.S. Nathke. 2001. A role for the Adenomatous Polyposis Coli protein in chromosome segregation. *Nat Cell Biol*. 3:429-32.

Mimori-Kiyosue, Y., N. Shiina, and S. Tsukita. 2000. Adenomatous polyposis coli (APC) protein moves along microtubules and concentrates at their growing ends in epithelial cells. *J Cell Biol*. 148:505-18.

Mitchison, T.J., and M.W. Kirschner. 1985. Properties of the kinetochore in vitro. II. Microtubule capture and ATP- dependent translocation. *J Cell Biol*. 101:766-77.

Morrison, E.E., B.N. Wardleworth, J.M. Askham, A.F. Markham, and D.M. Meredith. 1998. EB1, a protein which interacts with the APC tumour suppressor, is associated with the microtubule cytoskeleton throughout the cell cycle. *Oncogene*. 17:3471-7.

Nakamura, F., X.Z. Zhou, and K.P. Lu. 2001. Critical role for the EB1 and APC interaction in the regulation of microtubule polymerization. Curr. Biol.11:1062-1067.

Nathke, I.S., C.L. Adams, P. Polakis, J.H. Sellin, and W.J. Nelson. 1996. The adenomatous polyposis coli tumor suppressor protein localizes to plasma membrane sites involved in active cell migration. *J Cell Biol*. 134:165-79.

Rao, R.D., J.C. Buckner, and J.N. Sarkaria. 2004. Mammalian target of rapamycin (mTOR) inhibitors as anti-cancer agents. *Curr Cancer Drug Targets*. 4:621-35.

Su, L.K., M. Burrell, D.E. Hill, J. Gyuris, R. Brent, R. Wiltshire, J. Trent, B. Vogelstein, and K.W. Kinzler. 1995. APC binds to the novel protein EB1. *Cancer Res*. 55:2972-7.

Vaughan, K.T. 2004. Surfing, regulating and capturing: are all microtubule-tip-tracking proteins created equal? *Trends Cell Biol*. 14:491-6.

Vaughan, K.T., S.H. Hughes, C.J. Echeverri, N.F. Faulkner, and R.B. Vallee. 1999. Co-

localization of dynactin and cytoplasmic dynein with CLIP-170 at microtubules distal ends. *J. Cell Sci.* 112:1437-1447.

Vaughan, P.S., J.D. Leszyk, and K.T. Vaughan. 2001. Cytoplasmic dynein intermediate chain phosphorylation regulates binding to dynactin. *J Biol Chem.* 276:26171-9.

Vaughan, P.S., P. Miura, M. Henderson, B. Byrne, and K.T. Vaughan. 2002. A role for regulated binding of p150[Glued] to microtubule plus-ends in organelle transport. *J. Cell Biol.* 158.

Project 7: Fibrinolysis in the Growth, Dissemination, and Angiogenesis of Breast and Prostate Carcinoma

Victoria A. Ploplis, Ph.D.
Francis J. Castellino, Ph.D.

Abstract

Due to problems associated with the C3-Tag mouse model of breast and prostate cancer in the C57BL/6J genetic strain, we have altered the tumor model for this project. Several clinical studies have identified components of the hemostatic system in regulating colon cancer. While a number of genes have been implicated in various stages of this disease, mutations in the adenomatous polyposis coli (*APC*) gene have been found during the early stages of adenoma formation, and it is believed that this gene is involved in tumor development and progression. Mutations of this gene results in familial adenomatous polyposis (FAP) which is characterized by the formation of multiple colonic adenomatous polyps which predisposes to the development of colon carcinoma. A mouse model (*APC^{Min+}*) has been developed that mimics the clinically features of FAP. Specifically this study will: 1) utilize a murine model of spontaneous colon cancer, the *APC^{Min+}* mouse, with additional alterations in expression of components of the hemostasis system and compare tumor development and dissemination in these various genotypically-distinct groups. This will involve analyses of tumor growth rate and the spatial and temporal involvement of proteins and other host cells; 2) identify and quantitate the relative abundance of angiogenic factors in primary and metastatic tumors utilizing real-time RT-PCR and determine the spatial expression patterns of these proteins by *in situ* hybridization; and 3) determine the relative contributions of host or tumor expression of hemostatic proteins in regulating tumor growth and dissemination.

Subject Terms: prostate cancer, breast cancer, fibrinolysis, angiogenesis

<center>**Progress Report**</center>

<center>**Fibrinolysis in the Growth, Dissemination, and Angiogenesis of Breast and Prostate Carcinoma**</center>

<center>Victoria A. Ploplis, Ph.D. and Francis J. Castellino, Ph.D.
Principal Investigators</center>

Introduction

The fibrinolytic system is a component of hemostasis and is the major physiological pathway involved in maintaining vascular patency through the degradation of fibrin clots. However, cell surface expression of specific receptors for plasminogen (Pg) and its physiological activators implicates Pm expression in cell mediated proteolytic processes, such as extracellular matrix degradation and directional cell migration events. Therefore, this system has also been implicated in regulating other physiological events such as wound healing (1), atherosclerosis (2), angiogenesis (3), and cancer (4).

An association of fibrinolysis and tumor tissue has been reported as early as 1911 (5). Since then, additional studies have indicated that neoplastic cells express elevated levels of uPA, tPA and/or uPAR suggesting that this pathway is involved in pathophysiological events such as tumor growth and metastasis (6). Studies have demonstrated that malignant cells often secrete higher amounts of plasminogen activators relative to their normal counterparts (7). For example, the cell types responsible for production of uPA in colonic tumors have been identified, utilizing stringent *in situ* hybridization techniques, as the tumor epithelium and not stromal tissue (8). In addition, the expression of uPA receptor on a variety of transformed cells is well documented (7). Overexpression of this receptor has been reported in several types of human gastrointestinal, adenocarcinomas including gastric cancer and pancreatic cancer (9-11). As a result, the assembly of plasminogen activators on cell surfaces can result in local activation of Pg and focal proteolysis which can contribute to a malignant phenotype of cells by enhancing invasive processes mediated by cell matrix degradation. In support of this observation, earlier studies of primary tumor and metastases of Lewis lung carcinoma cells, utilizing antibodies to uPA, demonstrated intense staining at the sites of invasive growth of the tumor and degradation of normal tissue (6). Additional studies, utilizing antibodies reactive with the catalytic site of uPA, prevented morphological changes and extracellular matrix degradation associated with Rous sarcoma virus-transformed fibroblasts (12). Clinically, elevated levels of uPA and/or its receptors have been associated with carcinomas of breast, colon, skin, prostate, lung, kidney, and brain (13). Indeed, the expression of uPA in breast carcinomas has been found to be an independent and strong prognostic marker for relapse and reduced survival. While there appears to be a strong correlation between the enhanced expression of components of the fibrinolytic system and tumor growth and metastasis, the specific *in vivo* mechanisms by which this system contributes to these processes are still unclear.

A number of transgenic models of prostate and breast cancer have been developed. One particular model, TgN(C3-1-Tag)cJeg (*C3-1-Tag$^{+/o}$*), involves the transgene for the SV-40 large tumor antigen (Tag) driven by the rat prostatic steroid binding protein (C3(1)) promoter (14). This transgene functions in stimulating gene transcription and forms complexes with the cell cycle-regulatory proteins Trp53 and Rb1, both of which have been implicated in breast cancer. Male transgenic mice develop hyperplastic changes in the epithelium of the prostate, which eventually progress to prostate adenocarcinoma predominantly by 8 months of age. In females, hyperplasia of mammary ducts and acini occurs by 3 months of age and progress to multifocal mammary adenocarcinomas by 6 months of age. In both genders, pulmonary metastasis has been observed.

However, when these mice are backcrossed into the C57BL/6J strain, they lose the phenotypes associated with prostate and breast cancer and instead demonstrate enhanced lesions of heterotopic bone formation that was associated with mixed tumor formation arising from eccrine sweat glands in the foot pads of mice as well as in the ischiocavernosus muscle adjacent to bulbourethral glands and occasionally the salivary and mammary glands (15). There was no obvious differences between the crosses associated with these lesions.

As recommended by the last review, a statement of work change was sent to the P.I. of this grant. The change involved altering the tumor model to one with 100% penetrance in the C57BL/6J strain. The new tasks are incorporated in the Body of this report.

Body

Task 1. **Generate and perform necropsy of $APC^{Min/+}$ mice with alterations in expression of components of the fibrinolytic system.**

a) Generate colonies of $APC^{Min/+}$ mice that are additionally deficient for urokinase or plasminogen activator inhibitor-1.

The $APC^{Min/+}/UPA^{-/-}$ and $APC^{Min/+}/PAI-1^{-/-}$ mice needed for the studies described have been successfully obtained through initial crossings of $APC^{Min/+}$ with $UPA^{-/-}$ or $PAI-1^{-/-}$ mice followed by crossings of $APC^{Min/+}/UPA^{+/-}$ or $APC^{Min/+}/PAI-1^{+/-}$ mice.

b) Perform necropsy (measure tumor size, determine tumor location and dissemination) and collect tissue from $APC^{Min/+}$ mice and $APC^{Min/+}$ mice that are also deficient for urokinase or plasminogen activator inhibitor-1 at various timepoints during the progression of the disease (12-30 wk).

Most of the work to date has been on 20 week old $APC^{Min/+}$, $APC^{Min/+}/PAI-1^{-/-}$, and $APC^{Min/+}/UPA^{-/-}$ mice. Tumor burden at this age demonstrated that $APC^{Min/+}/UPA^{-/-}$ mice have significantly diminished levels of intestinal polyps/tumors relative to the other genotypes (2 ± 2 vs. 15 ± 6 for $APC^{Min/+}$ and 21 ± 10 for $APC^{Min/+}/PAI-1^{-/-}$). There were no significant differences in tumor size between $APC^{Min/+}$ and $APC^{Min/+}/UPA^{-/-}$ (1.2 ± 0.2 mm vs. 1.4 ± 0.3 mm, respectively). However, $APC^{Min/+}/PAI-1^{-/-}$ tumors appeared to be somewhat larger at this timepoint (1.7 ± 0.3 mm). There was no evidence that tumor disseminated to other organs at this timepoint.

Task 2. **Perform histology and immunohistology on tumor and control tissue.**

a) Histology stains will include, but will not be limited to, H&E (cellular identification and morphology) and Masson's and Gomori Trichrome (extent of fibrosis).

Fig 1. (H&E staining of $APC^{Min/+}$). Showing a general view of a circumferential tumor near the muscularis mucosae, columnar epithelial cells and enlarged hyperchromatic nuclei. (100X mag.)

Fig.2 (H&E staining of $APC^{Min/+}/UPA^{-/-}$). A small polypoid lesion with adjoining normal mucosa. (100X mag.)

Fig. 3. (H&E staining of $APC^{Min/+}/PAI-1^{-/-}$). The expanding tumor mass consists of disorganized and crowded cells. There is no significant loss of polarity in the crypts. (100X mag.)
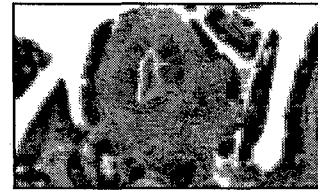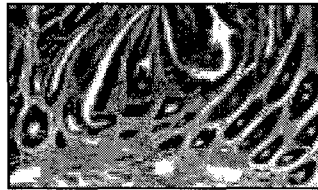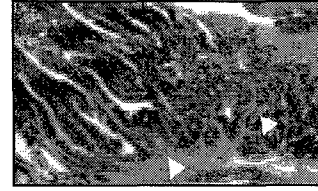
Fig. 4. (Masson's and Gomori Trichrome stain of $APC^{Min/+}$). Diffuse collagen deposition is noted at the base of the tumor (blue) arising from the mucosae. (Top – 100X, Bottom – 200X mag.)

Fig.5. (Masson's and Gomori Trichrome stain of $APC^{Min/+}/UPA^{-/-}$). There is normal collagen deposition in the mucosa with minimal distribution in the polypoid lesion. (Top – 100X, Bottom – 200X mag.

Fig. 6. (Masson's and Gomori Trichrome stain of $APC^{Min/+}/PAI-1^{-/-}$). Light collagen deposition diffusely distributed throughout the tumor. (Top – 100X, Bottom – 200X mag.)

b) Immunohistochemistry for expression of vWF, CD105, CD31 (neovessel formation); thrombospondin, angiopoietin-1, VEGF (angiogenesis); CD45 (leukocytes); fibronectin, laminin, and vitronectin (extracellular matrix proteins); PAI-1, Pg, uPA, uPAR, fibrin(ogen) (fibrinolytic markers) and other stains that will be identified during the progression of the project.
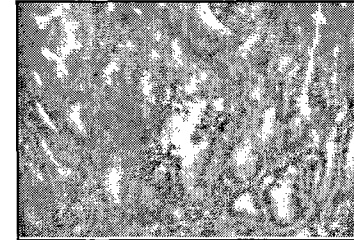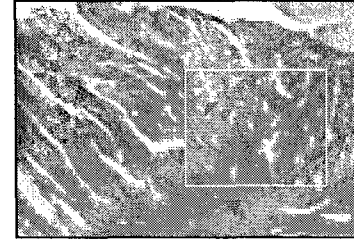
Fig. 7. (Fibrin(ogen) immunostaining in $APC^{Min/+}$). Strong diffuse accumulation and distribution of fibrin from the mucosae to the tumor. (Top panel – 100X and bottom panel 200X mag.)

Fig. 8. (Fibrin(ogen) immunostaining in $APC^{Min/+}/UPA^{-/-}$). Low deposition of fibrin in the tumor. (Top panel – 100X and bottom panel – 200X)

Fig. 9. (Fibrin(ogen) immunostaining in $APC^{Min/+}/PAI-1^{-/-}$). Increase deposition of fibrin from the muscularis throughout the tumor. (Top panel – 100X and bottom panel – 200X)

21
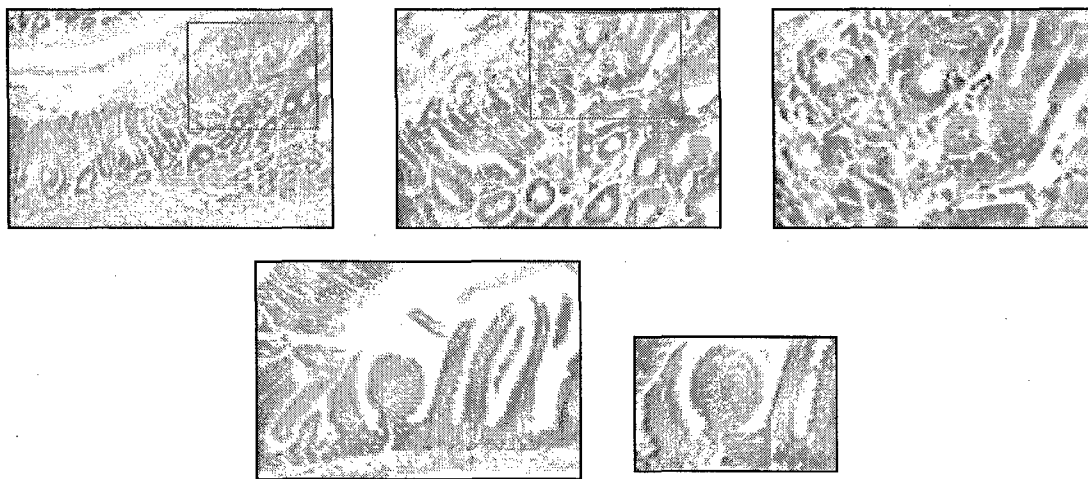
Fig. 10. PAI-1 immunostaining of $APC^{Min/+}$ (Top 3 panels, 100X, 200X, 400X mag.) demonstrating low Diffuse expression of PAI-1 in the upper part of the tumor with low grade atypia. PAI-1 immunostaining of $APC^{Min/+}/UPA^{-/-}$ (Bottom 2 panels, left – 100X and right – 200X mag.) demonstrating an absence of PAI-1 expression
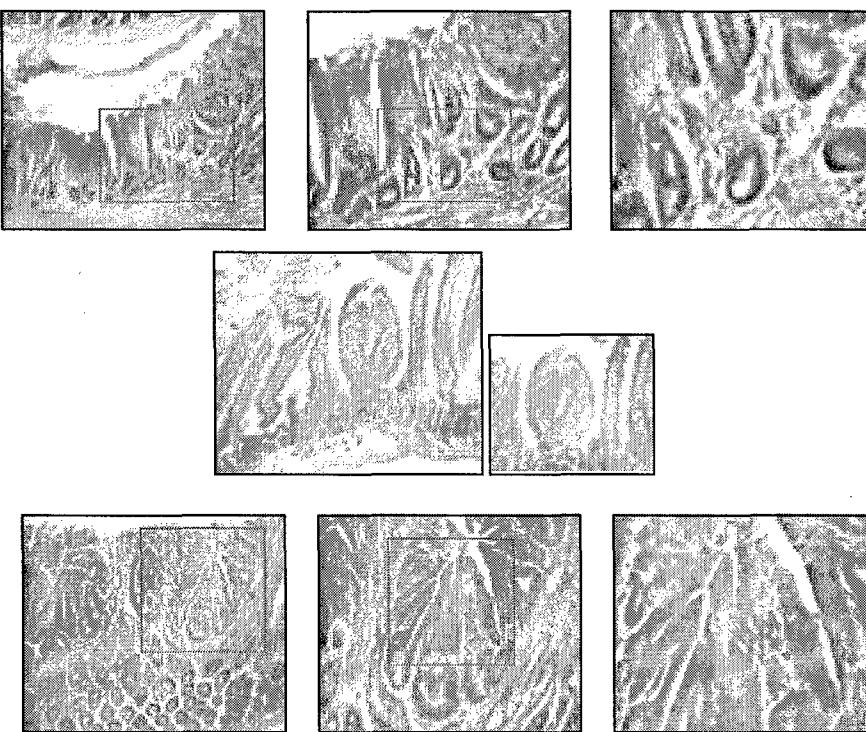
Fig. 11. UPAR immunostaining of $APC^{Min/+}$(Top panels, 100X, 200X, and 400X mag.) demonstrating low focal expression of UPAR mainly in lymphoid cells of lamina propia. UPAR immunostaining of $APC^{Min/+}/UPA^{-/-}$ (Middle two panels, 100X and 200X mag.) demonstrating no expression of uPAR. UPAR immunonostaining of $APC^{Min/+}/PAI-1^{-/-}$ (Lower three panels, 100X, 200X, and 400X mag.) demonstrating highly diffuse expression of UPAR throughout the tumor with increased deposition in the crypts.

22

Other immunostainings will include inflammatory cell markers *i.e.,* CD45; extracellular matrix protein *i.e.,* fibrinectin, laminin, and vitronectin; angiogenic regulators *i.e.,* angiopoietin, VEGF, and thrombospondin-1; and other components of the hemostasis system.

Task 3. **Determine expression of angiogenic regulators and extent of neovascularization.**

a) Utilizing real time RT PCR for specific mRNA determinations, expression of angiogenic regulatory factors will be determined as a function of disease progression.

Projected for following no cost extension year.

b) Neovessel formation will be quantitated from tumor tissue derived from $APC^{Min/+}$ mice and compared with mice having an additional deficiency of either urokinase or plasminogen activator inhibitor-1.

We have stained some of the tissue for CD31, a marker of neovessels, and are in the process of determined vessel density. Completion projected for following no cost extension year.

Key Research Accomplishments

a) Differences in tumor incidence in $APC^{Min/+}$ mice with an additional deficiency of urokinase ($APC^{Min/+}/UPA^{-/-}$)

b) Diminished expression of uPA in these mice parallel altered expression of other components of the fibrinolytic system *i.e.,* uPAR, the receptor for uPA, fibrin(ogen), and PAI-1.

Reportable Outcome

Manuscript in initial stages of preparation.

Conclusions

Colorectal tissue is the third most common site of new cases and deaths from carcinomas in both men and women. Several clinical studies have identified components of the hemostasis system in regulating the pathology of colon cancer. While a number of genes have been implicated in various stages of this disease, mutations in the adenomatous polyposis coli (*APC*) gene have been found during the early stages of adenoma formation, and it is believed that this gene is involved in tumor development and progression. Mutations of this gene results in familial adenomatous polyposis (FAP) which is characterized by the formation of multiple colonic adenomatous polyps which predisposes to the development of colon carcinoma. A mouse model (APC^{Min+}) has been developed that mimics the clinically features of FAP and results from these studies indicate that urokinase plays a key role in the early develop of this disease.

References

1. Carmeliet P, Collen D (1994). Evaluation of the plasminogen/plasmin system in transgenic mice. Fibrinolysis 8:269-276.
2. Moons L, Shi C, Ploplis V, Plow E, Haber E, Collen D, Carmeliet P (1998). Reduced transplant arteriosclerosis in plasminogen-deficient mice. J Clin Invest 102:1788-1797.
3. Mignatti P (1993). The fibrinolytic system and angiogenesis. Fibrinolysis 7:20-21.
4. DeVries TJ, Vanmuijen GNP, Ruiter DJ (1996). The plasminogen activation system in tumour invasion and metastasis. Pathol Res Pract 192:718-733.
5. Lambert RA, Hanes FM (1911). Characteristics of growth of sarcoma and carcinoma cultivated in vitro. J. Exp. Med. 13:495-504.
6. Skriver L, Larsson LI, Kielberg V, Nielsen LS, Andresen PB, Kristensen P, Dano K (1984). Immunocytochemical localization of urokinase-type plasminogen activator in Lewis lung carcinoma. J Cell Biol 99:752-757.

7. Dano K, Andraesen PA, Grondahl-Hansen J, Kristensen P, Nielsen LS, Skriver L (1985). Plasminogen activators, tissue degradation, and cancer. Adv Cancer Res 44:139-266.

8. Harvey SR, Sait SN, Xu Y, Bailey JL, Penetrante RM, Markus G (1999). Demonstration of urokinase expression in cancer cells of colon adenocarcinoma by immunohistochemistry and in situ hybridization. Am J Pathol 155:1115-1120.

9. Wang SN, Miyauchi M, Koshikawa N, Maruyama K, Kubota T, Miura K, Kurosawa Y, Awaya A, Kanai Y (1994). Antigen expression associated with lymph node metastasis in gastric adenocarcinomas. Pathol Int 44:844-849.

10. Cantero D, Fries H, Deflorin J, Zimmermann A, Brundler MA, Riesle E, Korc M, Buchler MW (1997). Enhanced expression of urokinase plasminogen activator and its receptor in pancreatic carcinoma. Br J Cancer 75:388-395.

11. Park IK, Kim BJ, Goh YJ, Lyu MA, Park CG, Hwang ES, Kook YH (1997). Co-expression of urokinase-type plasminogen activator and its receptor in human gastric-cancer cell lines correlates with their invasiveness and tumorigenicity. Int J Cancer 71:867-873.

12. Quigley JP (1979). Phorbol-ester induced morphological changes in transformed chick fibroblasts: Evidence for direct catalytic involvement of plasminogen activator. Cell 17:131-141.

13. Kwaan HC (1992). The plasminogen-plasmin system in malignancy. Cancer Met Rev 11:291-311.

14. Maroulakou IG, Anver M, Garrett L, Green JE (1994). Prostate and mammary adenocarcinoma in transgenic mice carrying a rat C3(1) simian virus 40 large tumor antigen fusion gene. Proc Natl Acad Sci USA 91:11236-11240.

Synthesis and Studies of Amamistatins and Analogs, Novel Anticancer Agents

Marvin J. Miller

Abstract

The focus of this research continues to be the design new compounds for the treatment of specific cancers, based on the structures of amamistatins. Amamistatins **A** and **B** were isolated from the actinomycete *Nocardia asteroids*. Amamistatin **A** was found to have anti-proliferative activity against a variety of cancer cell lines, with $IC_{50} < 1$ µM against MCF-7 breast, A549 lung, and MKN45 stomach cancer, respectively. Amamistatins **A** and **B** also both show cytotoxicity against mouse lymphocytic leukemia cells P388 (IC_{50} 15 and 16 ng/mL). This activity alone makes the amamistatins interesting synthetic targets. In addition to the wide range of biological activity, these compounds are interesting due to their structural similarity to mycobactins which are a class of siderophores, iron-chelating compounds. Like mycobactins, amamistatins bind iron (or zinc ion) and other metals using two lysine-based hydroxamate ligands and a hydroxyphenyl oxazole, and this ability to chelate metals essential for targeted enzyme activity is hypothesized to be responsible for the anti-tumor activity. The metal-chelating compounds secreted by mycobacteria to sequester physiologically essential iron, coupled to the structural similarity of components of the amamistatins and mycobactins to histone deacetylase inhibitors, suggests that carefully planned synthetic and biological studies can lead to the generation of novel anticancer agents. The last report indicated that the total synthesis of a mycobactin analog, **YPX-1-145** was performed and then ten mycobactin analogs and nineteen synthetic intermediates had been submitted for preliminary biological evaluation, with several demonstrating anticancer activity as predicted. Over the past year major progress has been made on the synthesis of target molecules and analogs to generate over **200 unique samples** that have or are being submitted for testing.

Subject Terms: cancer, breast, lung and stomach cancer, inhibitors, therapeutic agents, design and syntheses

INTRODUCTION

Breast, lung, stomach and other cancers account for a significant fraction of mortality and disability annually. Amamistatins and related mycobactins are structurally novel compounds with notable anticancer activity. Synthetic access to these novel compounds and analogs will allow detailed SAR studies to be performed. The results will either confirm the hypothesis that these compounds act as novel histone deacetylase inhibitors or help determine their activity by an alternate mode of action.

Amamistatins A and B were isolated from the actinomycete *Nocardia asteroids*, and their structures elucidated to be as shown in Figure 1. When tested for activity on a variety of cancer cell lines, they showed antiproliferative effects against MCF-7 breast, A549 lung, and MKN45 stomach cells, with IC_{50} values of 0.48, 0.56, and 0.24 μM, respectively. Anti-tumor activity has also been found in the series of structurally related compounds BE-32030 A-E isolated from *Nocardia sp.* A32030.[1] Two compounds known as nocobactin and formobactin were also isolated from strains of *Nocardia*,[2,3,4,5] with formobactin showing anti-lipid peroxidation activity, reduction of (L)-glutamate toxicity in neuronal cells, and suppression of apoptotic cell death by oxygen radical producers. In addition to the wide range of biological activity, these compounds are interesting due to their structural similarity to mycobactins, which have been studied in our lab for the possible treatment of tuberculosis and other mycobacterial infections.[6] Mycobactins are a class of siderophores, iron-chelating compounds, secreted by mycobacteria to aid in the acquisition of physiologically insoluble, yet essential Fe(III) from their environment. Mycobactins bind iron using three bidentate ligands: a hydroxyphenyl oxazoline and two hydroxamic acids. It has been suggested that metal-binding ability is also responsible for the activity of the amamistatins and related compounds. From the range of biological activity exhibited by this group of structurally related compounds, it is clear that structure-activity relationship (SAR) studies are necessary for future work in this area.
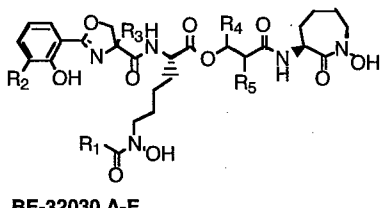

BE-32030 A-E

A-C, R_2=R_5=H, R_3=R_4=Me
A, R_1=(CH$_2$)$_{11}$Me
B, R_1= (CH$_2$)$_{13}$Me
C, R_1= (CH$_2$)$_6$CH=CH(CH$_2$)$_7$Me
D, R_1=(CH$_2$)$_{11}$Me, R_2=OH
E, R_1= (CH$_2$)$_4$CH=CH(CH$_2$)$_7$Me, R_2=OH
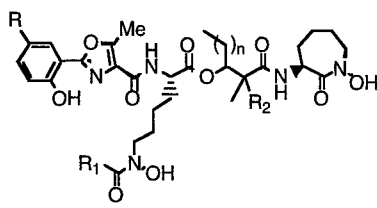
nocobactin, R=R_2=H, R_1=Me n = 9 & 11
formobactin, R=R_1=H, R_2=Me n = 8
  lipid peroxidation and other inhibitory activity
Amamistatin A, R=OMe, R_1=H, R_2=Me
Amamistatin B, R=R_1=H, R_2=Me, n=6
<u>Growth inhibition for human tumor cell lines</u>
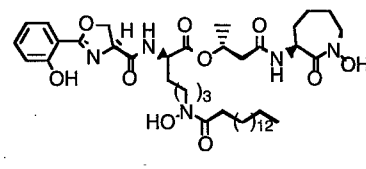
Mycobactin T
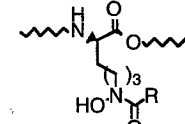
ε-*N*-hydroxy-ε-*N*-acyl-L-lysine, key metal binding component

Figure 1: Structure of Amamistatins and Related Compounds

While the exact mode of action responsible for the anticancer activity of the amamistatins and related mycobactin-like compounds is not known, and will also be part of the proposed study, one of the metal binding components, the ε-*N*-hydroxy-ε-*N*-acetyl-L-lysine, resembles known inhibitors of histone deacetylases, enzymes with activity that has been linked to cancer.[7,8,9,10,11,12] Histones are a family of basic proteins that are normally associated with DNA in most cells of eukaryotic organisms, including humans. These essential proteins are rich in the basic amino acids arginine and lysine. Consequently, at physiological pH, the proteins are highly charged and bind tightly to negatively charged DNA to provide structural order that plays an important role in gene expression. Removal of the charge by acylation alters the DNA-histone interaction. Acylation of the ε-amino group of the lysine components of nuclear histones is regulated by acetyl-transferase and deacetylase[13] and affects key processes including DNA replication, transcription, repair and rearrangements during differentiation. Thus, in normal cells, a critical balance must be maintained between histone acyl transferase (HAT) and histone deacylase (HDAC) activity to allow cell specific gene expression. Alterations of the HAT/HDAC balance by changes in histone acylation have recently been linked to proliferation of malignant tumors. Thus, significant research efforts have led to the discovery of HDAC inhibitors with *in vivo* anticancer activity. These inhibitors all incorporate chemical functionality that can bind or interact with the essential components of the HDAC deactylation reaction.[14,15,16,17,18,19,20,21,22] <u>However, none of the recently reported HDAC inhibitors incorporate</u>

the natural lysine substrate or a form of it that might also bind the essential zinc. The ε-N-hydroxy-ε-N-acyl-L-lysine component of the amamistatins and mycobactins closely mimics the natural acetyl-L-lysine substrate of HDAC, yet contains a hydroxamate to bind the essential Zn atom of HDAC and thus possibly serve as a potent inhibitor of HDAC.

Upon initial inspection, the structure of amamistatins and related mycobactins seems rather complex and the development of effective, practical syntheses for SAR studies would seem daunting. However, as shown below, both types of compounds can be retrosynthetically disconnected into the same four types of fragments: a hydroxyphenyl oxazole (or oxazoline) **1**, linear (**2**) and cyclic (**4**) hydroxamic acids, and a β-hydroxy linker **3** (XH = OH, Y &/or Z=alkyl, for the natural compounds).

Amamistatin A: G = OMe
Amamistatin B: G = H
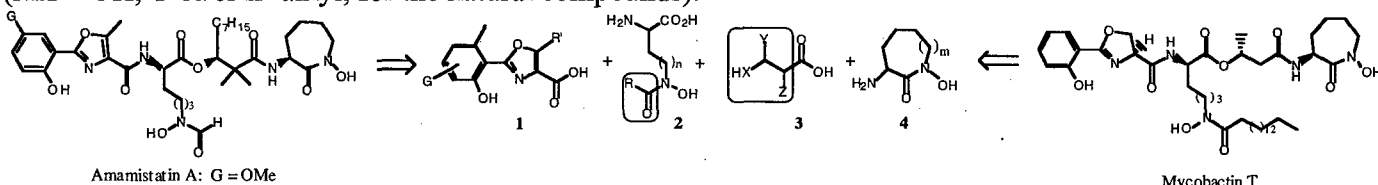
Mycobactin T

During our earlier syntheses of mycobactins and analogs, we developed very efficient methods for the syntheses of each of the core components of the mycobactins and their effective incorporation into mycobactins and analogs. Preparation of each of the four core components and their use in the syntheses of mycobactins and analogs is summarized below.

As shown below, the oxazoline fragment (**1**) was formed by coupling salicylic acid and L-serine, followed by dehydrative cyclization using either the Burgess reagent or, on larger scale, a low temperature treatment with thionyl chloride.
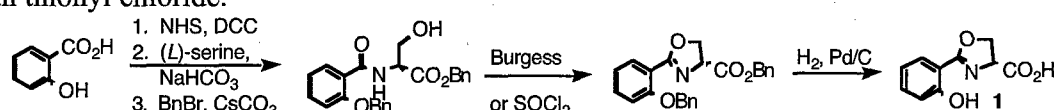
Both the linear (**2**) and cyclic hydroxamic acids (**4**) were derived from lysine, using methodology developed in our group. This conversion was originally carried out via a direct oxidation method using dimethyl dioxirane and acetone.[23] This method was later replaced by indirect oxidation, shown below, which allows for isolation of the very stable intermediate nitrone.[24] The nitrone can then be stored for later conversion to the hydroxamate. Thus, N^{α}-protected lysine was condensed with benzaldehyde to form the corresponding imine, then converted to the oxaziridine using m-CPBA and isomerized to the nitrone with TFA.
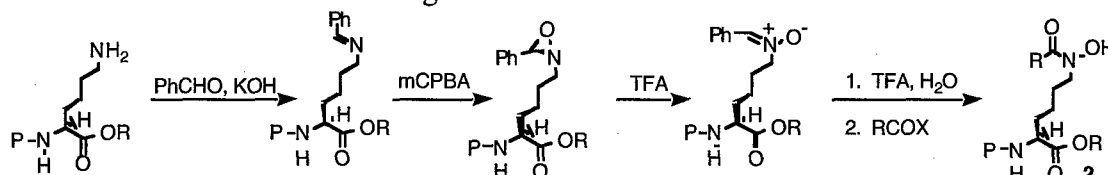
For the linear hydroxamate portion, the nitrone was converted to the hydroxylamine using TFA/H$_2$O and acylated immediately with the appropriate side chain (RCOX). Alternatively, the nitrone could be left in place and acylated at the end of the synthesis to create a series of compounds differing by only the hydroxamate side chain. The oxazole and linear hydroxamic acid fragments were then coupled using EDC/HOAt to form the mycobactic acid half of mycobactins. The cyclic hydroxamate was formed from the same N^{α}-protected nitrone by treating it with NH$_2$OH•HCl, followed by cyclization with DCC, DMAP, and DMAP•HCl.
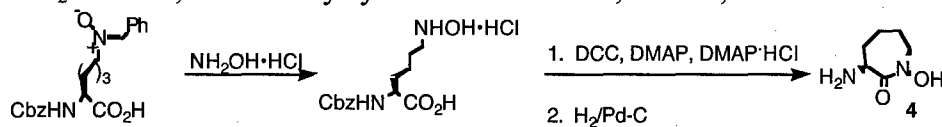
β-Hydroxy acids, corresponding to fragment **3** (XH=OH, Y &/or Z=variable alkyl) have been obtained from asymmetric aldol reactions or asymmetric reduction of the corresponding β-keto acids. Coupling of the linker (component **3**) and cyclic hydroxamate (component **4**) with DCC completed the cobactin half of the molecule. The stereocenter at the central ester linkage of the mycobactins (designated * in structures below) was easily controlled by the conditions used for the final coupling reaction. The use of a coupling agent gave retention of configuration, while Mitsunobu coupling led to inversion of stereochemistry. Using this methodology, our group has completed the synthesis of Mycobactins S and T,[25] as well as a variety of

mycobactin analogs. The scheme below summarizes the syntheses and emphasizes the practicality of the processes that allow assembly of the components without use of hydroxamate and phenol protecting groups.

L-serine
1. 2-(CO$_2$H, OBn)benzene /EDC
2. MeO$_2$CNSO$_2$N(Et)$_3$ (Burgess reagent)
3. H$_2$/Pd-C → 1

1 + 2 → EDC, HOAt → 5

6 → 1. H$_2$/Pd-C 2. (7, form of 3) HO-Me-CO$_2$H / DCC → 8

1. NaOH (-Me ester)
2. 8 + coupling agent or Mitsunobu

mycobactins S and T
n=2 in all natural forms
* = (S)configuratin for mycobactin S
and (R) configuration for mycobactin T
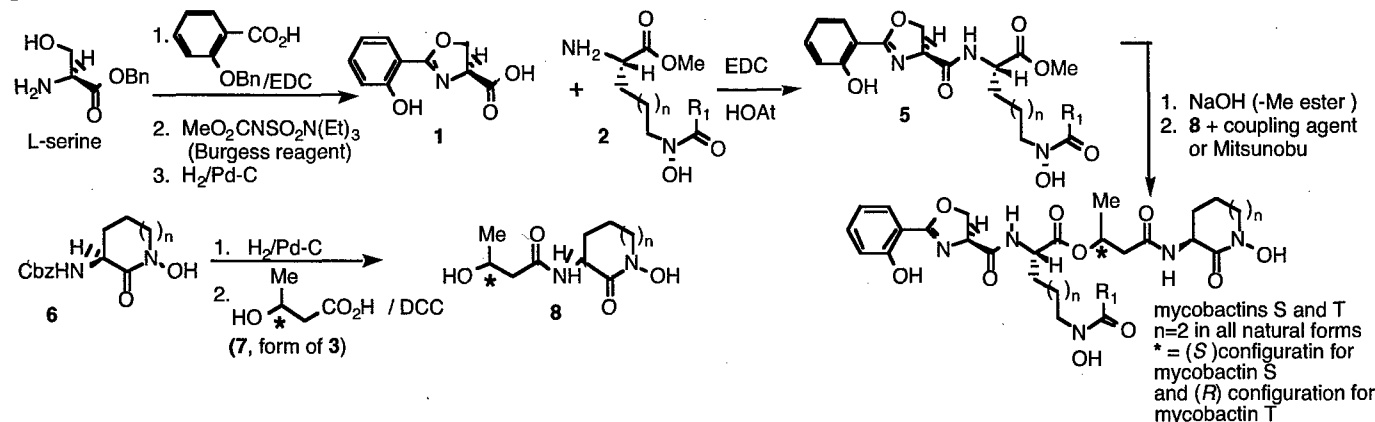
As shown below, substitution of the usual β-hydroxy acid component **3** of the mycobactins with the β-lactam derived β-amino acids during the syntheses allowed preparation of novel, unnatural, but more stable analogs, such as **YPX-1-145**, that proved to be potent inhibitors of tuberculosis.[26]

9 → H$_2$NOBn, EDC → 10 → PPh$_3$, CCl$_4$, TEA → 11 → LiOH → 12, 80% overall from Boc-L-serine

12 + 4 → 1. EDC/HOAt 2. H$_2$, Pd-C 91% overall → 13

1 + 14 → 1. EDC, HOAt 2. LiOH 90% for 2 steps → 15 → EDC/HOAt DMAP, 13 (-Boc) 85% → YPX-1-145
antiTB MIC = <0.2 μg/mL
IC$_{50}$ = 1 μg/mL
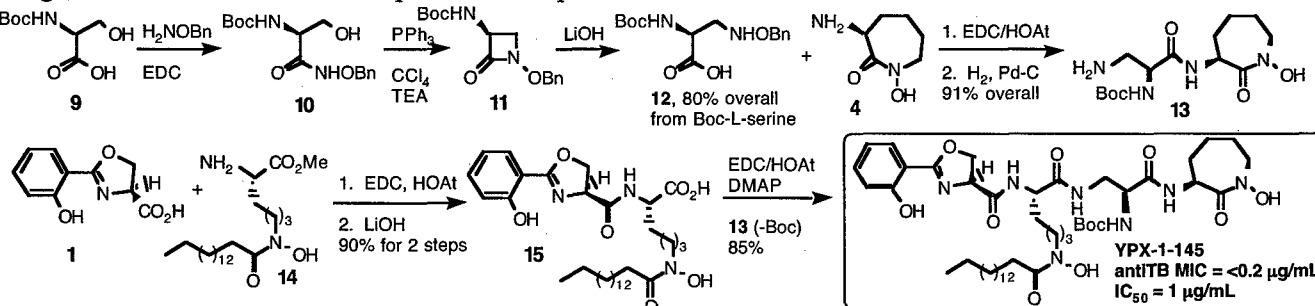
Thus, fundamental methodologies for the preparation of the key components of the mycobactins have been developed and their utility demonstrated in practical syntheses of mycobactins and analogs. The structural similarity of the mycobactins to the amamistatins, nocobactins and formobactins indicated that similarly effective syntheses of these interesting natural products and analogs could be developed.

Using the synthetic methodology developed for the mycobactins, the synthesis of Amamistatins A and B has been initiated by preparation of all of the components. Thus, in the case of amamistatin B, the oxazole fragment (component **1**) was formed by coupling salicylic acid (R=H) and L-threonine, followed by dehydrative cyclization and oxidation to the oxazole ring as shown below. For the synthesis of amamistatin A, methoxy substituted salicylic acid (R=OMe) will be substituted for salicylic acid itself.

1. NHS, DCC
2. (L)-threonine, NaHCO$_3$
3. BnBr, CsCO$_3$
→ Burgess → 1. DDQ 2. H$_2$, Pd/C
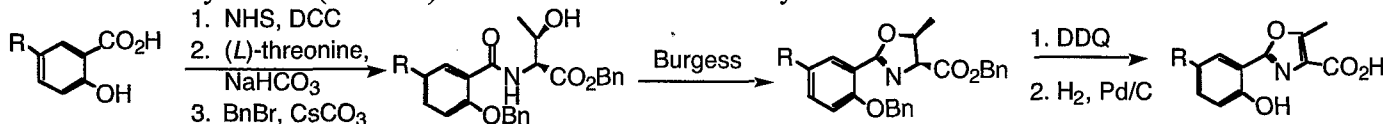
The key linear lysine component (**2**) has been prepared using the practical and effective indirect oxidation process described earlier, but with substitution of the appropriate side chain (H) by use of formylacetic anhydride as the reagent RCOX. A significant variety of analogs can now be prepared by simple variation of the acylating agent RCOX to provide SAR information and perhaps optimizing inhibitory activity by filling the 14 Angstrom "cavity" revealed in the X-ray crystallographic studies.

As proposed, the β-hydroxy acid linker (a form of component **3**) has been made using an enantioselective aldol reaction with octanal and methyl trimethylsilyl dimethylketene acetal (**16**), using a chiral oxazaborodolidinone (**17**).[27]

C$_7$H$_{15}$CHO + 16 → 17, THF, -78 °C → C$_7$H$_{15}$...CO$_2$Me → aq. NaOH, MeOH → C$_7$H$_{15}$...CO$_2$H
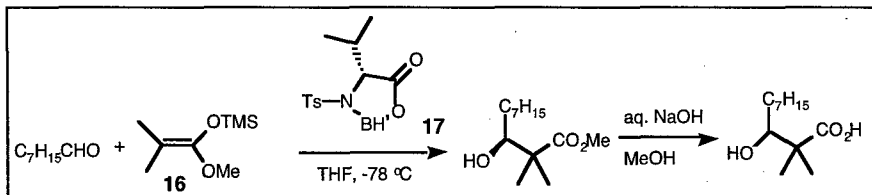
The remaining cyclic lysine-based hydroxamate (component **4**) is available from our previous mycobactin syntheses.

With all four components in hand, coupling reactions have been used to assemble **1** and **2** into "mycobactic acid" portion ("left" half) and fragments **3** and **4** were coupled to provide the "cobactin" portion ("right" half, **20** shown above). As indicated in the last report, the final synthetic challenge was expected to be the sterically hindered coupling between the two halves ("left" and "right") of the amamistatins. We are pleased to indicate that we have very recently optimized chemistry that allows effective formation of the key ester linkage in model compounds and penultimate precursors of fully protected amamistatin. We anticipate that application of this technology will allow completion of the total synthesis of amamistatin.

In addition to completing the syntheses of all of the components of amamistatin B, the total synthesis of a mycobactin analog, **YPX-1-145**, was completed along with several related derivatives. **YPX-1-145** and its resynthesized form, **HZ-1-296-3**, represent new mycobactin analogs originally designed as antiTB agents. With their long C-16 acyl side chain on the ε-nitrogen of the linear lysine, they were anticipated to not be substrates for histone deacetylase and, in fact, showed no anticancer activity. As of the last report, ten mycobactin analogs and nineteen synthetic intermediates were prepared and submitted for biological evaluation in a prostate cancer (PC-3) cell assay. As proposed, **HZ-2-82**, with a simple acetyl side chain does inhibit the growth of the PC-3 (prostate) cancer cells. Unexpectedly, and very interestingly, two other partial structures, **HZ-2-56** and **HZ-2-117**, are also active. **HZ-2-56** lacks the linear lysine component while **HZ-2-117** contains the linear lysine component, but also an extended acyl side chain. In the last report, we indicated that these very interesting results would be augmented by further synthetic studies and biological assays to further elaborate important structure-activity-relationships (SAR) of these novel anticancer agents. During this past year, more than 200 new samples have been prepared and many have already been submitted for biological studies.

Previously Completed Syntheses
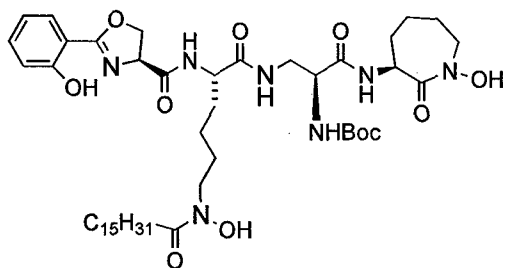
YPX-I-145-2   antiTB MIC = 0.48 ug/mL
            IC_{50} = 9.88 ug/mL

HZ-I-296-3   antiTB MIC = 0.98 ug/mL
            IC_{50} = 9.97 ug/mL
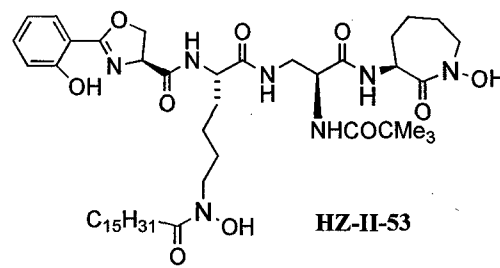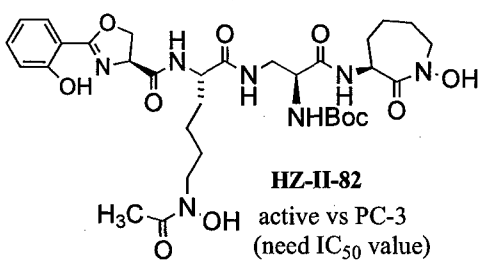
HZ-II-82
active vs PC-3
(need IC_{50} value)
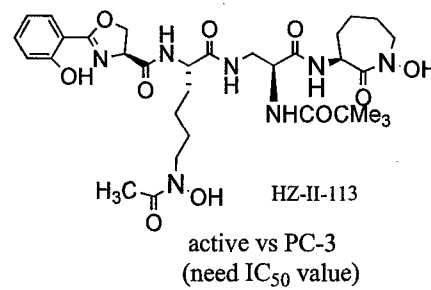
HZ-II-113
active vs PC-3
(need IC_{50} value)
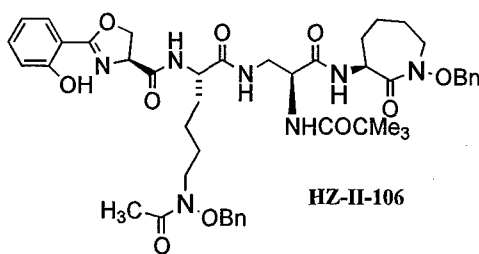
HZ-II-106
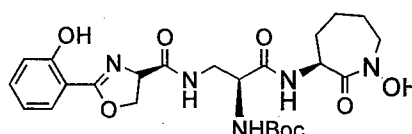
HZ-II-56   active vs PC-3
            (need IC_{50} value)

30

HZ-II-117

active vs PC-3
(need IC$_{50}$ value)

HZ-II-119

HZ-II-120

HZ-II-128
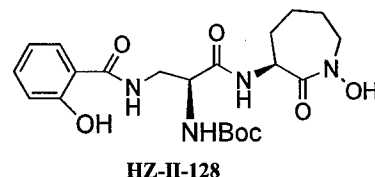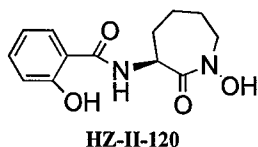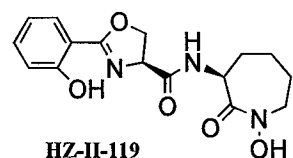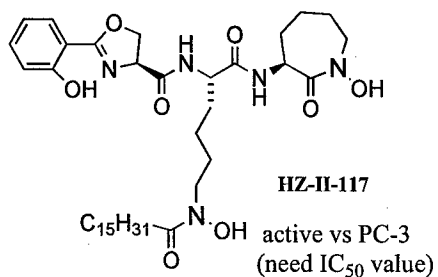
Previously Prepared Synthetic Components and Fragments for Additional Syntheses and SAR Studies

HZ-I-207

HZ-II-30

HZ-I-215b

HZ-I-249

HZ-I-137

HZ-I-179

HZ-I-238

HZ-I-257

HZ-I-226

HZ-I-252

HZ-I-295

HZ-II-134

HZ-I-291

HZ-II-59

HZ-I-202

HZ-II-45

HZ-II-63

31

HZ-II-74

HZ-II-109
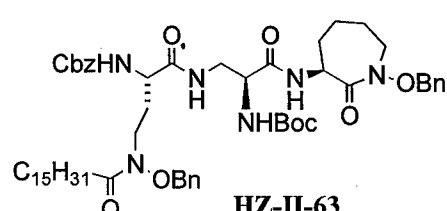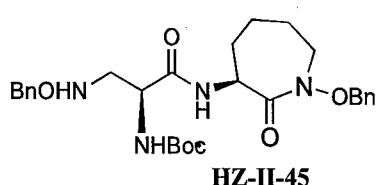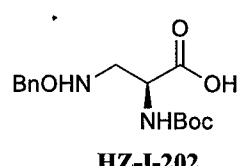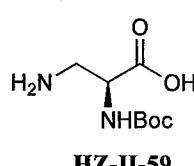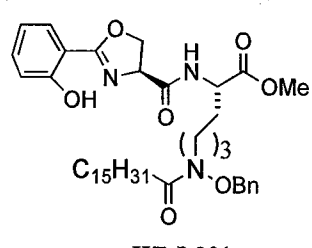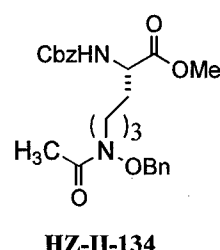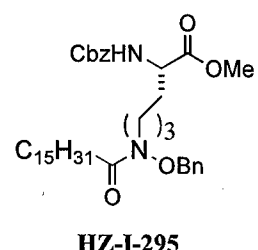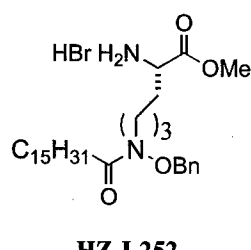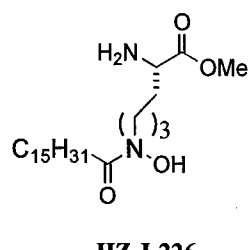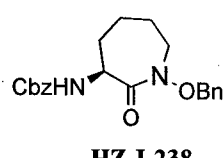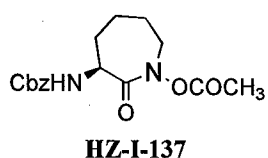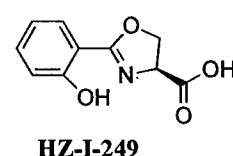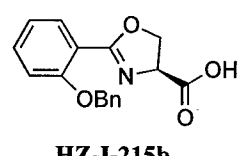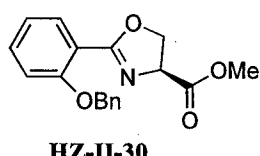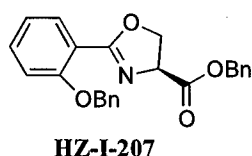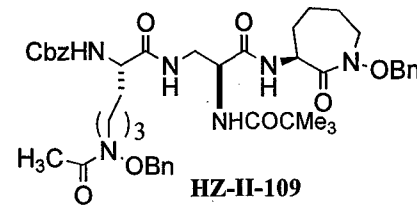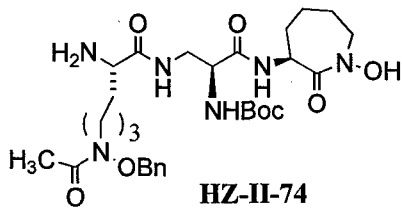
A list of the structures, ID numbers and preliminary assay results of over 170 of the more than 200 samples prepared this year is attached to this report. While bioassays are still being performed on many of the more than 200 unique compounds prepared so far, preliminary results indicate that even some of the synthetic intermediates have low micromolar activity. This is especially interesting in the series of easily prepared oxazoline derivatives that represent forms of **1**, the first component of the mycobactic acid section of the mycobactins and amamistatins. Thus, as indicated by the substantial number of related compounds in the set of over 200 that we have prepared, we are initiating a structure-activity relationship (SAR) study of this portion of the overall target structures. If the SAR of this small component can be optimized, it will result in the identification of a novel class of anticancer agents that is readily synthesized and suitable for additional elaboration.

Partial list of additional compounds prepared and preliminary biological assays against PC3 (prostate cancer) and MCF7 (breast cancer) cell lines as well as anti TB screening results:

Compound	MolWt	MABA GAS NRP-TB	MABA GAST low iron NRP-TB	VERO cells GAS	LORA 7H12	SI	PC-3 cells 96 hrs.	MCF-7 (%)
		MIC (uM)	MIC (uM)	IC50 (uM)	MIC(uM)		IC50 (uM)	vs. control (100%)
BSB-I-164-1	225.2	>128	>128					
BSB-I-147-3, HZ-I-215	311.34	118	>128					117.7
BSB-I-213-3, JH-3-122, HZ-I-47	387.44	7.42 (45 @ level 2)	7.18 (>128 @ level 2)	>128 (>128 @ level 2)	50.2	18		114
BSB-I-214-1	281.31	5.3 (62 @ level 2)	3.82 (>128 @ level 2)	>128 (>128 @ level 2)	63	24		
BSB-I-219-4, HZ-II-249	207.19	>128	>128					98.9
KAS-I-246-1	219.2	>128	>128					
KAS-I-264-2	399.45	28.3	>128	101		356		
KAS-I-210-1	401.46	>128	>128				30.0	
KAS-II-87-1	203.19	>128	>128					
KAS-I-288-1	293.32	3.92	15.2	34.9	58.5	9		

32

KAS-I-293-1, KAS-84-1	251.31	>128	>128					
KAS-I-267-1	351.43	>128	>128					
BSB-I-205-4	470.57	>128	>128		43.1			
BSB-I-210-4	470.57	>128	>128					
KAS-I-295-2	385.44	>128	>128					
KAS-I-247-1 (HBr salt)	234.3 (315.20	>128	>128				0.0	
KAS-II-62-1	414.46	29.6	39.3	102		3		
KAS-II-79-1	456.5	14.2	46.2					
KAS-II-56-1, HZ-I-238	368.44	>128	>128					60.9
KAS-II-84-2	442.51	>128	>128		46.8			
KAS-II-34-1	479.54	>128	>128					
BSB-I-180-2	501.54	109	>128					83.4
KAS-II-39-1	507.55	61	>128		61.3			
KAS-II-53-1	605.69	>128	>128				7.5	
KAS-II-44-1	419.48	30.9	>128	112	28.6	4		
BSB-I-172-3	223.23	>128	>128					
BSB-I-208-3	405.45	>128	97.5	>128	26			
BSB-I-209-3	299.33	>128	>128					
BSB-I-203-4	228.25	>128	>128					
HZ-I-179, HZ-I-167	278.31	>128	>128					88.7% (140.2%)
HZ-I-284	526.64	>128	>128					
HZ-II-119	333.35	>128	>128					98.7
HZ-II-120	264.28	>128	>128					86.3
HZ-II-139	554.65	>128	73.5	>128				
AS-138	548.77	>128	>128		13.1		7.0	
2AS-196-1	458.64	>128	108		63.5		20.0	
2AS-186 (H2SO4)	358.52 (456.6)	>128	120		60.4		35.0	
KAS-I-299-4	216.32	118	109	>128			0.0	
KAS-II-63-4	432.61	>128	>128					

BSB-I-148-4	289.29	>128	>128					
BSB-I-165-3	455.51	46.6	46.3	39.2	59	0.8		
BSB-I-166-1	303.31	>128	>128					
KAS-II-45-4	313.36	>128	>128					
HZ-II-238	393.4	>128	>128					
HZ-I-285b	693.93	>128	<128					
HZ-II-63	1027.4	>128	>128					123.5
HZ-II-246, YPX-2-145	902.15	>128	8.95	35.3		4		
HZ-II-232	1082.4	>128	128					
HZ-II-245	872.12	>128	>128				12.0	
HZ-II-185	519.56	>128	101				10.0	
HZ-II-223	609.68	>128	>128					
HZ-II-231	503.56	>128	>128					
HZ-II-206	677.72	>128	79.4	>128			19.0	135.3
HZ-II-144	519.56	>128	122					-50.7
HZ-II-233	766.85	>128	>128					
HZ-II-186	705.77	>128	122					
HZ-II-208	676.73	>128	125				17.0	-36.1
TEL-II-87, danoxamin	619.72							
TBD-II-190-2	217.27	>128	>128		>128			
TBD-II-301-2	311.43	64	>128		109			
TBD-III-234-2	233.31	>128	>128		>128			
TBD-III-241-2	266.39	8	59		61			
TBD-III-267-2	217.27	>128	>128		>128			
KAS-II-65-3	198.31	>128	>128		>128			
KAS-II-114-3	303.45	>128	>128		>128			
KAS-II-133-2	303.45	111	>128		>128			
TBD-II-180-2	331.5	>128	64		128			
2AS-229	603.2							
KAS-II-28-3	495.54	>128	>128		>128			
KAS-II-51-3	329.35	>128	>128		>128		0.0	
KAS-II-136-3, BSB-I-179	483.52	>128	>128		>128		8.0	33.2
KAS-II-95-3	205.21	>128	>128		>128			

AFV-I-106-2	401.46	32	>128		64			
KAS-II-125-2	230.35	126	>128		>128	....	....	
KAS-II-126-2	230.35	115	>128		>128			
KAS-II-128-2	216.32	>128	>128		>128			
KAS-II-129-2	321.46	59	>128		>128			
KAS-II-130-2	321.46	82	>128		>128			
KAS-I-245-3	352.39	>128	>128		>128			
KAS-II-117-3	442.47	>128	>128		>128			
KAS-II-118-3	428.49	102	>128		>128			
BSB-I-266-2	241.29	>128	>128		>128			
BSB-I-249-4	255.32	>128	>128		>128			
TBD-IV-269-1	684.88							
TBD-IV-271-1 (di-HCl)	524.75 (597.67)							
LFZ-I-227b	401.38							
LFZ-I-223b	401.38							
LFZ-I-205	523.63	>128	>128		>128			
LFZ-I-279	445.48							
LFZ-I-255	399.41							
LFZ-I-233	419.39							
LFZ-I-284	285.26							
LFZ-I-276	285.26							
BSB-I-225-3	467.52	>128	>128		>128		37.0	
BSB-I-226-2	559.62	>128	>128		>128		15.0	
BSB-I-227-2	543.62	>128	>128		>128		17.0	
BSB-I-228-2	559.62	>128	>128		>128		~2.5	
BSB-I-229-4	543.62	>128	>128		>128		15.0	
BSB-I-220-4	191.19	>128	>128		>128			
BSB-I-233	312.33	127	>128		>128		11.0	
BSB-I-259-4	222.2	>128	>128		>128			
BSB-I-241	296.33	>128	>128		>128		0.0	
GM1-60-5	221.21	>128	>128		>128			

35

2AS-228	637.82							
2AS-231	621.82	>128	>128		>128			
2AS-234	653.89	>128	>128		>128			
2AS-233	223.25	>128	>128		>128		37.0	
2AS-232	403.13	28	112		>128			
hwq-I-271	322.32	>128	>128		>128			
hwq-I-246	422.4	71	>128		29			
hwq-II-144	238.24	63	>128		>128			
hwq-I-259	381.43	>128	>128		>128			
hwq-I-270	347.41	>128	>128		>128			
hwq-I-215	287.36	>128	>128		>128			
hwq-II-11	472.45	>128	>128		>128			
hwq-II-19	392.36	>128	>128		>128			
GPN-III-26	233.23						0.0	
EAM-I-189	269.35							
EAM-I-133	243.31						0.0	
EAM-I-190	255.32						0.0	
EAM-I-64	229.28						0.0	
EAM-I-45	203.24						0.0	
EAM-I-183	215.25						7.0	
EAM-I-68	163.18						13.0	
MDS-IV-293B	289.38							
MDS-IV-98B	339.39						50.0	
PY-III-30	445.41						0.0	
PY-III-31	346.28						0.0	
PY-III-56	502.46						0.0	
PY-III-59	348.27						0.0	
PY-III-62	330.28						0.0	
PY-III-74	599.58						0.0	
PY-III-82	344.3						0.0	
PY-III-128	766.9						0.0	
HZ-II-53	886.15	>128	45.43		>128			-42.3
HZ-II-145	425.53							135
HZ-I-137	320.35							68.2
HZ-II-113	204.23							92.1
HZ-II-59	689.77							122
HZ-II-56	519.56							-0.2
HZ-II-213	234.3							106
HZ-II-106	870.02							81.9
HZ-II-128	450.49							75
HZ-I-291	693.93							86.8
HZ-II-117	715.94							-78
HZ-II-134	442.51							100.4
HZ-II-201	403.44							62.2
HZ-I-226	414.63							13
HZ-II-82	705.77							81.4
HZ-II-141	497.55							-80.3

HZ-II-45	526.64							99.3
HZ-I-295	638.89							115
HZ-I-252	504.76							116
HZ-II-109	830.98							58.8
HZ-I-296	902.15							-21.1
HZ-II-30	311.34							50.6
EAM-I-68	163.18							58.7
EAM-I-183	215.25							23.7
EAM-I-189	269.35							66.7
EAM-I-133	243.31							71.2
EAM-I-190	255.32							85.6
EAM-I-64	229.28							67.8
EAM-I-045	203.24							120
EAM-I-164	189.22							113
JKB-I-021	247.3							
JKB-I-053	339.39							
HZ-I-202	310.35							137
2AS-243	575.69							
GZ-1-170-2	449.49	>128	126		>128			
DS04-209-A	678.9	14	>128		118			
DS04-209-B	692.9	>128	>128		31			

KEY RESEARCH ACCOMPLISHMENTS (year 2 of 2)

- All of the components of the amamistatins and mycobactins have been prepared.
- Methodology has been developed that will allow formation of the very hindered ester linkage of the amamistatins. Thus, it is anticipated that the total synthesis should be able to be completed in less than one additional year.
- More than 200 components and fragment analogs have been prepared. These unique samples are undergoing biological studies.
- Preliminary biological assays indicate that several of the analogs and even truncated versions have activity against prostate and breast cancer, while others have activity against tuberculosis.
- Thus, indications are that appropriate continued synthetic and SAR studies will provide new leads for the development of novel, readily synthesized anticancer agents.

Presentations given.

"Amamistatin B Analogs as Potential Anti-Cancer and Anti-TB Agents." Fennell, K.; Miller, M. J. 36th Central Regional Meeting 2004, Indianapolis, IN June 2-5, 2004.

"Amamistatin B Analogs as Potential Anti-Cancer and Anti-Tuberculosis Agents." Fennell, K. A.; Miller, M. J. Walther Cancer Institute Annual Scientific Retreat, August 6, 2004.

"Synthesis and Studies of Amamistatins and Analogs Novel Anticancer Agents." Zhu, H.; Miller, M. J. Walther Cancer Institute Annual Scientific Retreat, August 6, 2004.

"Synthesis of a Conformationally Constricted Siderophore Conjugate as Potential NAALADase Inhibitor and Diagnostic Agent." Ding, P.; Helquist, P.; Miller, M. J. Walther Cancer Institute Annual Scientific Retreat, August, 2004.

"Synthesis of Siderophore Drug Conjugates." Miller, M. J. 4th International Biometals Symposium, Garmisch Partenikirchen Germany, September 3-5, 2004.

"Salmycins – Natural Siderophore-Drug Conjugates: Prospects for Modification and Investigation Based on Successful Total Synthesis." Möllmann, U.; Dong, L.; Miller, M. J. 4th International Biometals Symposium, Garmisch Partenikirchen Germany, September 3-5, 2004.
<u>Abstracts of papers presented at Scientific Meetings. (cont'd)</u>

"DNA Microarray Analysis of the Mode of Action of Salmycin B. " Allard, M.; Moisan, H.; Bellemare, J.; Ladouceur M.-E.; Dong, L.; Miller M. J.; Jacques, M; Lacasse, P.; Diarra, M. S.; Malouin, F. ICAAC Symposium, Washington, DC, October 30, 2004.

"Design, Syntheses and Studies of Mycobacterial Siderophores with Selective antiTB Activity." M. J. Miller, J. Hu, Y. Xu, A. J. Walz, H. Zhu, K. Fennell, B. Bodnar, A. Sheinkman, G. Moraski, S. Franzblau, U. Moellmann, Tuberculosis: Integrating Host and Pathogen Biology (D1), Whistler, Canada, April 2-7, 2005.

"Synthesis and Studies of Amamistatins and Analogs, Novel Anticancer Agents", Zhu, H.; Miller, M.J. Walther Cancer Institute Retreat in Indianapolis, August, **2003**.

CONCLUSIONS

During this second year of support, significant additional progress has been made towards accomplishing the main synthetic goals and preliminary assays indicate that several of the synthetic products have anticancer activity. The syntheses of all of the components have been simplified to allow extensive core and peripheral modification. These results have allowed us to prepare over 200 unique compounds to facilitate extensive SAR studies. These studies are anticipated to generate new leads for the discovery of novel selective anti TB and anti cancer agents.

REFERENCES

1. Tsukamoto, M.; Murooka, K.; Nakajima, S.; Abe, S.; Suzuki, H.; Hirano, K.; Kondo, H.; Kojira, K.; Suda, H. "BE-32030 A, B, C, D, and E, New Antitumor Substances Produced by *Nocardia* sp. A32030," *J. Antibiot.*, **1997**, *50*, 815-821.
2. Ratledge, C.; Patel, P. V. "The Isolation, Properties and Taxonomic Relevance of Lipid-Soluble, Iron-Binding Compounds (the Nocobactins) from Nocardia," *J. Gen. Microbiol.* **1976**, *93*, 141-152.
3. Ratledge, C.; Snow, G. A. "Isolation and Structure of Nocobactin NA, a Lipid-Soluble Iron-Binding Compound from *Nocardia asteroides*," *Biochem. J.* **1974**, *139*, 407-413.
4. Patel, P. V.; Ratledge, C. "Isolation of Lipid-Soluble Compounds that Bind Ferric Ions from *Nocardia* Species," *Biochem. Soc. Trans.* **1973**, *1*, 886-888.
5. Murakami, Y.; Kato, S.; Nakajima, M.; Matsuoka, M.; Kawai, H.; Shin-Ya, K.; Seto, H. "Formobactin, a Novel Free Radical Scavenging and Neuronal Cell Protecting Substance from *Nocardia* sp.," *J. Antibiotics.* **1996**, *49*, 839-845.
6. Vergne, A. F.; Walz, A. J.; Miller, M. J. "Iron Chelators from Mycobacteria (1954-1999) and Potential Therapeutic Applications," *Nat. Prod. Rep.* **2000**, *17*, 99-116.
7. Sun, J. M.; Chen, H. Y.; Moniwa, M.; Samuel, S.; Davie, J. R. "Purification and Characterization of Chicken Erythrocyte Histone Deacetylase 1," *Biochemistry*, **1999**, *38*, 5939-5947.
8. Lin, R. J.; Nagy, L.; Inoue, S.; Shao, W. L.; Miller, W. H.; Evans, R. M. "Role of the Histone Deacetylase Complex in Acute Promyelocytic Leukaemia," *Nature*, **1998**, *391*, 811-814.

9. Lopezrodas, G.; Brosch, G.; Georgievea, E.; Sendra, R.; Franco, L.; Loidl, P. "Histone Deacetylase – A Key Enzyme for the Binding of Regulatory Proteins to Chromatin," *FEBS Lett.* **1993**, *317*, 175-180.

10. Yoshida, M.; Furumai, R.; Nishiyama, M.; Komatsu, Y.; Nishino, N.; Horinouchi, S. "Histone Deacetylase as a New Target for Cancer Chemotherapy," *Cancer Chemother. Pharmacol.* **2001**, *48*, S20-S26.

11. Marks, P. A.; Richon, V. M.; Rifkind, R. A. "Histone Deacetylase Inhibitors: Inducers of Differentiation or Apoptosis of Transformed Cells," *J. Natl. Cancer Inst.* **2000**, *92*, 1210-1216.

12. Kiefer, S. M.; McDill, B. W.; Yang, J.; Rauchman, M. "Murine Sall Represses Transcription by Recruiting a Histone Deacetylase Complex," *J. Biol. Chem.* **2002**, *277*, 14869-14876.

13. Saito, A.; Yamashita, T.; Mariko, Y.; Nosaka, Y.; Tsuchiya, K.; Ando, T.; Suzuki, T.; Tsuruo, T.; Nakanishi, O. "A Synthetic Inhibitor of Histone Deacetylase, MS-27-275, with marked *in vivo* Antitumor Activity Against Human Tumors," *Proc. Natl. Acad. Sci. USA*, **1999**, *96*, 4592-4597.

14. Jung, M; Brosch, G.; Kölle, D.; Scherf, H.; Gerhäuser, C.; Loidl, P. "Amide Analogues of Trichostatin A as Inhibitors of Hisone Deacetylase and Inducers of Terminal Cell Differentiation," *J. Med. Chem.* **1999**, *42*, 4669-4679.

15. Jung, M. "Inhibitors of Histone Deacetylase as New Anticancer Agents," *Curr. Med. Chem.* **2001**, *8*, 1505-1511.

16. Furumai, R.; Komatsu, Y.; Nishino, N.; Khochbin, S.; Yoshida, M.; Horinouchi, S. "Potent Histone Deacetylase Inhibitors Built from Trichostatin A and Cyclic Tetrapeptide Antibiotics Including Trapoxin," *Pro. Natl. Acad. of Sci. U.S.A.* **2001**, *98(1)*, 87-92.

17. Su, G. H.; Sohn, T. A.; Ryu, B.; Kern, S. E. "A Novel Histone Deacetylase Inhibitor Identified by High-Throughput Transcriptional Screening of a Compound Library," *Cancer Res.* **2000**, *60*, 3137-3142.

18. Richon, V. M.; Emiliani, S.; Verdin, E.; Webb, Y.; Breslow, R.; Rifkind, R. A.; Marks, P. A. "A Class of Hybrid Polar Inducers of Transformed Cell Differentiation Inhibits Histone Deacetylases," *Proc. Natl. Acad. Sci. USA,* **1998**, *95*, 3003-3007.

19. Marks, P. A.; Richon, V. M.; Breslow, R.; Rifkind, R. A. "Histone Deacetylase Inhibitors as New Cancer Drugs," *Curr. Opin. Onc.* **2001**, *13*, 477-483.

20. Remiszewski, S. W.; Sambucetti, L. C.; Atadja, P.; Bair, K. W.; Cornell, W. D.; Green, M. A.; Howell, K. L.; Jung, M.; Kwon, P.; Trogani, N.; Walker, H. "Inhibitors of Human Histone Deacetylase: Synthesis and Enzyme and Cellular Activity of Straight Chain Hydroxamates," *J. Med. Chem.* **2002**, *45*, 753-757.

21. Sternson, S. M.; Wong, J. C.; Grozinger, C. M.; Schreiber, S. L. "Synthesis of 7200 Small Molecules Based on a Substructural Analysis of the Histone Deacetylase Inhibitors Trichostatin and Trapoxin," *Org. Lett.* **2001**, *3*, 4239-4242.

22. Grozinger, C. M.; Schreiber, S. L. "Deacetylase Enzymes: Biological Functions and the Use of Small-Molecular Inhibitors," *Chem. Biol.* **2002**, *9*, 3-16.

23. Hu, J.; Miller, M. J. "A New Method for the Synthesis of N^ε-Acetyl-N^ε-hydroxy-L-lysine, the Iron-Binding Constituent of Several Important Siderophores," *J. Org. Chem.* **1994**, *59*, 4858-4861.

24. For an early related approach, see; Naegeli, H.-U.; Keller-Schierlein, W. "Stoffwechselprodukte von Mikroorganismen 174. Mitteilung, Eine neue Synthese des Ferrichroms; *enantio*-Ferrichrom," *Helv. Chim. Acta.* **1978**, *61*, 2088-2094.

25. Hu, J. H.; Miller, M. J. "Total Synthesis of a Mycobactin S, a Siderophore and Growth Promoter of *Mycobacterium Smegmatis*, and Determination of its Growth Inhibitory Activity against *Mycobacterium tuberculosis*" *J. Am. Chem. Soc.* **1997**, *119*, 3462-3468.

26. Xu, Y.; Miller, M. J. "Total Syntheses of Mycobactin Analogues as Potent Antimycobacterial Agents Using a Minimal Protecting Group Strategy," *J. Org. Chem.* **1998**, *63*, 4314-4322.

27. Yokokawa, F.; Izumi, K.; Omata, J.; Shioiri, T. "Total Synthesis of Amamistatin A, an Antiproliferative Linear Peptide from an Actinomycete" *Tetrahedron* **2000**, *56*, 3027-3034.

Improved Methods of Mearsuring the Efficacy of Anticancer Drugs in Early Stages of Treatment

Bradley D. Smith, Ph.D.

Abstract

The appearance of phosphatidylserine (PS) on the cell surface is a hallmark of the intermediate stages of cell apoptosis. A fluorescent sensor for PS appearance is an attractive apoptosis detection strategy that has the potential to improve the treatment of cancer patients by allowing rapid, objective, patient-by-patient assessment of the efficacy of tumor cell killing. At present, the best method of detecting externalized PS is to use the dye-labeled protein, Annexin V, which has a strong affinity for PS. However, Annexin V has a number of limitations, and a low-molecular-weight, synthetic substitute is needed. A series of dye-labeled, organozinc compounds will be prepared and evaluated for their abilities to detect the appearance of PS on the surface of apoptotic cells. Flow cytometry will be used to compare their PS-detection abilities with Annexin V, the naturally occurring peripheral protein that is currently employed. The goal of this proposal is to find a synthetic PS-sensor that can replace Annexin V and provide a measure of apoptotic index for heterogeneous samples such as blood, spleen, lymph nodes and bone marrow.

INTRODUCTION

A wide variety of chemotherapeutic agents exert their effect by inducing cell apoptosis and necrosis. Resistance to anticancer treatment is widely believed to involve mutations that lead to deregulated cell-proliferation and suppression of mechanisms that control apoptosis. Serial biopsies in breast cancer patients indicate that response to therapy correlates with early post-treatment increases in tumor apoptotic index. However, an appropriate method for early detection of apoptosis, that is clinically applicable to peripheral blood and tissue samples freshly obtained from cancer patients, has not yet been established. The appearance of phosphatidylserine (PS) on the cell surface is a hallmark of the intermediate stages of cell apoptosis and can be detected before morphological changes can be observed. A fluorescent sensor for PS appearance is an attractive apoptosis detection strategy that has the potential to improve the treatment of cancer patients by allowing rapid, objective, patient-by-patient assessment of the efficacy of tumor cell killing. At present, the best method of detecting externalized PS is to use the dye-labeled protein, Annexin V, which has a strong affinity for PS. However, Annexin V has a number of limitations, and a low-molecular-weight, synthetic substitute is needed. A series of dye-labeled, organozinc compounds will be prepared and evaluated for their abilities to detect the appearance of PS on the surface of apoptotic cells. Flow cytometry will be used to compare their PS-detection abilities with Annexin V, the naturally occurring peripheral protein that is currently employed. The goal of this proposal is to find a synthetic PS-sensor that can replace Annexin V and provide a measure of apoptotic index for heterogeneous samples such as blood, spleen, lymph nodes and bone marrow.

BODY

Our initial studies in year 1 with PSS-380 (compound **2** in original proposal) used a fluorophore with non-optimal properties,[1] but the work produced important structural information which has led us in year 2 to develop the modular, three component design shown in Scheme 1.[2]
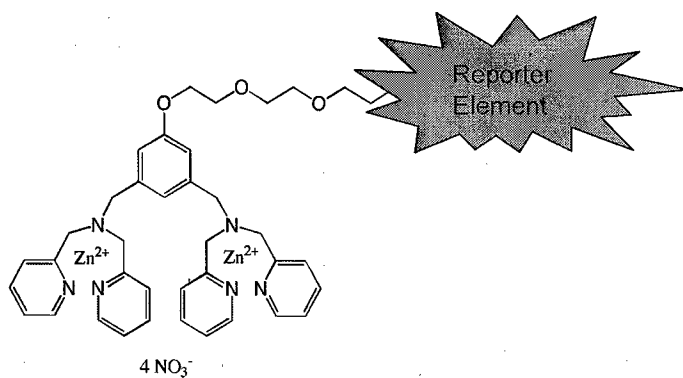
Scheme 1

Shown below are three examples of this design PSS-480, PSS-biotin, and PSS-greenQD.[3] Each is capable of detecting the appearance of phosphatidylserine on the membrane surface of apoptotic cells (Jurkat, CHO, HeLa). In the case of PSS-greenQD the CdSe/CdS quantum dot is a probe suitable for prolonged observation without photobleaching. Apoptosis can be detected under a wide variety of conditions, including variations in temperature, incubation time, and binding media. Binding of each sensor appears to be restricted to the cell membrane exterior, because no staining of organelles or internal membranes is observed.

4 NO$_3^-$

R =

PSS-480

R =

PSS-Biotin

PSS-green QD
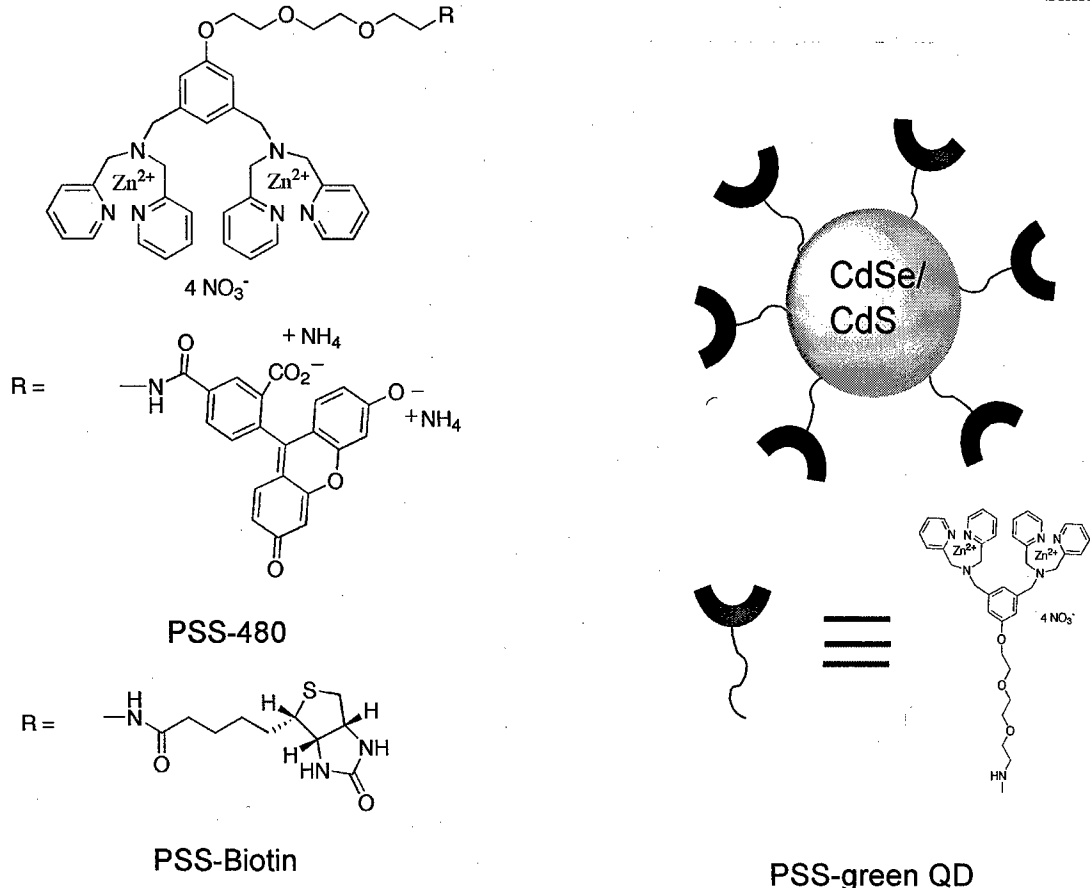
The utility of PSS-480 in flow cytometry was demonstrated using a population of Jurkat cells treated with camptothecin (10 μM, 16 h) to induce apoptosis. The histograms in Figure 1 indicate that approximately 30% of the cells were stained with PSS-480, while less than 5% of the cells were stained by 7AAD (the necrotic subpopulation). With untreated cells, less than 5% of the total population was stained with PSS-480 and 7AAD.

Another application of this sensing technology is to produce assays for screening of compounds that have potential anticancer activity (Figure 2). Thus, a series of three Zn2+-dipicolylamine coordination compounds were developed to bind selectively to membranes containing phosphatidylserine and act as a colorimetric chemosensing ensemble when combined with the UV-visible indictor pyrocatechol violet.[4] A similar displacement assay uses a coumarin methylsulfonate derivative as a fluorescent indicator, and a third assay involves quenching of calcein fluorescence by Cu2+ and subsequent fluorescence restoration upon addition of phosphatidylserine. In the best case, vesicle membranes containing as little as 5% phosphatidylserine could be detected under physiologically relevant conditions using as little as 10 μM sensing ensemble, and two of the three systems allow vesicles containing 50% phosphatidylserine to be detected by the naked eye.
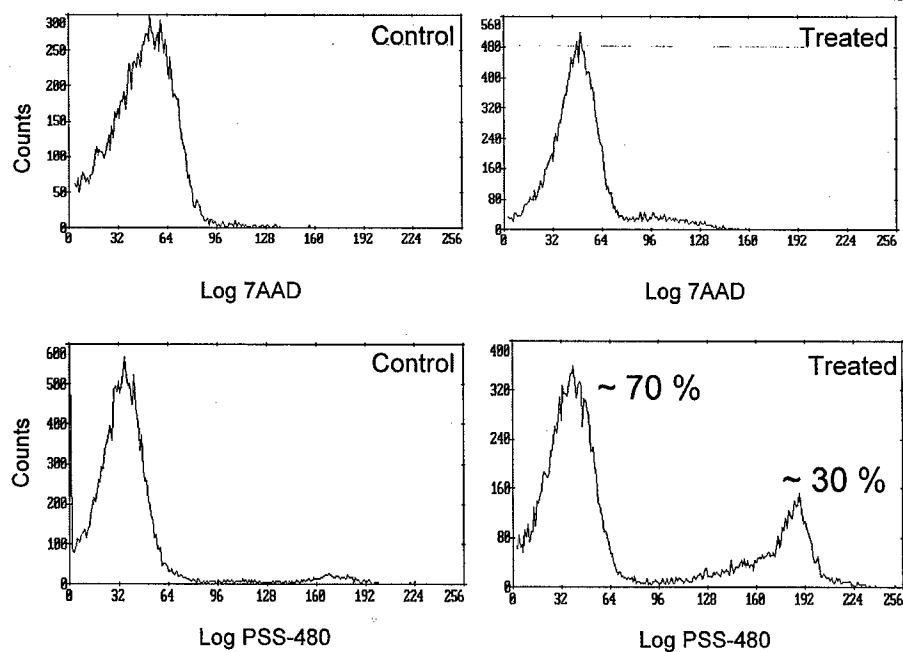
Figure 1: Flow cytometry histograms illustrating staining of Jurkat cells by PSS-480 and 7AAD. Control cells (top and bottom left) and treated cells (top and bottom right) exhibit similar levels of staining by 7AAD, indicating the same level of necrotic cells in the population (less than 5% in each case). Cells treated with camptothecin exhibit significantly more staining by PSS-480 than do control cells. Approximately 30% of treated cells were identified as apoptotic using PSS-480, while less than 5% of the untreated cells were stained with PSS-480. Nearly identical percentages of apoptotic cells were identified in each group using annexin V-FITC (data not shown).
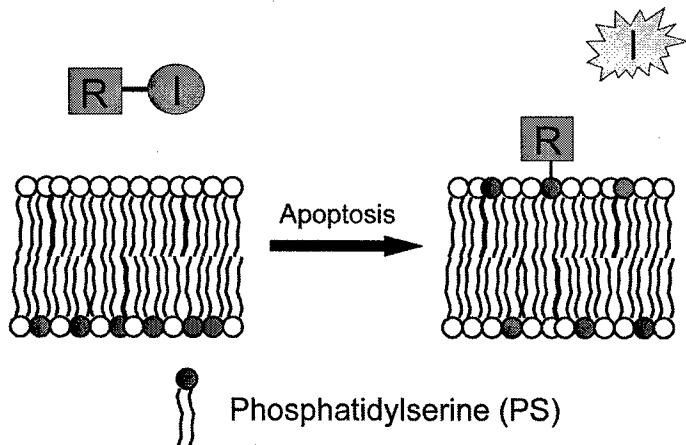
Figure 2: Displacement assay for apoptosis: Following phosphatidylserine externalization to the outer membrane monolayer, the indictor (I) is displaced from the receptor-indicator complex (R-I) by the phosphatidylserine headgroup, generating a detectable signal by restoration of the spectral properties of the indicator.

KEY RESEARCH ACCOMPLISHMENTS (year 2)

Showed that second generation sensing compound called PSS-480 is excellent sensor of cell apoptosis.
Showed that second generation sensing compound called PSS-biotin is excellent sensor of cell apoptosis.
Showed that second generation sensing compound called PSS-greenQD is excellent sensor of cell apoptosis.
Developed a new indicator displacement assay for screening of chemical agents that may have anticancer activity.

REPORTABLE OUTCOMES

Publications

1) Fluorophore Linked Zinc (II) Dipicolylamine Coordination Complexes as Sensors for Phosphatidylserine Containing Membranes. Lakshmi, C. Hanshaw, R. G.; Smith, B. D. *Tetrahedron*, 2004, *60*, 11307-11315.

Presentations

1)   Smith, B. D., "Chemical agents that sense and influence biomembrane function", Bowling Green University, October 2004.

2)   Smith, B. D., "Chemical agents that sense and influence biomembrane function", University of Maryland, November 2004.

3)   Smith, B. D., "Chemical agents that sense and influence biomembrane function", NIST, Washington DC, November 2004.

4)   Smith, B. D., "Chemical agents that sense and influence biomembrane function", NYU, March 2005.

5)   Smith, B. D., "Chemical agents that sense and influence biomembrane function", Washington University, St Louis, March 2005.

Sensor Distribution

6)   Free samples of PSS-380 and PSS-480 have been distributed to approximately ten academic research laboratories around the world.

CONCLUSIONS

Three sensors were developed to detect externalized PS, namely, PSS-480, PSS-biotin, and PSS-greenQD. Each is capable of detecting the appearance of phosphatidylserine on the membrane surface of apoptotic cells (Jurkat, CHO, HeLa). In the case of PSS-greenQD the CdSe/CdS quantum dot is a probe suitable for prolonged observation without photobleaching. Apoptosis can be detected under a wide variety of conditions, including variations in temperature, incubation time, and binding media. Binding of each sensor appears to be restricted to the cell membrane exterior, because no staining of organelles or internal membranes is observed. Another application of this sensing technology is to produce assays for screening of compounds that have potential anticancer activity. Thus, a series of three Zn2+-dipicolylamine coordination compounds were developed to bind selectively to membranes containing phosphatidylserine and act as a colorimetric or fluorescent chemosensing ensemble when combined with an appropriate dye.

REFERENCES

(1)   Detection of Apoptotic Cells using a Synthetic Fluorescent Sensor for Membrane Surfaces that Contain Phosphatidylserine. Koulov, A. V.; Stucker, K.;. Lakshmi, C.; Robinson, J. P.; Smith, B. D. *Cell Death Diff.* 2003, 10, 1357-1359.

(2)   Fluorophore Linked Zinc (II) Dipicolylamine Coordination Complexes as Sensors for Phosphatidylserine Containing Membranes. Lakshmi, C. Hanshaw, R. G.; Smith, B. D. *Tetrahedron*, 2004, 60, 11307-11315.

(3)   Fluorescent Detection of Apoptotic Cells using a Family of Zinc Coordination Complexes with a Selective Affinity for Membrane Surfaces that are Enriched with Phosphatidylserine. Hanshaw, R. G.; Lakshmi, C. Lambert, T. N.; Smith, B. D. *ChemBiochem.* In press.

(4)   Indicator Displacement Assays that Detect Bilayer Membranes Enriched in Phosphatidylserine. Hanshaw, R. G.; O'Neil, E. J.; Foley, M.; Carpenter, R. T.; Smith, B. D. J. Materials Chem. 2005, 15, (Advance Article) DOI: 10.1039/b500522a

Mechanism of Action of Nonsteroidal Anti-Inflammatory Drugs in the Prevention and Treatment of Colorectal Adenomatous Polyps

Francis J. Castellino, Ph.D.

Abstract

Individuals with familial adenomatous polyposis (FAP) have multiple intestinal adenomas that progress to colorectal carcinomas if left untreated. This syndrome is linked to germline mutations in the adenomatous polyposis coli (*APC*) gene. Clinical trials studying the effects of nonsteroidal anti-inflammatory drugs (NSAIDs) in FAP patients showed that sulindac and the selective cyclooxygenase-2 inhibitor, celecoxib, were effective at both inhibiting the growth of adenomatous polyps and causing regression of existing polyps. Mice heterozygous for a dominant mutation in the APC gene ($APC^{Min/+}$) are an experimental model of FAP and APC-related colorectal cancer. These mice develop spontaneous intestinal adenomatous polyps that progress to carcinomas. As in FAP patients, polyp formation in $APC^{Min/+}$ mice is dramatically reduced by treatment with NSAIDs. Despite promising experimental and clinical results, questions remain concerning the safety, efficacy, and mechanism of action of NSAID in the treatment of FAP and in the prevention of colorectal carcinomas.

This study proposes to use DNA microarray analyses to identify the biological pathways and individual molecules in normal intestine and adenomatous polyps of $APC^{Min/+}$ mice that are affected by NSAID treatment. The results of these studies will lead to new hypotheses regarding the mechanism of action of NSAID for polyp prevention/regression.

Subject Terms: NSAID, sulindac, adenomatous polyposis coli

Mechanism of action of nonsteroidal anti-inflammatory drugs in the prevention and treatment of colorectal adenomatous polyp

P.I. Francis J. Castellino, Ph.D.

Introduction

Individuals with familial adenomatous polyposis (FAP) have multiple intestinal adenomas that progress to colorectal carcinomas if left untreated. This syndrome is linked to germline mutations in the adenomatous polyposis coli (*APC*) gene (1). Clinical trials studying the effects of nonsteroidal anti-inflammatory drugs (NSAIDs) in FAP patients showed that sulindac and the selective cyclooxygenase-2 inhibitor, celecoxib, were effective at both inhibiting the growth of adenomatous polyps and causing regression of existing polyps (2,3). Mice heterozygous for a dominant mutation in the *APC* gene ($APC^{Min/+}$ mice) are an experimental model of FAP and APC-related colorectal cancer (4). These mice develop spontaneous intestinal adenomatous polyps that progress to carcinomas. As in FAP patients, polyp formation in $APC^{Min/+}$ mice is dramatically reduced by treatment with NSAIDs (5). Despite promising experimental and clinical results, questions remain concerning the safety, efficacy, and mechanism of action of NSAID in the treatment of FAP and in the prevention of colorectal carcinomas.

This study proposed to use DNA microarray analyses to identify the biological pathways and individual molecules in normal intestine and adenomatous polyps of $APC^{Min/+}$ mice that are affected by NSAID treatment. The results of these studies will lead to new hypotheses regarding the mechanism of action of NSAID for polyp prevention/regression.

Body

Sulindac, an NSAID drug, was administered to 80 day-old $APC^{Min/+}$ mice, in order to study the molecular changes that this COX-1/COX-2 inhibitor induces in the regulation of adenoma formation and growth.

As mentioned in the previous report, a 6 day treatment with sulindac (0.6mg sulindac / mouse / day in 2 x 0.5 mL doses) resulted in an unequivocal reduction in tumor burden (Fig. 1). In order to be able to follow the molecular response induced by this NSAID, tumor tissue was collected after 2 days of treatment and RNA isolated from cells which were captured from frozen sections by laser capture microdissection. Six wild type (*WT*) mice were administered vehicle only, 7 $APC^{Min/+}$ mice were administered vehicle only, and 9 $APC^{Min/+}$ mice were administered sulindac at the above designated dose.

From each experimental group, 3 samples have been isolated, amplified, and profiled. The genechips used (Affymetrix, Mouse Expression Array 430A) have been analyzed in a 3 x 3 matrix using the Affymetrix (GCOS) software (Fig. 2). Nine transcripts were found to have been significantly upregulated, while 7 were significantly downregulated relative to vehicle-treated $APC^{Min/+}$ mice (Table 1 and 2).

APC$^{(Min/+)}$: Sulindac and Tumor Number

p = 0.001

Untreated   Sulindac

Condition
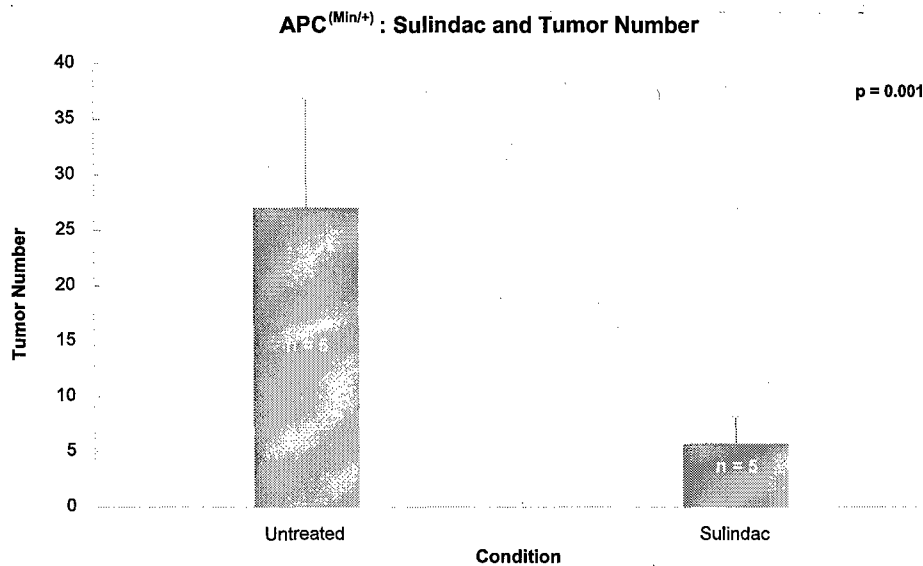
Fig. 1. Tumor burden in 80 day old $APC^{Min/+}$ mice treated with sulindac (n-5) or vehicle alone (n=5).

Vehicle   Sulindac
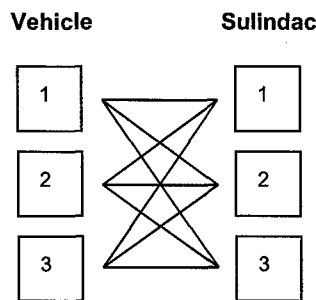
Fig. 2. 3x3 matrix analysis for data comparison between the different treated groups.

Two of the 9 genes that were upregulated were Cdx2 and Col1a2 (Table 1). Cdx2 is a transcription factor involved in intestinal development, differentiation, and homeostasis (6). It has a wide range of targets, such as enzymes associated with tumor suppression and E2F transcription factors utilized for apoptosis and DNA repair. Recently it has been shown that its' homologue Cdx1 reduces beta-catenin/T-cell factor transcriptional activity and ultimately results in inhibition of human colon cancer cell proliferation (7). Col1a2, is a protein responsible for cell adhesion and defense responses and is very likely involved in arresting tumor proliferation. DNA hypermethylation of this gene near the transcription start site has been found to occur in primary colorectal cancers (8). Additionally, genes associated with ubiquitin-mediated protein degradation are also upregulated.

Two of the 7 genes downregulated were neuronal pentraxin 2 and cyclin D2 (Table 2.), Neuronal pentraxin 2 forms a complex with a calcium binding protein, and therefore could be associated with regulating Ca^{2+} transport (9). Cyclin D2 plays a role in the proliferative decline of aged CD4 T(+) cells (10).

Table1. Upregulated Gene List of APC$^{(Min/+)}$ mice after 2 days of treatment with sulindac

Gene	Fold Change	Symbol	Gene Ontology
ADAM-like, decysin 1	2.6	Adamdec1	integrin-mediated signaling pathway proteolysis and peptidolysis
caudal type homeo box 2	1.8	Cdx2	Development pattern specification regulation of transcription DNA-dependent
procollagen, type I, alpha 2	2.0	Col1a2	cell adhesion, phosphate transport
C-type lectin related f	2.9	Clrf	cellular defense response
ribonuclease L (2', 5'-oligoisoadenylate synthetase-dependent)	2.1	Rnasel	protein amino acid phosphorylation
interferon activated gene 203	2.1	Ifi203	immune response
lysosomal-associated protein transmembrane 5	1.9	Laptm5	
D site albumin promoter binding protein	1.6	Dbp	circadian rhythm regulation of transcription, DNA-dependent
phospholipase C, beta 3	1.4	Plcb3	intracellular signaling cascade lipid catabolism lipid metabolism, signal transduction

Table 2. Downregulated Gene List of APC$^{(Min/+)}$ mice after 2 days of treatment with sulindac

Gene	Fold Change	Symbol	Gene Ontology
regenerating islet-derived family, member 4	-2.4	Reg4	
deiodinase, iodothyronine, type II	-3.1	Dio2	thyroid hormone catabolism
serine (or cysteine) proteinase inhibitor, clade A, member 3N	-4.3	Serpina3n	
neuronal pentraxin 2	-2.5	Nptx2	
RIKEN cDNA 2610312B22 gene	-1.3	2610312B22Rik	cytokine and chemokine mediated signaling pathway
cyclin D2	-1.4	Ccnd2	cell cycle cytokinesis, regulation of cell cycle
hypoxia inducible factor 1, alpha subunit	-1.8	Hif1a	Angiogenesis, cell differentiation, regulation of transcription DNA-dependent, response to hypoxia signal transduction

Valuable preliminary data is already being obtained in this study. However, more replicates are needed in order to achieve statistical validity. The ultimate goal is to have 6 replicates from each group and to perform data mining utilizing different approaches (GCOS and GeneSpring) in order to achieve reliable and clinically relevant results. Once conclusive results are obtained, a more detailed study of the gene ontology and pathways will be performed.

Key Research Accomplishments

● Three samples from sulindac-treated or vehicle alone-treated *APC$^{Min/+}$* mice have been processed and applied to gene chips.

● Initial data mining on these samples have identified a number of gene expression differences between these two groups.

Reportable Outcome

Too early to report findings. Need data from other replicates.

Conclusions

Results from these studies indicate that NSAIDs, such as sulindac, can attenuate the growth of adenomas in $APC^{Min/+}$ mice that mimics their effect in the clinical setting. Therefore, the $APC^{Min/+}$ model is an appropriate model to determine effects on gene profile of these tumors in response to treatment. RNA samples have een obtained from 3 vehicle- and 3 sulindac-treated $APC^{Min/+}$ mice and gene profiling have identified differences in the genetic signatures of these mice.

References

1. Nakamura, Y., Nishisho, I., Kinzler, K.W., Vogelstein, B., Miyoshi, Y., Miki, Y., Ando, H., Horii, A., Nagase, H. (1991). Mutations of the adenomatous polyposis coli gene in familial polyposis coli patients and sporadic colorectal tumors. *Princess Takamatsu Symp.* 22:285-292.

2. Giadiello, F.M., Hamilton, S.R., Krush, A.J., Piantadosi, S., Hylind, L.M., Celano, P., Booker, S.V., Robinson, C.R., Offerhaus, G.J. (1993). Treatment of colonic and rectal adenomas with sulindac in familial adenomatous polyposis. *N. Engl. J. Med.* 328:1313-1316.

3. Nugent, K.P., Farmer, K.C., Spigelman, A.D., Williams, C.B., Phillips, R.K. (1993). Randomized controlled trial of the effect of sulindac on duodenal and rectal polyposis and cell proliferation in patients with familial adenomatosis polyposis. *Br. J. Surg.* 80:1618-1619.

4. Steinbach, G., Lynch, P.M., Phillips, R.K., Wallace, M.H., Hawk, E., Gordon, G.B., Wakabayashi, N., Saunders, B., Shen, Y., Fujimura, T., Su, L.K., Levin, B. (2000). The effect of celecoxib, a cyclooxygenase-2 inhibitor, in familial adenomatosis polyposis. *N. Engl. J. Med.* 342:1946-1952.

5. Fodde, R., Edelmann, W., Yang, K., van Leeuwan, C., Carlson, C., Renault, B., Breukel, C., Alt, E., Lipkin, M., Khan, P.M., Kucherlapati, R. (1994). A targeted chain-termination mutation in the mouse Apc gene results in multiple intestinal tumors. *Proc. Natl. Acad. Sci. USA* 91:8969-8973.

6. Guo, R-J., Suh, E.R., Lynch, J.P. (2004). The role of Cdx proteins in intestinal development and cancer. *Cancer Biol.* 3:593-601.

7. Guo, R.J., Huang, E., Ezaki, T., Patel, N., Sinclair, K., Wu, J., Klein, P., Suh, E.R., Lynch, J.P. (2004). Cdx1 inhibits human colon cancer cell proliferation by reducing beta-catenin/T-cell factor transcriptional activity. *J. Biol. Chem.* 279:36865-36875.

8. Sengupta P.K., Smith, E.M., Kim, K., Murnane, M.J., Smith, B.D. (2003). DNA hypermethylation near the transcription start site of collagen alpha2(I) gene occurs in both cancer cell lines and primary colorectal cancers. *Cancer Res.* 63:1789-1797.

9. Kirkpatrick, L.L., Matzuk, M.M., Dodds, D.C., Perin, M.S. (2000). Biochemical interactions of the neuronal pentraxins. Neuronal pentraxin (NP) receptor binds to taipoxin and taipoxin-associated calcium-binding protein 49 via NP1 and NP2. *J. Biol. Chem.* 275:17786-17792.

10. Hale, T.J., Richardson, B.C., Sweet, L.I., McElligott, D.L., Riggs, J.E., Chu, E.B., Glynn, J.M., LaFrenz, D., Ernst, D.N., Rochford, R., Hobbs, M.V. (2002). Age-related changes in mature CD4+ T cells: cell cycle analysis. *Cell. Immunol.* 220:51-62.

Macrolides as Potential Anticancer Drugs

Rudolph M. Navari, Ph.D., M.D.
Vincent Jo Davisson, Ph.D.
Martin Tenniswood, Ph.D.
Paul Helquist, Ph.D.

Abstract

The iejimalides are naturally occurring macrolides isolated in very small quantities (0.0003% wet weight) from a marine tunicate, *Eudistoma* cf. *rigida*, found near Okinawa, Japan. The current studies have confirmed the high potency of these compounds in inhibiting the growth of over 60 cancer cell lines, in many cases at nanomolar concentrations. Cell cycle studies demonstrate that the iejimalides promote S phase arrest. A preliminary study of acute toxicity has been conducted in mice. Comparison of activity profiles with over 30,000 other known anticancer compounds show limited indications of correlation with previously established mechanisms of action. Derivatives of the iejimalides have been obtained by reaction of their serine subunit hydroxy groups with functionalized isocyanates to produce carbamate derivatives that retain significant levels of activity. These derivatives have been employed in cellular target identification studies employing fluorescent and affinity labeled side chains. No effect has been seen on microtubule structure. The first total synthesis of the iejimalides is nearly complete. All of the subunits of the revised structure of the iejimalides have been obtained by synthetic methods, and their assembly into the intact iejimalide system is in progress.

MARINE MACROLIDES AS POTENTIAL ANTICANCER DRUGS

Vincent Jo Davisson, Martin Tenniswood, and Paul Helquist

1. INTRODUCTION

Extraction of *Eudistoma* cf. *rigida*, a tunicate or sea slug found near Okinawa, Japan, affords four macrolides known as iejimalides A-D. They are very rare compounds that were first reported by the laboratory Professor Junichi Kobayashi. In the first papers on these compounds, the structures **1-4** (Figure 1) were described along with potent activity against a few standard cancer cell lines.[i,ii] In much later studies, the Kobayashi laboratory presented a revised structure for iejimalide B as **2b**.[iii] Consequently, a working hypothesis is that the entire set of four iejimalides may be represented with structures **2a-d** (Figure 2). Note that the two sets of structures differ in the configuration of C(13)-C(14) alkene double bond. Also, whereas the configurations of the five stereogenic centers at C(4), C(9), C(17), C(22), and C(23) had not been assigned in the original studies, they were assigned for **2b**.

1a lejimalide A : $R^1 = R^2 = H$
1b lejimalide B : $R^1 = CH_3$, $R^2 = H$
1c lejimalide C : $R^1 = H$, $R^2 = SO_3Na$
1d lejimalide D : $R^1 = CH_3$, $R^2 = SO_3Na$
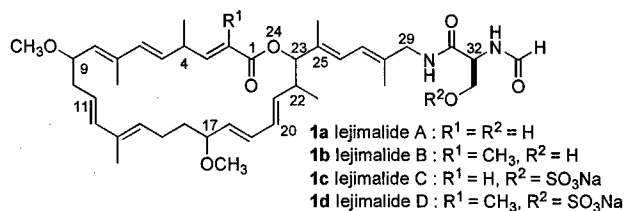
Figure 1. Originally assigned structures of the iejimalides

2a lejimalide A: $R_1 = R_2 = H$
2b lejimalide B: $R_1 = CH_3$, $R_2 = H$
2c lejimalide C: $R_1 = H$, $R_2 = SO_3Na$
2d lejimalide D: $R_1 = CH_3$, $R_2 = SO_3Na$
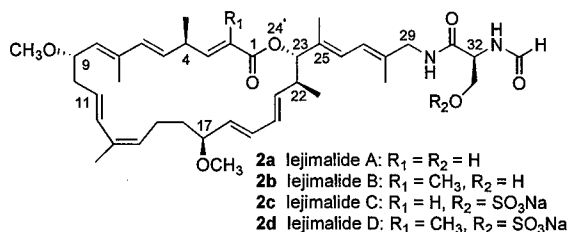
Figure 2. Revised structures of the iejimalides

The cancer cell data reported by the Kobayashi laboratory showed IC_{50} values as low as 1 ng/mL for the iejimalides, which suggested that these compounds could be investigated as possible anticancer agents. However, the earlier investigators did not provide the further types of data required for moving ahead with drug development studies. Nothing was known about cell line selectivity, cellular targets, and mechanism of action. Furthermore, the natural source of the iejimalides was much too limited to provide useful quantities for detailed investigations. Therefore, an alternative source of material was needed, namely in the form of a laboratory synthesis that would provide not only the iejimalides themselves but also appropriate analogues.

2. BODY

Our principal approved tasks include the following:
(1) Investigation of Cellular Activity;

(2) Efforts Toward Completion and Improvement of the Total Synthesis of the Iejimalides;

(3) Synthesis of Fluorescent and Immobilized Derivatives; and

(4) Identification of Cellular Targets.

We have summarized our progress for each of these tasks in the following sections.

1. Investigation of Cellular Activity. Our studies of activity are performed on samples of the naturally occurring iejimalides A and B isolated from the tunicate, *Eudistoma* cf. *rigida* collected near Okinawa, Japan. We do not isolate or study iejimalides C and D since they are significantly less active that the A and B compounds.

In a collaboration with Professors Tatsuo Higa and Junichi Tanaka, we have now made four collections of these compounds. The most recent collection was made in September, 2004. Although we harvest several kilograms of the organism during each trip, the low abundance of the iejimalides results in the isolation of only approximately 10 mgs of these compounds. This short supply of material will persist until a total synthesis has been completed in the laboratory.

In our annual report of April 2004, we summarized the results of activity studies in some 70 cell lines conducted in several laboratories, including those of the National Cancer Institute, Professor George R. Pettit at Arizona State University, Professor Martin P. Tenniswood at the University of Notre Dame, and Professor V. Jo Davisson at Purdue University. Iejimalide B is uniformly an order of magnitude more potent than iejimalide A. IC_{50} values for iejimalide B in the low nM range were seen in several cancer cell lines. Large differences in cell line responses were seen among the TGI values. Especially pronounced was the sensitivity of a colon cancer cell line. Very few cell lines show LC_{50} values below 100μM (micromolar).

Due to the very small quantities of the natural iejimalides that are available, detailed studies of acute toxicity have not been performed. However, in order to obtain preliminary indications of safe dosage levels for use in later animal tumor models, a very limited study was conducted to determine the *no observed effect level* (NOEL) of iejimalide A in mice in the Notre Dame animal facility. Two independent studies were conducted with 16 mice each, including controls. The mice (4 per group) were given a single intravenous dose by direct injection into the tail vein at doses of 0, 0.5, 1.0, and 2.0 mg/kg, observed for three days, and euthanized, and their organs were collected for histological analysis. No clinical or histopathological toxicity was seen at a dosage of 0.5 mg/kg of iejimalide A. The liver, kidneys, and brains were all normal. Mild subcutaneous edema, hemorrhage, and inflammation were seen at the site of injection. These effects were more severe at the higher dosage levels. More complete studies of toxicity will be performed upon availability of larger quantities of material.

Iejimalide B produces marked effects on the growth of PC-3 cells in a time and dose dependent manner (Figure 3). At doses of 10nM and above, iejimalide B shows a dramatic

Figure 3. Time Course and Dose Response of PC-3 Prostate Cancer Cells to Iejimalide B. PC-3 cells were plated in Gc medium in 96 well plates and incubated for the indicated time in the presence of increasing concentrations of Iejimalide B, administered once at time zero. Cell number was monitored using the crystal violet assay. Each time point is analyzed in triplicate. The experiment has been independently replicated three times.
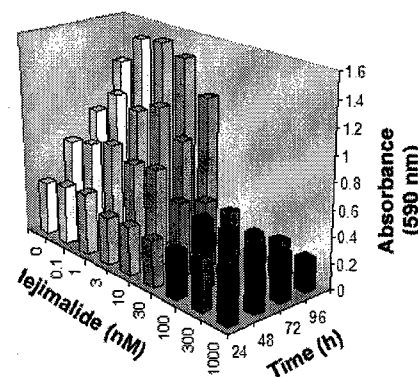
suppression of the growth of PC-3, but even at doses as high as 1mM (micromolar), it does not appear to be toxic to the cells. The effect of a single administration of the drug at the start of the experiment is sufficient to block the increase of cell number for at least 96 hours, implying that the drug is not rapidly metabolized in this cell line.

Using flow cytometry, we have analyzed the effect of Iejimalide B on cell cycle kinetics and apoptosis in PC-3 cells using multicycle analysis (M-plus). As shown in Table 1, iejimalide B has very dramatic effects on the cell cycle in causing a dose-dependent increase in the percentage of cells in S and G2/M phase, and a corresponding decrease in the proportion of the cells in G0/G1. Examination of the effects of iejimalide B on apoptosis in PC-3 cells, either by analysis of the sub G0 fraction after PI staining or by apo-BrdU analysis, suggests that iejimalide B does not induce apoptosis in this cell line.

Table 1. Effect of Iejimalide B on cell cycle kinetics and apoptosis in PC-3 cells after 48 hours of treatment

Treatment	sub Go	G1	S	G2/M	> 4N
Untreated	0.06	60.6	28.9	13.5	0
30nM Iejimalide B	0.22	47.4	40.9	1.7	10.7
300nM Iejimalide B	N.D.	51.6	26.2	15.7	18.7

The effect of iejimalide B on PC-3 cells suggests that the cells are arresting during S phase and that the transition through mitosis is being disrupted, as evidenced by the increase in the proportion of the cells in G2/M and the appearance of a significant proportion of the cells that are greater than 4N. Despite this obvious disruption, there is no evidence of apoptosis after treatment with iejimalide B (even at concentrations as high as 300nM), or at longer times of incubation (data not shown).

2. Efforts Toward Completion and Improvement of the Total Synthesis of the Iejimalides. An earlier co-worker in the Helquist laboratory, Dr. John Kane, had nearly completed a synthesis of the iejimalides based upon targeting the gross structures **1** originally assigned by the Kobayashi laboratory. In the course of this work, Dr. Kane and other co-workers had synthesized the C(1)-C(11),[iv] C(12)-C(20),[v] and C(21)-C(29)[vi] subunits in enantiopure form, and Dr. Kane had accomplished the coupling of the C(1)-C(11) and C(12)-C(20) subunits. However, very late in Dr. Kane's studies, Kobayashi published a revision of the structure, complete with assignment of all of the stereogenic centers as depicted by **2** above. This revision forced a partial reworking of the total synthesis, which has been pursued by more recent and current co-workers.

We described in the April 2004 report that one co-worker had succeeded in synthesizing the C(12)-C(19) subunit. However, during the current reporting period, other co-workers, Dr. Dirk Schweitzer and Mr. Daniel Strand, have developed superior syntheses of this subunit in the form of alkynal **5** (Scheme 1). The key step is the adaptation of the Carreira enantioselective alkynylation[vii] procedure to the aldehyde **3** to give the propargylic alcohol **4**. An alternative alkynylation method developed by Jiang has also been applied.[viii] Other methods that we have

Scheme 1
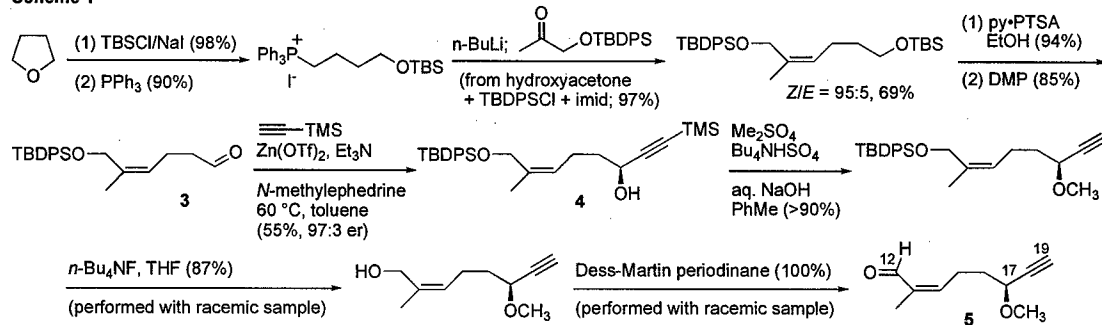
successfully employed for control of the C(17) stereogenic center have been preparation of the alcohol **4** in racemic form followed either by kinetic enzymatic resolution with a commercial lipase[ix] or oxidation to the ketone followed by a Noyori[x] or an Alpine[xi] enantioselective ketone reduction. We are presently investigating the application of a dynamic kinetic resolution procedure employing a dual organometallic/enzymatic catalytic system.[xii]

Building upon results from our April 2004 report, we have now completed the synthesis of the entire C(20)-C(34) subunit **13**, which provides the right-hand portion of the macrolide ring and the entire side chain, terminating in the *N*-formyl serine residue of the iejimalides (Scheme 2).[xiii] The diene portion **8** was obtained by a Heck reaction of alkenyl bromide **6** and *N*-methallyl phthalimide **7** in a manner similar to the case that we have published earlier,[vi] followed by

Scheme 2
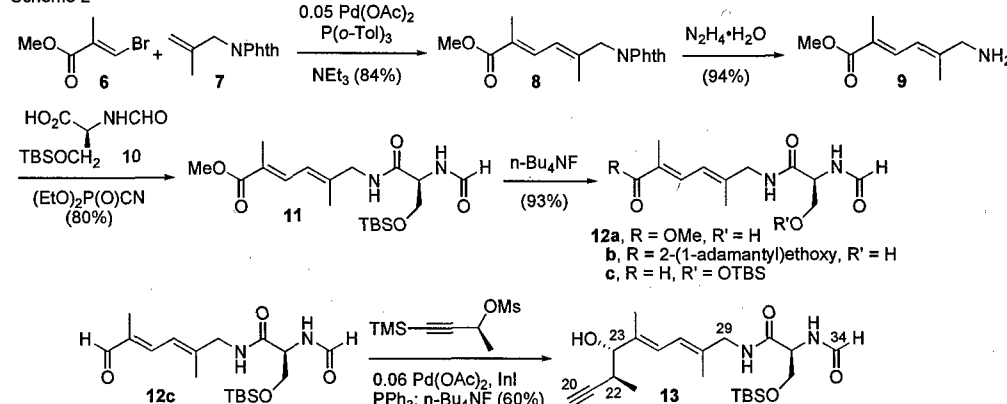
removal of the phthaloyl group to give the free amine **9**. Coupling with the serine derivative **10** that we describe in our April 2004 report and removal of the silyl protecting group then gave the C(23)-C(34) side chain **12a** of the iejimalides for the first time. By a slight modification of this route, the aldehyde **12c** was also obtained. This aldehyde was subjected to an asymmetric Marshall propargylation reaction.[xiv] The resulting alkyne **13** will next be employed in a hydrozirconation/iodination[xv] to elaborate this C(20)-C(34) subunit into the form of an alkenyl iodide that is required for coupling with the C(1)-C(19) subunit. Compatibility of the hydrozirconation with the diene subunit is well-precedented.[xvb]

The methyl ester **12a** was assayed for PC-3 cell growth inhibition, but no effect was seen for this very small fragment of the overall iejimalide structure. Likewise, the 2-(1-adamantyl)ethyl ester derivative **12b** was prepared to mimic the macrolide portion of the iejimalides, but again it was inactive. Other, more substantial subunits will be assayed systematically as the rest of the synthesis is pursued towards completion.

The total synthesis of the iejimalides is at a highly advanced stage of development. We have now performed a test coupling reaction of our previously reported C(1)-C(11) sulfone **14** with a racemic sample of alkynal **5** to afford the entire C(1)-C(19) subassembly in the form of **15**. With

Scheme 3
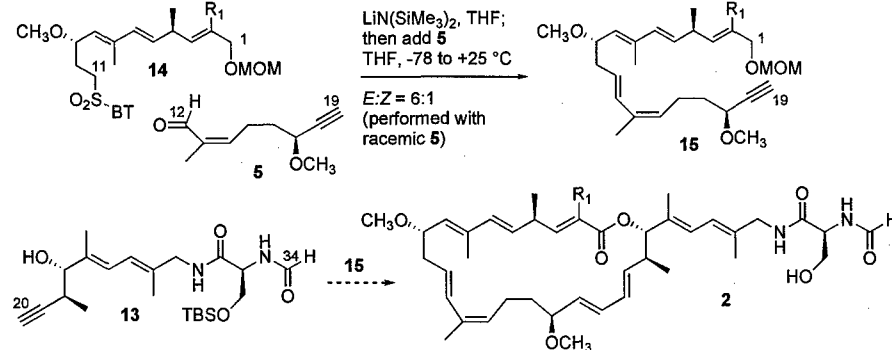
the major fragments **13** and **15** now available by efficient pathways, the goal of completing the first total synthesis of the iejimalides is ever closer (Scheme 3).

3. Synthesis of Fluorescent and Immobilized Derivatives. In order to obtain derivatives for cellular localization studies or for investigation of structure activity relationships, derivatives of the natural iejimalides must be obtained. However, the iejimalides have very few sites at which direct and selective derivatization can occur. The most accessible reactivity is provided by the hydroxy group of the serine subunit. We described in our April 2004 report the preparation of a series of ester and carbamate derivatives by reaction of acyl chlorides and isocyanates, respectively, with the serine hydroxy group. We had also demonstrated that this hydroxyl group

is a permissive site in that good activity was observed upon assaying some of these derivatives in the same cancer cell lines that have been employed with the natural iejimalides. The single most important compound that we obtained in these studies was the fluorescent coumarin derivative **16** (Scheme 4). It was found to retain potent activity as indicated by its IC_{50} of 20 nM in PC-3 prostate cancer cells.
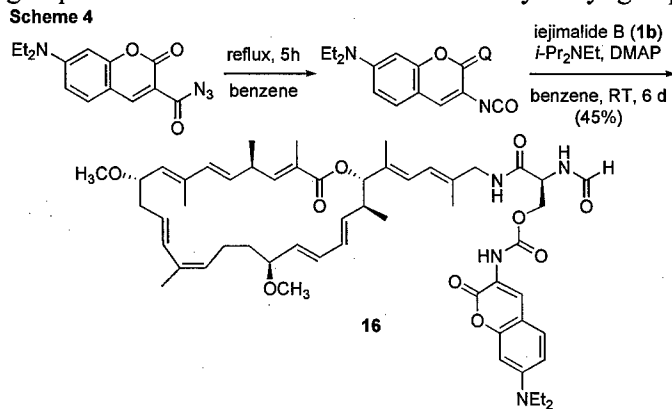
Scheme 4

Most recently, we have obtained the immobilized iejimalide derivatives **17** (Scheme 5) through use of a functionalized polystyrene resin having an isocyanate linker prepared in the

Davisson laboratory at Purdue University. This compound is currently being employed in affinity binding or "pulldown" assays of cellular binding sites. The cellular proteins that bind to this material will be identified by the Davison laboratory through use of mass spectrometry techniques. Therefore, the fluorescently labeled derivative **16** and the

Scheme 5

immobilized form **17** will provide very useful complements in identifying the localization of the iejimalides at both the cellular and molecular level.
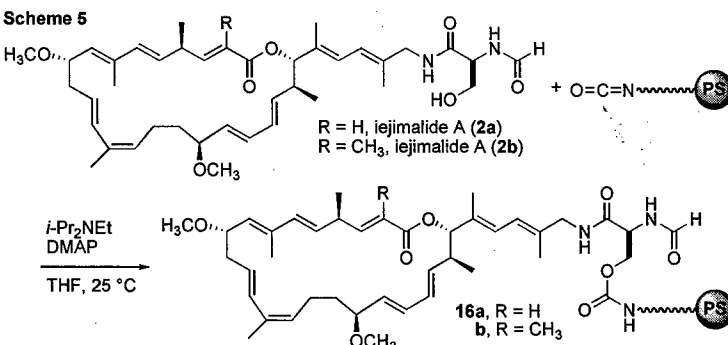
A key finding from this portion of our research is that the serine subunit provides a conveniently manipulated, permissive site for derivatization of the iejimalides without adversely affecting normal activity in some cell lines. This observation is useful for our cellular binding site identification studies, but it is also important for any future investigation of the iejimalides as lead compounds for cancer drug development. Derivatives will be needed to establish structure activity relationships, optimization of solubility and membrane transport properties, modification of metabolic pathways, development of possible prodrug forms, and attachment of ligands for selective drug delivery.

4. Identification of Cellular Targets. We described in our April 2004 report that, we had performed a COMPARE analysis[xvi] using the NCI cell data to probe for possible correlations of activity, cellular targets, and mechanisms of action of iejimalides A and B with other previously

studied compounds.[xvii] Fairly good correlations were found with destruxin B, podophyllotoxin, and a colchicine derivative (Figure 4). A few studies indicate that destruxin B is a specific, dose-dependent, and reversible inhibitor of vacuolar-type ATPase.[xviii] It is well-known that podophyllotoxin, colchicine, and their derivatives inhibit cell division by preventing the development of spindles as the nuclei are dividing. Podophyllotoxin and its derivatives (e.g. etoposide) are cytostatic, antimitotic agents that block the cell cycle at the G1 and S phases and induce apoptosis by a mechanism involving inhibition of microtubule assembly or inhibition of topoisomerase activity leading to DNA damage.[xix] Colchicine and its derivatives also block cell division by inhibiting microtubule polymerization required for the formation of spindles.[xx] A recent X-ray study of a tubulin-colchicine complex showed that colchicine binds at a location such that curved tubulin is not able to adopt the straight conformation that is required for microtubule assembly.[xxi] The results of the COMPARE analysis have therefore provided some suggestions of cellular targets and mechanisms to probe initially as possible modes of action for the iejimalides.

S236580
(Destruxin B)

S24818
(Podophyllotoxin)

S648784
(Colchicine derivative)
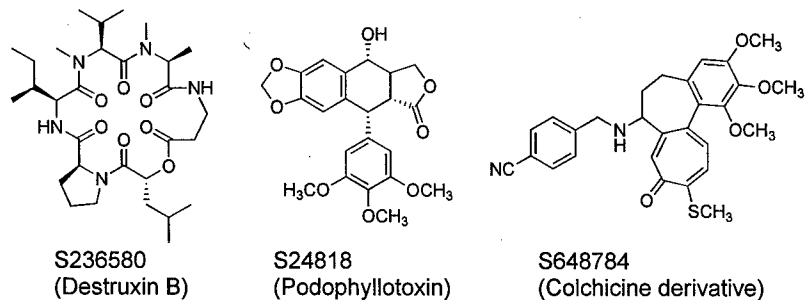
Figure 4. Compounds showing COMPARE correlations with iejimalides A and B

The Davisson laboratory at Purdue University has performed preliminary cellular studies of the coumarin derivative **16** in MCF-7 and PC-3 cells. Shown in Figure 5 is a set of confocal images of PC-3 cells treated with the iejimalide-coumarin conjugate **16** and with benzyl coumarin control (TOP). These images highlight the cellular localization of the redistribution of the coumarin dye specific to the iejimalide drug component. Tubulin staining of fixed PC-3 cells after treatment with either iejimalide B or paclitaxel also highlights the distinctions in the microtubule structures (BOTTOM). The microtubule structure is not disrupted in the iejimalide B treated PC-3 cells when compared to paclitaxel treated cells. Under these experimental conditions, a comparison cannot fully distinguish differences in the microtubule structures. However, the highly filamentous structure of microtubules leading outwards to the cell membrane is apparent in the iejimalide treated cells. It is clear that the iejimalide derivative has no strong effect on microtubule structure.
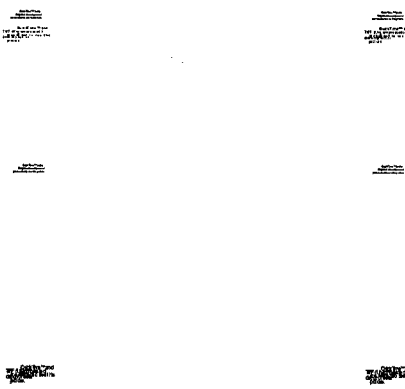
Figure 5. **TOP.** Confocal image of iejimalide B-coumarin **16** treated PC-3 cells (upper left) and PC-3 cells treated with the benzyl-coumarin standard (upper right). PC-3 cells were treated with either 200 nM iejimalide-coumarin **14** or 200 nM coumarin standard for 3 h and washed with PBS three times. Live cell images were obtained by confocal microscopy. Scale bar, 10mm. **BOTTOM.** Tubulin staining of fixed PC-3 cells treated with (A) 10 nM iejimalide B for 12 h (bottom left) and (B) 100 nM paclitaxel for 12 h (bottom right). Cells were treated with 10 nM iejimalide and 100 nM paclitaxel, respectively, for 12 h, and were then fixed and stained with mouse monoclonal anti microtubule antibody. Scale bar, 10 mm.

Possible, albeit speculative, explanations at this early point are that the iejimalide-coumarin conjugate binds to the nuclear end rather than the membrane end of the microtubules, to other proteins associated with microtubule formation, to the nuclear membrane, to the endoplasmic reticulum, or in the mitochondria. Preliminary comparison of the localization patterns of the iejimalide-coumarin conjugate **16** with localization patterns of mitochondrial tracking agents (not shown) show close similarities. For this preliminary study, PC3 cells were fixed with paraformaldehyde, stained with 200 nM iejimalide B-coumarin conjugate for 30 min, and washed with PBS three times. The resulting fluorescent images (Figure 6) resembles the distribution of mitochondria. Differential staining of iejimalide B-coumarin conjugate and mitrotracker will be done in both fixed cells and live cells to test the co-localization of the coumarin-conjugated drug with mitochondria. The actual binding site, whether it is in the mitochondria or elsewhere, must be determined in these and other further studies.

Figure 6. Localization of iejimalide B-coumarin **16** in PC-cells showing a pattern resembling mitochondrion distribution.

The Davisson laboratory has also obtained initial results using the immobilized iejimalide derivatives **17** in a pull-down assay. For this experiment, both iejimalide A and iejimalide B carbamates linked to polystyrene beads **17a** and **17b** were used, along with a methyl carbamate latex bead as a control. MCF7 cells were grown under normal conditions in DMEM F12 Ham's

media, supplemented with 10% fetal bovine serum, and harvested using trypsin-EDTA treatment to release the cells from their culture flasks. The cells were rinsed in Hank's saline solution and centrifuged, and the cell pellet was stored at -80 °C for later analysis.

For the cell lysis procedure, two buffers were prepared: a wash buffer, consisting of 50 mM Tris-HCl, pH 7.4, 100 mM NaCl, 1 mM EDTA and EGTA, with 0.5% nonionic detergent P40; and a non-denaturing lysis buffer is the same with the following detergent supplements: 1% deoxycholic acid, 0.1% SDS, 1% Triton X-100, and protease inhibitors: 1 ug/uL leupeptin, and the Halt protease inhibitor cocktail from Pierce. Six million MCF7 cells were lysed in 2 mL of lysis buffer, and lysis was allowed to proceed for 30 minutes on ice, and with gentle shaking. This lysate was then diluted 1:1 with wash buffer to a final volume of 4 mL. The total protein content was determined to be 0.4 mg/ml by a Bradford protein assay.

In a first experiment, 3 mg of control beads was weighed and suspended in 1 mL of water, followed by sonication to disperse the beads. This procedure of weighing a dried bead was challenging due to the static nature of the polystyrene beads relative to experimental handling with metal spatula, rubber gloves, and plastic sample vials. Therefore in the second experiment, the three latex bead conjugates were resuspended in their original vials with 1 mL of water and sonicated to disperse the beads. In the first experiment, the control beads were incubated with 1 mg of protein lysate, diluted at a 1:10 dilution with detergent-free wash buffer (rather than the 1:1 dilution described above).

In the second experiment, 80 uL of each bead suspension (i.e. 8% of the total bead preparation) were incubated with aliquots of 0.5 mg protein lysate, on ice with shaking overnight. The next day the samples were centrifuged (at 12 x g) for 2 minutes, and the supernatant was reserved. The pellet was then resuspended in detergent-free Tris-HCl wash buffer, centrifuged, and the wash was removed. The bead pellet was then resuspended in SDS loading buffer and heated at 96 C° for 10 min in preparation for one-dimensional SDS-PAGE analysis.

The SDS-PAGE gel (Figure 7) shows the results of three pull-downs. The gel was stained with silver stain according to the Schevchenko method. In lane 1 is a broad range protein ladder from Biorad, covering a molecular weight range of 7 to 209 kDa on this 4-20% acrylamide, Tris-glycine gel. Lane 2 contains 15 uL of cell lysate before the pull down (too low of a concentration to analyze). Lane 3 contains 15uL of the supernatant sample taken off of the control bead incubated with 1:10 diluted detergent-containing buffer, and Lane 5 contains the proteins that were stripped from this same control bead by the SDS loading buffer. The increased percentage of detergent in the 1:1 diluted control bead preparation causes loss of resolution between bands, seen in this second control bead pull down sample in Lane 4. The most interesting bands in this gel are the Iejimalide A and Iejimalide-B pull down samples in lanes 6 and 7, respectively. In spite of low resolution, there are clear differences between iejimalides A and B. Iejimalide B has a distinct protein pattern from A in Lane 6 and the control bead in Lane 4, with a collection of higher molecular weight proteins in the 49-80 kDa range that pull-down specifically. The supernatants for the three samples are in Lanes 8, 9 and 10, for control, Iejimalide A and Iejimalide B respectively. There are essentially no differences between the supernatant lanes.

The conclusions that can be made are encouraging. Iejimalide B pulls down a different set of proteins than does Iejimalide A. Iejimalide A has very little difference with the control bead. This observation is consistent with the greater potency of iejimalide B over A, and suggests a protein-binding affinity that survives a pull-down experiment. We are actively pursuing a 2-dimensional SDS-PAGE analysis of these samples, and we plan to isolate the proteins that specifically bind to the iejimalide B (and possibly A) over control for identification by mass spectrometric sequencing analysis.
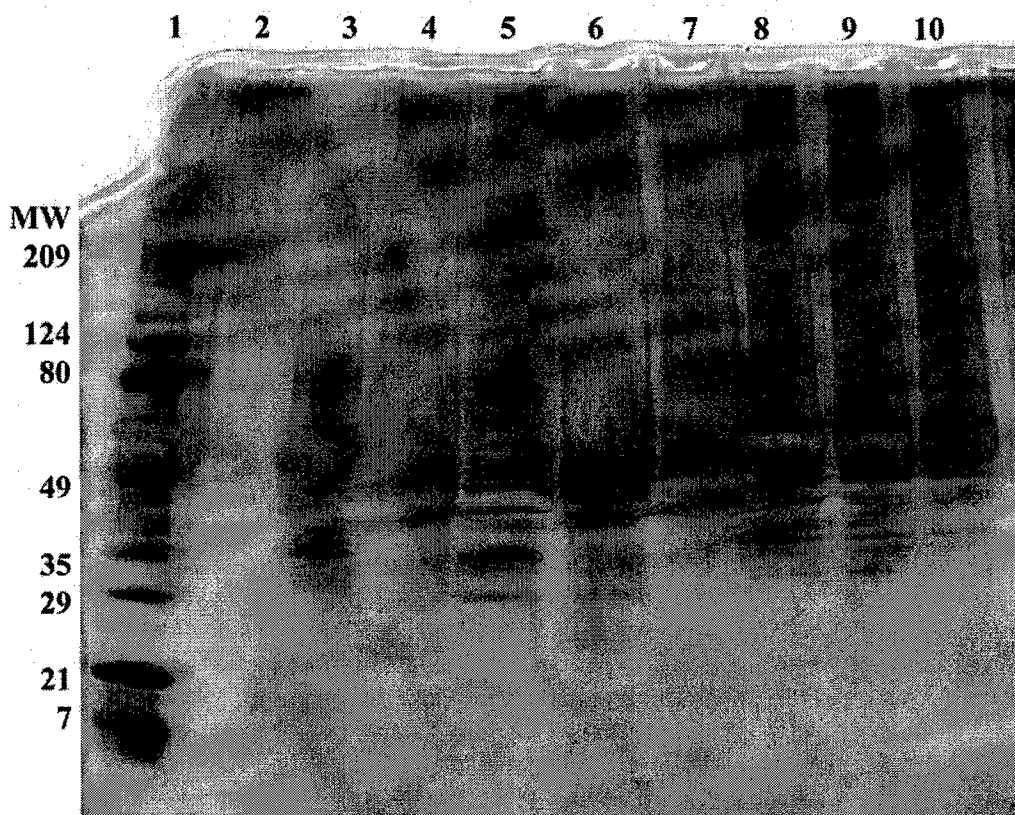
Figure 7. Preliminary results of pull-down assays of binding of MCF-7 cellular proteins to immobilized iejimalide derivatives **17a** and **17b**. See description of results in the accompanying text.

3. KEY RESEARCH ACCOMPLISHMENTS

• completion of fourth re-isolation of additional samples of the naturally occurring iejimalides

• demonstration of growth inhibition effects and cell cycle arrest in cancer cell cultures

• preliminary study of acute toxicity of the iejimalides in mice

• improved laboratory syntheses of all of the subunits of the iejimalides

• semi-synthesis of fluorescent and immobilized derivatives of the iejimalides that retain activity against cancer cell lines

• observation of localization of a fluorescent iejimalide derivative in cancer cells and lack of effect on microtubules

• observation of selective cellular protein affinity by an immobilized iejimalide derivative

4. REPORTABLE OUTCOMES

Manuscript prepared for submission for publication:
> Schweitzer, D.; Zhu, J.; Jarori, G.; Tanaka, C.; Kane, J. J.; Davisson, V. J.; Helquist, P. "Synthesis of Carbamate Derivatives of Iejimalides. Retention of Normal Antiproliferative Activity" (2005)

Presentations:
> University of Minnesota, Department of Chemistry, "Chemical and Biological Studies of Macrocyclic Natural Products", October 1, 2004.

> 36th Great Lakes Regional Meeting of the American Chemical Society, Illinois Central College, Peoria, Illinois, Abstract No. 23, Invited Lecture, "Chemical and Biological Studies of Macrocyclic Natural Products", October 17, 2004.

Degree obtained:
> Jamie L. Zigterman, M.Sc., University of Notre Dame, May, 2004.

5. CONCLUSIONS

This work had previously confirmed that the iejimalides show potent growth inhibition effects in some 70 cell lines. A dose and time response study in PC-3 prostate cancer cells has shown that the growth inhibition effects persist in a concentration range of 10-100 nM for at least 96 hours. Studies of cell cycle effects indicate that the iejimalides promote S phase arrest in cancer cell cultures.

The first total synthesis of the iejimalides is very close to completion. Improved, second-generation syntheses of all of the subunits of the iejimalides have been completed. Assembly of these subunits is now underway to compete the total synthesis. This synthesis will provide an alternative, more abundant source of the iejimalides compared to the very limited quantities available from the natural source. The synthesis will also provide numerous analogues for later drug development efforts.

Semi-synthetic derivatives of the iejimalides are readily available by direct esterification or carbamoylation of the free hydroxy group of the side chain serine residue. Normal cell growth inhibition activity is retained for derivatives obtained in this manner. A fluorescently labeled derivative is localized within the cytoplasm of PC-3 prostate cells. Although a COMPARE analysis suggested that the iejimalides may have a microtubule-based mechanism of action, we have observed no effects on microtubules in PC-3 cells. An immobilized derivative of an iejimalide has been prepared successfully and has been employed in a preliminary affinity isolation study to identify the cellular protein target(s) of the iejimalides.

The scientific and medical significance of these results is summarized by the following key points:

(1) potent cell-growth inhibition is observed for the iejimalides in several cancer cell lines;

(2) total synthesis of the iejimalides is at an advanced stage and will provide increased quantities of the iejimalides and synthetic analogues for conducting more extensive pre-clinical drug development studies.

(3) direct derivatization of the iejimalides provides labeled compounds that can be employed in cellular target identification efforts.

6. REFERENCES

i. (a) Kobayashi, J.; Cheng, J.; Ohta, T.; Nakamura, H.; Nozoe, S.; Hirata, Y.; Ohizumi, Y.; Sasaki, T. "Iejimalides A and B, Novel 24-Membered Macrolides with Potent Antileukemic Activity from the Okinawan Tunicate *Eudistoma* cf. *Rigida*" *J. Org. Chem.* **1988**, *53*, 6147-6150. (b) Kikuchi, Y.; Ishibashi, M.; Sasaki, T.; Kobayashi, J. "Iejimalides C and D, New Antineoplastic 24-Membered Macrolide Sulfates from the Okinawan Marine Tunicate *Eudistoma* cf. *Rigida*" *Tetrahedron Lett.* **1991**, *32*, 797-798.

ii. Kikuchi, Y.; Ishibashi, M.; Sasaki, T.; Kobayashi, J. "Iejimalides C and D, New Antineoplastic 24-Membered Macrolide Sulfates from the Okinawan Marine Tunicate *Eudistoma* cf. *Rigida*" *Tetrahedron Lett.* **1991**, *32*, 797-798.

iii. Tsuda, M.; Nozawa, K.; Shimbo, K.; Ishiyama, H.; Fukushi, E.; Kawabata, J.; Kobayashi, J. "Stereochemistry of iejimalide B" *Tetrahedron Lett.* **2003**, *44*, 1395-1399.

iv. Mendlik, M. T.; Cottard, M.; Rein, T.; Helquist, P. "Stereocontrolled Synthesis of the C(1)-C(11) Subunit of the Iejimalides", *Tetrahedron Lett.* **1997**, *38*, 6375-6378.

v. Pedersen, T. M.; Hansen, E. L.; Kane, J. ; Rein, T.; Helquist, P.; Norrby, P.-O.; Tanner, D. "Enantioconvergent Sequential Asymmetric Horner-Wadsworth-Emmons Reaction and Palladium-Catalyzed Allylic Substitution" *J. Am. Chem. Soc.* **2001**, *123*, 9738-9742.

vi. Cottard, M.; Kann, N.; Rein, T.; Åkermark, B.; Helquist, P. "Synthesis of a Major Fragment of the Iejimalides" *Tetrahedron Lett.* **1995**, *36*, 3115-3118.

vii. Frantz, D. E.; Fässler, R.; Carreira, E. M. "Facile Enantioselective Synthesis of Propargylic Alcohols by Direct Addition of Terminal Alkynes to Aldehydes" *J. Am. Chem. Soc.* **2000**, *122*, 1806-1807.

viii. Jiang, B.; Chen, Z.; Xiong, W. "Highly enantioselective alkynylation of aldehydes catalyzed by a readily available chiral amino alcohol-based ligand" *Chem. Commun.* **2002**, 1524-1525.

ix. Commercially obtained Amano AK lipase was employed with vinyl acetate as an acylating agent under standard conditions. Marshall, J. A.; Chobanian, H. R.; Yanik, M. M. "Lipase-Mediated Resolution of 4-TMS-3-butyn-2-ol and Use of the Mesylate Derivatives as a Precursor to a Highly Stereoselective Chiral Allenylindium Reagent" *Org. Lett.* **2001**, *3*, 3369-3372.

x. Matsumura, K.; Hashiguchi, S.; Ikariya, T.; Noyori, R. "Asymmetric Transfer Hydrogenation of ąb-Acetylenic Ketones" *J. Am. Chem. Soc.* **1997**, *119*, 8738-8739.

xi. (a) Van de Weghe, P.; Bourg, S.; Eustache, J. "Electrophilic selenocyclization in 2-ene-1,5-diol systems: unexpected oxetane vs. tetrahydrofuran formation" *Tetrahedron* **2003**, *59*, 7365-7376. (b) Tueting, D. R.; Echavarren, A. M.; Stille, J. K. "Palladium catalyzed coupling of organostannanes with vinyl epoxides" *Tetrahedron* **1989**, *45*, 979-992. (c) Oestreich, M.; Fröhlich, R.; Hoppe, D. "(-)-Sparteine-Mediated Stereoselective Intramolecular Carbolithiation of 4-Substituted 5-Hexynyl Carbamates. Synthesis of Enantiopure 1,3-Difunctionalized Alkylidene Cyclopentanes" *J. Org. Chem.* **1999**, *64*, 8616-8626.

xii. (a) Persson, B. A.; Larsson, A. L. E.; Ray, M. L.; Bäckvall, J.-E. "Ruthenium- and Enzyme-Catalyzed Dynamic Kinetic Resolution of Secondary Alcohols" *J. Am. Chem. Soc.* **1999**, *121*, 1645-1650. (b) Kim, M.-J.; Chung, Y. I.; Choi, Y. K.; Lee, H. K.; Kim, D.; Park, J. "(S)-Selective Dynamic Kinetic Resolution of Secondary Alcohols by the Combination of Subtilisin and an Aminocyclopentadienylruthenium Complex as the Catalysts " *J. Am. Chem. Soc.* **2003**, *125*, 11494-11495.

xiii. Hill, D. R.; Hsiao, C.-N.; Kurukulasuriya, R.; Wittenberger, S. J.; "2,2,2-Trifluoroethyl Formate: A Versatile and Selective Reagent for the Formylation of Alcohols, Amines, and *N*-Hydroxylamines" *Org. Lett.* **2002**, *4*, 111-113.

xiv. (a) Marshall, J. A.; Chobanian, H. R.; Yanik, M. M. "Lipase-Mediated Resolution of 4-TMS-3-butyn-2-ol and Use of the Mesylate Derivatives as a Precursor to a Highly Stereoselective Chiral Allenylindium Reagent" *Org. Lett.* **2001**, *3*, 3369-3372. (b) Johns, B. A.; Grant, C. M.; Marshall, J. A. "Synthesis and Utilization of Indium(I) Iodide for in situ Formation of Enantioenriched Allenylindium Reagents and Their Addition to Aldehydes: (2R,3S,4S)-1-(tert-Butyldiphenylsilyloxy)-2,4-dimethyl-5-hexyne-3-ol" *Org. Synth* **2002**, *79*- 59-71.

xv. (a) Lipshutz, B. H.; Keil, R.; Ellsworth, E. L. "A New Method for the *in situ* Generation of $Cp_2Zr(H)Cl$ (Schwartz' Reagent)" *Tetrahedron Lett.* **1990**, *31*, 7257-7260. (b) Kalish, V. J.; Shone, R. L.; Kramer, S. W.; Collins, P. W.; Babiak, K. A.; McLaughlin, K. T.; Ng, J. S. "An Improved Procedure for the Synthesis of Prostaglandin Analogues" *Synth. Commun.* **1990**, *20*, 1641-1645.

xvi. http://itbwork.nci.nih.gov:8080/CompareServer/ CompareServer

xvii.   Paull K. D.; Shoemaker R. H.; Hodes L.; Monks, A.; Scudiero D. A.; Rubinstein L.; Plowman J.; Boyd M. R. "Display and analysis of patterns of differential activity of drugs against human tumor cell lines: Development of mean graph and COMPARE algorithm" *J. Natl. Cancer Inst.* **1989**, *81*, 1088-1092.

xviii.   (a) Muroi, M.; Shiragami, N.; Takatsuki; A. "Destruxin B, a specific and readily reversible inhibitor of vacuolar-type H^+-translocating ATPase" *Biochem. Biophys. Res. Commun.* **1994**, *205*, 1358-1365. (b) Togashi, K.; Kataoka, T.; Nagai, K. "Characterization of a series of vacuolar type H^+-ATPase inhibitors on CTL-mediated cyto-toxicity" *Immunol. Lett.* **1997**, *55*, 139-144. (c) Bandani, A. R.; Amiri, B.; Butt, T. M.; Gordon-Weeks; R. "Effects of efrapeptin and destruxin, metabolites of entomogenous fugi, on the hydrolytic activity of a vacuolar type ATPase identified on the brush border membrane vesicles of *Galleria mellonella* midgut and on plant bound hydrolytic enzymes" *Biochim. Biophys. Acta* **2001**, *1510*, 367-377.

xix. (a) Rudolf, E.; Cervinka, M. "Topoisomerases and tubulin inhibitors: a promising combination for cancer treatment" *Curr. Med. Chem. Anti-Canc. Agents* **2003**, 421-429. (b) Miao, L.; Yi, P.; Wang, Y.; Wu, M. "Etoposide upregulates Bax-enhancing tumour necrosis factor-related apoptosis inducing ligand-mediated apoptosis in the human hepatocellular carcinoma cell line QGY-7703" *Eur. J. Biochem.* **2003**, *270*, 2721-2731. (c) Kanbe, E.; Abe. A.; Towatari, M.; Kawabe, T.; Saito, H.; Emi, N. "DR1-like element in human topoisomerase IIalpha gene involved in enhancement of etoposide-induced apoptosis by PPARgamma ligand" *Exp. Hematol.* **2003**, *31*, 300-308. (d) Desbene, S.; Giorgi-Renault, S. "Drugs that inhibit tubulin polymerization: the particular case of podophyllotoxin and analogues" *Curr. Med. Chem. Anti-Canc. Agents* **2002**, *2*, 71-90. (e) Gordaliza, M.; Castro, M. A.; del Corral, J. M.; Feliciano, A. S. "Antitumor properties of podophyllotoxin and related compounds" *Curr. Pharm. Des.* **2000**, *6*, 1811-1839.

xx. (a) Jordan, M. A. "Mechanism of action of antitumor drugs that interact with microtubules and tubulin" *Curr. Med. Chem. Anti-Canc. Agents* **2002**, *2*, 1-17. (b) Molad, Y. "Update on colchicine and its mechanism of action" *Curr. Rheumatol. Rep.* **2002**, *4*, 252-256. (c) Chaudhuri, A. R.; Seetharamalu; P.; Schwarz, P. M.; Hausheer, F. H.; Luduena, R. F. "The interaction of the B-ring of colchicine with alpha-tubulin: a novel footprinting approach" *J. Mol. Biol.* **2000**, *303*, 679-692. (d) Bai, R.; Covell, D. G.; Pei, X. F.; Ewell, J. B.; Nguyen, N. Y.; Brossi, A.; Hamel, E. "Mapping the binding site of colchicinoids on beta -tubulin. 2-Chloroacetyl-2-demethylthiocolchicine covalently reacts predominantly with cysteine 239 and secondarily with cysteine 354" *J. Biol. Chem.* **2000**, *275*, 40443-4052.

xxi. Ravelli, R. B. G.; Gigant, B.; Curmi, P. A.; Jourdain, I.; Lachkar, S.; Sobel, A.; Knossow, M. "Insight into tubulin regulation from a complex with colchicines and a stathmin-like domain" *Nature* **2004**, *428*, 198-202.

ARF6-Mediated Regulation of Breast Epithelial Cell Invasion

Crislyn D'Souza-Schorey
Jeff Schorey

Abstract

The acquisition of a motile and invasive phenotype is an important step in the development of epithelial cell tumors, and ultimately for metastasis. The progression of epithelia-derived primary tumors to a metastatic phenotype is a multistage process involving aberrant functions of the tumor cell including detachment from neighboring cells via junction disassembly, increased local proteolysis, degradation of extracellular matrix components, invasion, adhesion to the vascular basement membrane, migration through the latter, and proliferation at distant sites. Thus, multiple changes including alterations in cell morphology and changes in gene expression, occur during tumor progression. To goal of our proposal is to investigate the molecular mechanisms of ARF6-regulated adherens junction disassembly and cell motility in human breast carcinoma cells. We hypothesize that via its effect on membrane traffic activation of ARF6 regulates the stability of adherens junctions, whereas via its effect on actin remodeling, ARF6 controls the process of cell invasion.

INTRODUCTION

The acquisition of a motile and invasive phenotype is an important step in the development of epithelial cell tumors, and ultimately for metastasis. The progression of epithelia-derived primary tumors to a metastatic phenotype is a multistage process involving aberrant functions of the tumor cell including detachment from neighboring cells via junction disassembly, increased local proteolysis, degradation of extracellular matrix components, invasion, adhesion to the vascular basement membrane, migration through the latter, and proliferation at distant sites. Thus, multiple changes including alterations in cell morphology and changes in gene expression, occur during tumor progression (Birchmeier and Birchmeier, 1993; Hanahan and Weinberg, 2000). Until date, we have only a rudimentary understanding of the molecular mechanisms underlying morphological changes that occur during breast carcinoma metastasis. Members of the Ras-related GTPases can regulate these morphological changes either directly via their effect on the actin cytoskeleton or indirectly via changes in gene transcription (Hall, 1999; Van Aelst and D'Souza-Schorey, 1997). Recent studies by others and us demonstrated a role for members of the ARF and Rho GTPases, of the Ras superfamily, in cellular activities such as adhesion, and motility. Of particular interest to this proposal is our recent findings that sustained activation of ARF6, conferred increased migratory potential to epithelial cells (Palacios et al., 2001). The ARF6 GTPase has been show to regulate endosome recycling and actin cytoskeletal remodeling, both of which can impinge on cell motility. ARF6-GTP-induced increased cell migration in epithelia resulted from a) the redistribution of E-cadherin from adherens junctions to the cytoplasm and b) the ruffling of the lateral plasma membrane. In contrast, expression of a dominant negative mutant of ARF6, ARF6(T27N) blocked hepatocyte growth factor-induced internalization of·cadherin-based junctional components into the cytoplasm, as well as basal cell migration. The enhanced cell migratory capacity was not observed by expression of activated 'effector domain' ARF6 mutant selectively incapable of actin remodeling. This suggests that both, ARF6-induced adherens junctions disassembly and membrane ruffling, are required for the acquisition of a migratory phenotype in epithelia.

To goal of our proposal is to investigate the molecular mechanisms of ARF6-regulated adherens junction disassembly and cell motility in human breast carcinoma cells. We hypothesize that via its effect on membrane traffic activation of ARF6 induces the disassembly of adherens junctions, whereas via its effect on actin remodeling and MAPK kinase signaling, ARF6 controls the process of cell invasion. We proposed a highly focused set of investigations, which aimed to elucidate the cellular mechanisms that lead to increased motility upon ARF6 activation. Questions that will be specially addressed are **1.** How does nucleotide exchange and GTP hydrolysis on ARF6 control E-cadherin traffic? **2.** How do extracellular matrix proteins influence ARF6-GTP-induced cell migration? **3.** What are the signaling pathways involved in ARF6-induced ERK activation, which leads to invadopodia formation?

BODY

This section is intended to summarize the data obtained that led to investigations during the award period and describe key findings obtained during the award period.

1. Preliminary investigations in support of the proposal.

The investigations described here build on our exciting discovery that the ARF6 GTPase, by virtue of its regulation of endocytic traffic, modulates the spatial distribution of E-cadherin and is a critical determinant of epithelial cell migration. Like all other GTPases of the Ras superfamily, ARF6 cycles between its active GTP and inactive GDP-bound conformations and as such can serve as a molecular switch to regulate cellular processes. GTP hydrolysis is mediated by GAPs (GTPase activating proteins), whereas exchange of bound-GDP for GTP is mediated by GEFs (guanine nucleotide exchange factors). ARF6-GTP-induced adherens junctions disassembly did not require actin rearrangements but was dependent on the internalization of E-cadherin into the cytoplasm via vesicle transport. Treatment of cells with hepatocyte growth factor (HGF)/scatter factor induced the activation of endogenous ARF6 and ARF6 activation was accompanied by a marked increase in the migratory potential of epithelia. In contrast, dominant negative ARF6, ARF6(T27N), localized to AJs and enhanced the epithelial phenotype. Expression of ARF6(T27N) blocked HGF-induced internalization of cadherin-based junctional components into the cytoplasm, as well as cell migration. The enhanced cell migratory capacity was not observed by expression of activated 'effector domain' ARF6 mutant selectively incapable of actin remodeling. Thus, ARF6-induced adherens junctions disassembly and membrane ruffling, are required for the acquisition of a migratory phenotype in epithelia. Finally, we have shown that ARF6-activation is preceded by c-Met activation and $pp60^{v-Src}$-mediated phosphorylation of junctional components, during adherens junction disassembly. The above findings document an essential role for ARF6-regulated membrane traffic in adherens junction disassembly and epithelial cell migration.
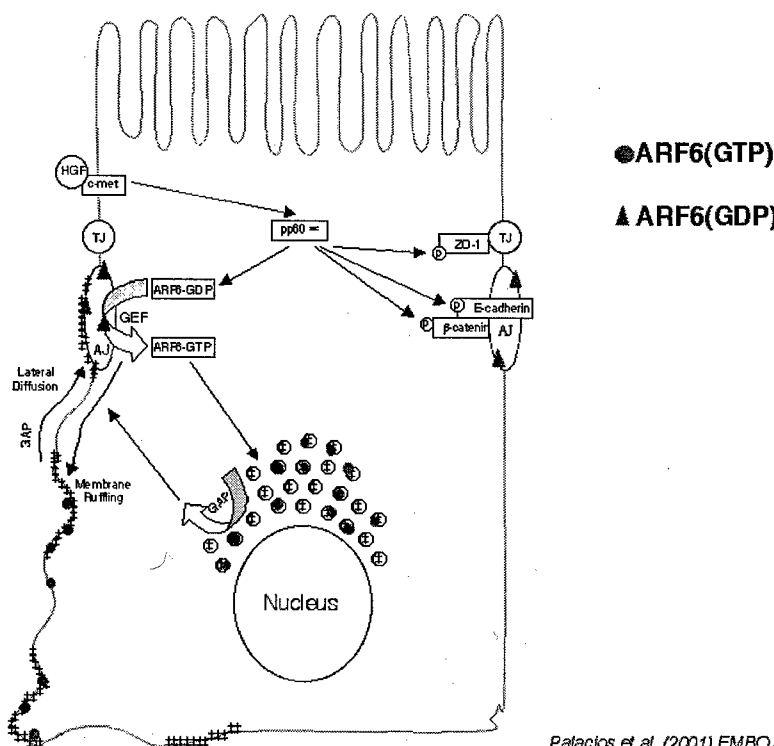
Figure 1: Working model for the regulation of adherens junction turnover by the ARF6 GTPase cycle. Activation on ARF6 at the AJs (by GEFs) occurs in response to extracellular stimuli and downstream of Src activation. This in turn promotes AJ disassembly and ruffling of the lateral membrane, although both processes are mediated by distinct effector pathways. GTP hydrolysis on ARF6 (by GAPS) at perinuclear compartments and the lateral membrane, results in redistribution of E-cadherin to and at the lateral membrane to re-assemble AJs.

●ARF6(GTP)

▲ARF6(GDP)

Palacios et al.,(2001) EMBO J. 20: 4973

2. Previous findings (year 1)

We found that GTP hydrolysis on ARF6 is required for the redistribution of E-cadherin back to the cell surface.

Our results suggest that a regulatory step exists at the perinuclear compartment where E-cadherin and the and other basolateral membrane proteins are segregated and recycled via two distinct pathways, one being dependent on GTP hydrolysis of ARF6 (E-cadherin recycling) and the other being independent of ARF6 (Tfn-R recycling).

Role of ARF6 in cell invasion: Our recent studies have shown that AFR6 localizes to invadopodia, on the adherent surface of the invasive melanoma cell and breast cancer cell lines. We found that sustained activation of ARF6 facilitates the formation of invadopodia and cell invasive potential 5-6 fold over parental cells. We also showed that AFR6 regulates the process of invasion through activation of ERK 1/2. (Please refer to Tague et al., PNAS, 2004, included at end of report).

CURRENT PROGRESS

3. EFA6 (Exchange factor for ARF6) does not affect ARF6 functions at the adherens junctions. EFA6 has been described as a bone fide exchange factor for ARF6 (Franco et al, 1999). In contrast to other known ARF exchange factors, EFA6 is specific for ARF6. EFA6 is expressed exclusively in brain tissue. The protein contains a Sec7 domain required for nucleotide exchange, a PH (pleckstrin homology) domain, a coil-coil domain, and a polyproline region at the C-terminal end. Chavrier and colleagues have now isolated the ubiquitously expressed EFA6 homologue, designated EFA6.3 (P. Chavrier, personal communication).

EFA6.3 is structurally homologous to EFA6 and its expression in cells induces a phenotype that is identical to that of the brain isoform. Plasmids encoding wild type and mutant EFA6.3, as well as polyclonal antisera that reacts efficiently with endogenous EFA6.3, have been provided to us as part of an ongoing collaboration by Philippe Chavrier at Inst. Curie, Paris. We have found that EFA6.3 localizes to cell junctions (data not shown). Thus we sought we will determine whether EFA6 catalyzes nucleotide exchange on ARF6 to facilitate adherens junction disassembly.

For these investigations we made use of EFA6(E242K), an EFA6.3 mutant that is defective in nucleotide exchange, as well as MDCKpp60^{v-Src}cells, an MDCK cell line expressing a temperature sensitive mutant of pp60^{v-Src} (Palacios et al., 2001). We investigated whether expression of EFA6(E242K) blocked Src-induced cell scattering. Cells were transfected with plasmid encoding EFA6(E242K) at non-permissive temperatures. Cells were then be shifted to permissive temperatures for Src expression and cell scattering was monitored using phase contrast time lapse and microscopy. Cells were also labeled for E-cadherin to monitor whether the internalization of E-cadherin into endosomal compartments is inhibited by expression of EFA6(E242K). These studies have revealed that expression of EFA6(E242K) had no effect on Src-induced disassembly of adherens junctions and E-cadherin was efficiently internalized (data not shown).

4. Kock-down of endogenous ARF6 in tumor cell lines. Using pSuper plasmid (Oligoengine) encoding small interfering RNAs against ARF6 we have been able to knock down ARf6 expression in melanona and breast cancer cell lines. We have been able to select for cells expressing the siRNA plasmid on the basis of resistance to the aminoglycoside, G418. With 4 days of selection we observe nearly complete knock-down of ARF6 expression in the LOX cell line (figure 2). In contrast transfection of cells with plasmid expressing 'control luciferase' siRNA, or vector plasmid alone had no effect on ARF6 expression. Thus we will now be able to complement our investigations using dominant negative ARF6, by also investigating the effects of knocking-down ARF6 expression.
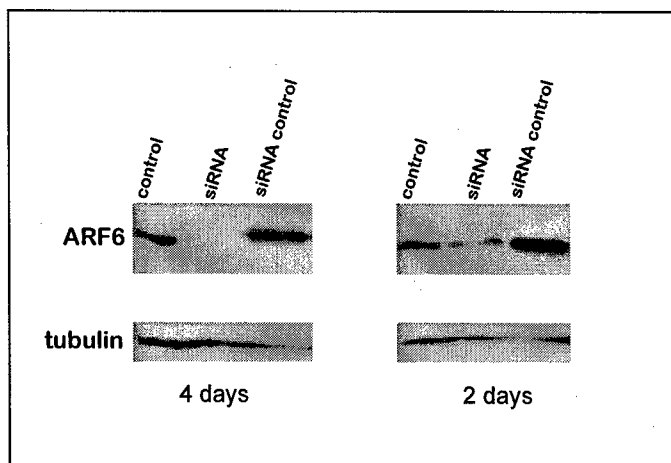

Figure 2: ARF6 knock-down using siRNA in LOX cells. Lysates were prepared from LOX cells transfected with pSuper plasmid encoding ARF6 siRNA or a non-relevant siRNA sequence or empty plasmid alone and subjected to western blot analysis. The blot was probed for ARF6 and α-tubulin using monoclonal antibodies.

5. The GTPase cycle of ARF6 controls ERK activation. Using LOX cells stably expressing ARF6(Q67L) or ARF6(T27N) proteins, we have been able to monitor the effect of ARF6 mutants on ERK activity by using in vitro biochemical assays which measure ERK activity in cell extracts by monitoring the phosphorylation of Elk-1 protein as a substrate. The commercially available p44/42 MAPK assay kit (Cell Signaling Technology) used for these studies, were performed according to the manufacturer's instructions. As seen in figure 3, a 41kD phospho-Elk (Ser 383) band is observed with LOX cells extracts indicative of high basal ERK activity in these cells, whereas additional hyper-phosphorylated bands are observed upon HGF treatment. (Additional ERK phosphorylation sites are present between amino acids 307 and 428 of the Elk protein). Importantly, when lysates of cells expressing ARF6(Q67L) were used in the assay, increased ERK activity was observed. On the other hand, expression of ARF6(T27N) decreased both HGF-induced as well as basal levels of ERK activity. These studies support our earlier findings that activation of ARF6 results in increased phospho-ERK levels in tumor cells. These data also support our rationale for investigations to investigate the signaling pathways linking ARF6 to ERK activation.
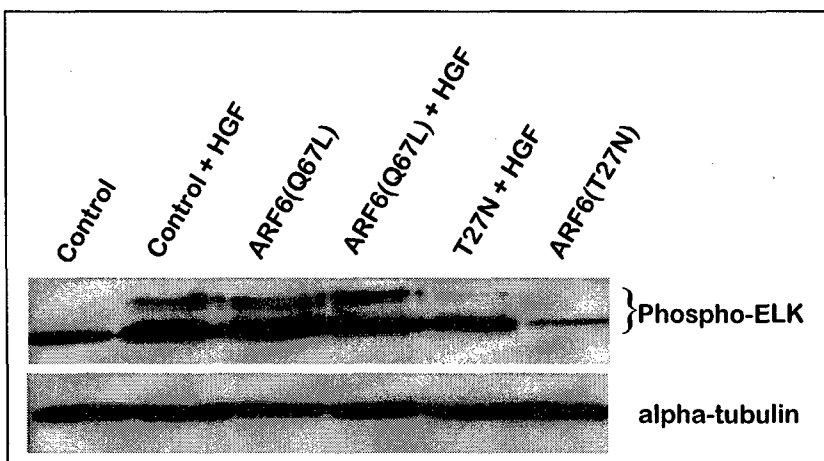
Figure 3: The ARF6 GTPase cycle modulates ERK activity. Extracts of untransfected LOX cells or cells expressing ARF6(Q67L) or ARF6(T27N) and treated with or without 40ng/ml HGF for 30 min, and assayed for ERK activity by measuring the phosphorylation of Elk as described above. Extracts were probed for phosphorylated Elk and for tubulin.

6. ARF6 is required for invasion induced by extracellular physiological stimuli. We had shown that addition of growth factors such as HGF and EGF to cells as well as engagement of the β1-integrin subunit has been shown to enhance invasion of melanoma cell lines. Expression of dominant negative ARF6 completely blocked HGF-induced LOX cell invasion. Moreover using an endogenous ARF6-GTP pull-down assay recently developed in our lab, we found that the levels of endogenous ARF6-GTP was increased as cells became more invasive with HGF treatment. We have now also examined the effect of the expressing the dominant negative ARF6 mutant on β1-integrin-induced invasion. For these studies, cells transfected with plasmids encoding ARF6(T27N), or those that were mock-transfected, were incubated with or without 11μg/ml of the PG411 antibody and the number of cells exhibiting gelatin degradation were scored. ARF6(T27N)-expression blocked PG411-stimulated gelatin degradation (Figure 4). Furthermore, as shown in figure 4B, activation of endogenous ARF6 was significantly increased as cells became more invasive in response to β1-integrin engagement. Thus ARF6-mediated regulation of LOX cell invasion is physiologically relevant.

A


B
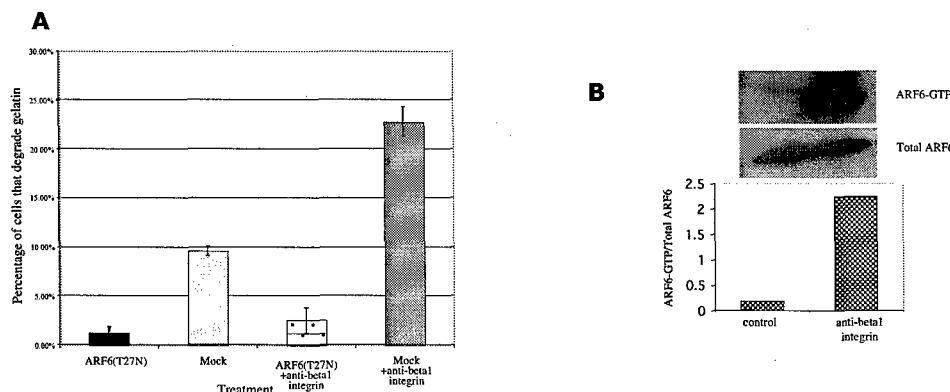
Figure 4. ARF6 activation occurs downstream and is required for β1-integrin-induced invasion. A) Cells were transfected with plasmids as indicated, seeded on gelatin-coated coverslips and treated with or without activating PG411. For each experimental condition, 150 cells were visualized and those exhibiting gelatin degradation underneath them were scored. The percentage of cells with gelatin degradation underneath them was calculated as an indicator of cell invasion. **B)** Cells were seeded on gelatin-coated tissue culture dishes and treated with or without PG411. Cells lysates were incubated with GST-MT2 beads as previously described. Bound ARF6-GTP and total ARF6 in lysates was visualized by western blot analysis.

Figure 5: Cells expressing Rac1(G12V) exhibit invadopodia. Cells expressing Rac1(G12V) were seeded in gelatin-coated coverslips (green) and labeled for Rac1 (red).
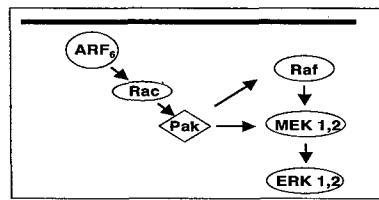
Figure 6: Rac1 functions downstream of ARF6 and recruits PAK, which in turn phosphorylates Raf1/ERK.

7. Is Rac1 required for ARF6-GTP-induced ERK activation? Preliminary investigations have shown that expression of constitutively activated Rac1, Rac1(G12V), in cells also enhances invadopodia formation and cell invasion (Figure 5), a process that was blocked by treatment of cells with inhibitors of MEK (our unpublished observations). Co-expression of ARF6(T27N) had no effect on Rac1(G12V)-induced invasive capacity, suggesting that Rac likely functions downstream of ARF6 to facilitate ERK activation. Infact Rac1 has been shown to function downstream of ARF6 in migrating non-polarized epithelial cells. How might Rac1 promote the activation of ERK? PAK (p21 adhesion kinase), a downstream target of Rac1, has been shown to phosphorylate Ser298, one of two sites in the catalytic domain of MEK1 thought to be important for stable association between Raf1 and MEK1 (6). PAK has

74

also been shown to phosphorylate Raf1 at Ser338, a process facilitating maximal activation of Raf1 by Ras (6). We will test whether Rac1 functions downstream on ARF6 and promotes ERK activation via the recruitment of PAK (see figure 6).

CONCLUSIONS We have made progress in deciphering the mechanisms involved in the breakdown of adherens junction disassembly as well as enhancement in cell invasion potential, both of which are critical for tumor progression. We have shown that the GTP hydrolysis on ARF6 specifically regulates the recycling of E-cadherin but not other proteins that are routed to the basolateral membrane of epithelial cells, suggesting that the trafficking of adhesion molecules is subject to more 'specialized' regulation. Our preliminary findings also suggest that EFA6, although localized to cell-cell contacts, may not play a role in the disassembly of the adherens junctions. We have also shown that ARF6 enhances tumor cell invasion via the activation of the extracellular signal regulated kinase. The GTPase cycle of ARF6 appears to regulate the activation of ERK. Activation of intergrin receptors that enhance invadopodia formation also enhance endogenous ARF6 activation. Depletion of ARF6 levels using siRNAs will be effective in further investigating the role of ARF6 in cell invasion. Expression of activated Rac1 can also promote invadopodia formation and our current studies are aimed at investigating whether Rac1 is required for ARF6 function.

KEY RESEARCH FINDINGS

✤ GTP hydrolysis on ARF6 is required for the recycling of E-cadherin molecules back to the lateral membrane for reassembly into cell junctions

✤ A mutant of EFA6 deficient in nucleotide-exchange does not block v-Src-induced adherens junctions disassembly.

✤ ARF6-GTP facilitates cell invasive capacity by activation of ERK.

✤ ARF6 activation occurs downstream and is required for β1-integrin-induced invasion.

✤ The GTPase cycle of ARF6 controls ERK activation.

LITERATURE CITED

1.   **Birchmeier, C., and W. Birchmeier** 1993. Molecular aspects of mesenchymal-epithelial interactions Annu Rev Cell Biol. **9**:511-40.

2.   **Franco, M., P. J. Peters, J. Boretto, E. van Donselaar, A. Neri, C. D'Souza-Schorey, and P. Chavrier** 1999. EFA6, a sec7 domain-containing exchange factor for ARF6, coordinates membrane recycling and actin cytoskeleton organization Embo J. **18**:1480-91.

3.   **Hall, A.** 1999. Signal transduction pathways regulated by the Rho family of small GTPases Br J Cancer. **80 Suppl 1**:25-7.

4.   **Hanahan, D., and R. A. Weinberg** 2000. The hallmarks of cancer Cell. **100**:57-70.

5.   **Palacios, F., L. Price, J. Schweitzer, J. G. Collard, and C. D'Souza-Schorey** 2001. An essential role for ARF6-regulated membrane traffic in adherens junction turnover and epithelial cell migration Embo J. **20**:4973-86.

6.   **Van Aelst, L., and C. D'Souza-Schorey** 1997. Rho GTPases and signaling networks Genes Dev. **11**:2295-322.

ADP-ribosylation factor 6 regulates tumor cell invasion through the activation of the MEK/ERK signaling pathway

Sarah E. Tague*†, Vandhana Muralidharan*†, and Crislyn D'Souza-Schorey*‡§

*Department of Biological Sciences and †The Walther Cancer Institute, University of Notre Dame, Notre Dame, IN 46556-0369

Tumor cell invasion through the extracellular matrix is accompanied by the formation of invadopodia, which are actin-rich protrusions at the adherent surface of cells at sites of extracellular matrix degradation. Using the invasive human melanoma cell line LOX as a model system, we demonstrate that the ADP-ribosylation factor 6 (ARF6) GTPase is an important regulator of invadopodia formation and cell invasion. We show that ARF6 localizes to invadopodia of LOX cells. Sustained activation of ARF6 significantly enhances the invasive capacity of melanoma as well as breast tumor cell lines, whereas dominant negative ARF6 abolishes basal cell invasive capacity as well as invasion induced by growth factors. Furthermore, using biochemical assays, we show that enhanced invasive capacity is accompanied by the activation of endogenous ARF6. Finally, we provide evidence that ARF6-enhanced melanoma cell invasion depends on the activation of the extracellular signal-regulated kinase (ERK), and that the ARF6 GTPase cycle regulates ERK activation. This study describes a vital role for ARF6 in melanoma cell invasion and documents a link between ARF6-mediated signaling and ERK activation.

An important characteristic of metastasizing cells is their ability to degrade and invade the extracellular matrix. Matrix degradation and cell invasion also occur during normal physiological processes, such as development and differentiation (1). The process of cell invasion is tightly regulated by a number of cell-signaling proteins, such as tyrosine kinases, Ras-related GTPases, and mitogen-activated protein kinase (MAPK) family proteins (2, 3). As an invading cell moves through the extracellular matrix, it extends actin-rich membrane protrusions into the matrix. These protrusions, called invadopodia, contain a number of actin-binding proteins and recruit various proteinases, including matrix metalloproteinases and serine proteases, which degrade matrix proteins at sites of cell invasion (4, 5). Studies on breast cancer and melanoma progression have shown that there appears to be a direct correlation between the ability of cells to form invadopodia and degrade matrix and the cells' invasive potential as measured by *in vitro* and *in vivo* assays for motility and invasion (4, 6, 7).

ADP-ribosylation factor 6 (ARF6) is a member of the Ras superfamily of small GTPases, and like most GTPases, ARF6 alternates between its active GTP-bound and inactive GDP-bound conformations. The ARF6 GTPase cycle has been shown to regulate endosome membrane trafficking, regulated exocytosis, and actin remodeling at the cell surface (8). These processes are important for controlling cell shape changes and can impinge on the acquisition of an invasive phenotype. In fact, previous work in our laboratory has shown that ARF6 promotes cell migration in epithelial cells by facilitating adherens junction disassembly through its effect on endocytosis (of adhesion molecules) and by inducing peripheral actin rearrangements (9). In addition, Santy and Casanova (10) have shown that overexpression of ARNO, a guanine nucleotide exchange factor for ARF6, also induces epithelial cell migration through the downstream activation of phospholipase D and the Rac1 GTPase.

In this study, we have examined the potential involvement of ARF6 during the process of tumor cell invasion. LOX cells, an invasive human amelanotic melanoma cell line, form prominent invadopodia and are capable of degrading gelatin, making it a good model system to study tumor cell invasion (11, 12). We describe an important role for ARF6 in the regulation of invadopodia formation and LOX cell invasion. We find that the activity of endogenous ARF6 increases as cells acquire invasive capacity and that activation of ARF6 is required for both basal level and growth factor-induced cell invasion. Finally, we show that the GTPase cycle of ARF6 regulates extracellular signal-regulated kinase (ERK) activation and that activation of ERK is essential for ARF6-induced melanoma cell invasion. This is the first report that links ARF6-mediated signaling to ERK activation.

Materials and Methods

Cell Lines, Plasmids, and Materials. The human amelanotic melanoma cell line, LOX, was kindly provided by Oystein Fodstad (The Norwegian Radium Hospital, Oslo). The hemagglutinin (HA)-tagged expression plasmids, ARF6(Q67L)–pCDNA3.1(−) and ARF6(T27N)–pCDNA3.1(−), have been previously described (13). Plasmids encoding activated and dominant negative MAPK/ERK kinase 1 (MEK-1) were kindly provided by Andrew Catling and Mike Weber (both from University of Virginia, Charlottesville). The rabbit anti-HA antibody was purchased from Babco (Richmond, CA), and the murine monoclonal anti-HA antibody was purchased from Covance (Princeton). Rhodamine-phalloidin and the murine anti-paxillin antibody were obtained from Molecular Probes. The DS1 polyclonal anti-ARF6 antibody was created from a 12-aa peptide close to the amino-terminal end, as previously described (14). The mouse monoclonal anti-phospho-p44/42 MAPK (Thr-202/Tyr-204) antibody, E10, and the anti-p44/42 MAPK rabbit polyclonal antibody were from Cell Signaling Technology (Beverly, MA), and the anti-transferrin receptor antibody was from Zymed. All secondary antibodies were purchased from Molecular Probes, except the goat anti-rat cy3 antibody, which was purchased from Chemicon. 5-(and-6)-Carboxyfluorescein diacetate, succinimidyl ester (CFDSE) and Texas red-X, succinimidyl ester were purchased from Molecular Probes. The MEK inhibitor, PD98059, was purchased from Calbiochem.

Cell Culture and Transfections. LOX cells were maintained in RPMI medium 1640 supplemented with 10% FBS, 2 mM L-glutamine, penicillin, and streptomycin. Plasmids were transfected into LOX cells via electroporation. LOX cells were trypsinized and washed twice in serum-free medium before electroporation. Cells ($\approx 1.5 \times 10^6$) from exponentially growing cultures were electroporated for 15 s at 230 V and 950 μF with a total of 15 μg of plasmid DNA.

CELL BIOLOGY

Electroporated cells were kept in complete RPMI medium 1640 at 37°C in 5% CO_2 for 48 h before further experimentation. Where indicated, LOX cells were also transfected with Metafectene transfection (Biontex Laboratories, Munich), according to the manufacturer's instructions.

Gelatin Degradation Assay. The gelatin degradation assay was modified from a previously published protocol (5). Briefly, coverslips were coated with 1% gelatin and allowed to dry overnight at 4°C. They were then rehydrated for 30 min in 2 ml of sterile H_2O. The gelatin was fixed onto the slide for 30 min with 1% paraformaldehyde. The coated coverslips were washed three times in PBS before being fluorescently labeled with 0.3–0.5 μM CFDSE or 2 μM Texas red-X, succinimidyl ester. The labeled coverslips were washed three times in PBS at 37°C before the seeding of $\approx 2 \times 10^5$ cells in 2 ml of complete RPMI medium 1640 per well. Cells were incubated on gelatin-coated coverslips for 8–24 h as indicated. For experiments with the MEK inhibitor, PD98059, cells were seeded on gelatin along with 18 μM PD98059.

For quantitation of cell invasion, cells were viewed under a fluorescent microscope coupled to a Bio-Rad MRC 1024 scanning confocal three-channel system (see below). For each experimental condition, 150 cells were visualized, and those exhibiting gelatin degradation underneath them were scored. The percentage of cells with gelatin degradation underneath them was calculated as an indicator of cell invasion. The data shown are a mean of three separate experiments.

Measurement of Endogenous ARF6-GTP. LOX cells plated at 80–85% confluency on gelatin-coated 100-mm tissue culture dishes were treated with or without 40 ng/ml HGF (hepatocyte growth factor) for 30–60 min. Analysis of the endogenous ARF6-GTP levels was performed with the MT-2 binding assay as previously described (14).

Immunofluorescent Staining and Microscopy. Immunofluorescent staining and microscopy techniques were conducted as previously described (13) except for staining with the E10 antibody. For immunofluorescent staining with the E10 antibody, cells were fixed and stained as recommended by Cell Signaling Technology. Immunofluorescent imaging was accomplished by using a Bio-Rad MRC 1024 scanning confocal 3 channel system, which uses a krypton–argon laser with excitation filters for 488 nm, 568 nm, and 647 nm and Bio-Rad LASERSHARP 2000 software (version 4.0).

Results

An Experimental System to Visualize Melanoma Cell Invasion. To examine the role of ARF6 in melanoma cell invasion, we used an invasion assay that was modified from a previously published protocol (5). Gelatin was immobilized on glass coverslips and then fluorescently labeled with either CFDSE (green) or Texas red-X, succinimidyl ester (red). LOX cells were seeded on fluorescently labeled gelatin-coated coverslips for 12 h. In the images shown in Fig. 1, LOX cells were labeled for actin, by using rhodamine–phalloidin. Gelatin degradation was visualized as dark spots underneath the cell, and invadopodia were found in areas of degraded gelatin (Fig. 1A). In the stacked side projection, invadopodia were observed as membrane protrusions extending into the gelatin (Fig. 1B). The number of invadopodia varied from one invading cell to another and appeared to emanate from actin-rich foci at the ventral surface of cells (Fig. 1C). These actin foci were also observed on the ventral surface of noninvading cells and may represent dynamic sites of invadopodia biogenesis.

Endogenous ARF6 Localizes to Invadopodia. To initiate our studies with ARF6, we characterized the localization of endogenous ARF6 in LOX cells. LOX cells plated on CFDSE-labeled gelatin-coated coverslips were permeablized and labeled for endogenous ARF6.
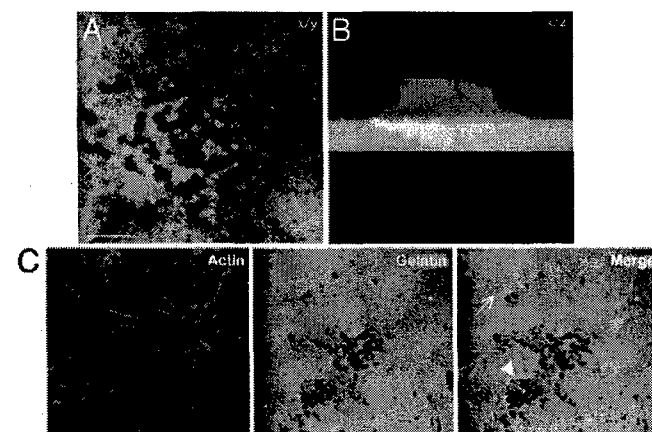
Fig. 1. CFDSE-labeled gelatin is degraded around actin-rich invadopodia formed by LOX cells. LOX cells were seeded on CFDSE-labeled gelatin (green) and allowed to invade for 12 h. The cells were then fixed, permeablized, and stained for actin by using rhodamine phalloidin (red). (A) The image on the left is a single confocal plane along the x/y axis at the tips of invadopodia. (B) The image on the right is a stacked side projection of the same cell along the x/z axis. (Bar = 10 μm.) (C) The image is taken along the ventral cell surface. The number of invadopodia varies from one invading cell to another (compare cells marked by arrow and arrowhead).

ARF6 staining was primarily perinuclear and in tubular compartments that did not overlap with endosomal markers such as the transferrin receptor (Tfn-R) (Fig. 2A) or with makers of the Golgi, the endoplamic reticulum, or lysosomes (data not shown). Thus ARF6 does not localize to classical early endosomes in LOX cells as described in Chinese hamster ovary (CHO), human embryonic kidney 293 (HEK293), PC12, and Madin–Darby canine kidney (MDCK) cells (9, 15–17) but to the tubular endosomal compartment that has previously been described in HeLa cells (18). In addition, endogenous ARF6 also localized to membrane protrusions that extended into areas of gelatin degradation (Fig. 2B).
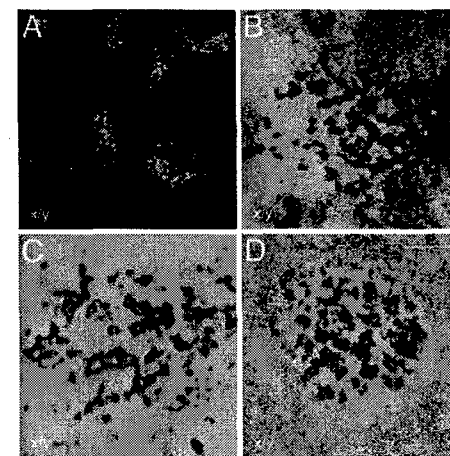
Fig. 2. Endogenous ARF6 localizes to invadopodia along with actin and paxillin. (A) LOX cells were processed for immunofluorescence microscopy and labeled for endogenous ARF6 (red) and Tfn-Rs (green). The image is taken across a single confocal plane at the cell body (x/y axis). (B–D) LOX cells plated on CFDSE-labeled gelatin (green) were fixed, permeablized, and immunofluorescently labeled for endogenous ARF6 (B–D) and actin (C), or paxillin (D). Images are across a single confocal plane along the x/y axis at the tips of invadopodia. (B) Endogenous ARF6 (red) can be seen extending into invadopodia, which are actively degrading gelatin. (C and D) Actin (red) and paxillin (red) localizes along with endogenous ARF6 (blue) in invadopodia. (Bar = 10 μm.)
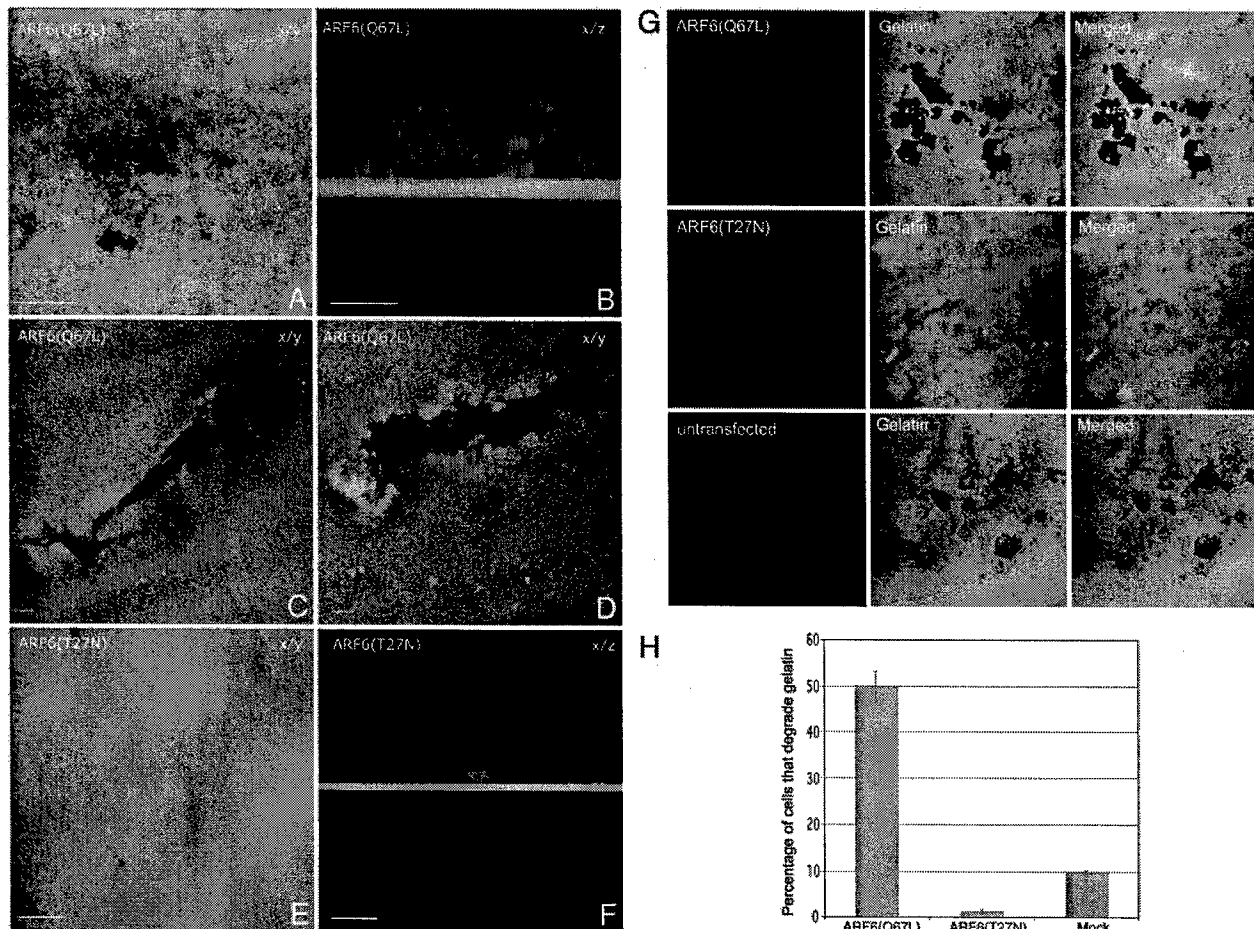
Fig. 3. Constitutively active ARF6 enhances cell invasion, whereas the dominant negative mutant of ARF6 prevents invadopodia formation and gelatin degradation. (*A–F*). LOX cells were transfected with plasmid encoding the HA-tagged ARF6(Q67L) (*A–D*) or the HA-tagged ARF6(T27N) (*E* and *F*). Images are shown along the *x*/*y* (*A* and *C–E*) or *x*/*z* axis (*B* and *F*). For all images, the HA-tagged ARF6 mutants were immunofluorescently labeled red and the gelatin is green. (Bar = 10 μm.) (*G*) MDA-MB-231 were transfected with plasmid encoding the HA-tagged ARF6(Q67L) or the HA-tagged ARF6(T27N). Images are shown along the *x*/*y* axis. (*H*) Quantitation of cell invasion by ARF6 GTP/GDP mutants. LOX cells were transfected with plasmids as indicated and seeded on gelatin-coated coverslips. After 24 h on gelatin, the percentage of transfected cells with gelatin degradation underneath them was calculated as an indicator of invasion and was compared to the percentage of untransfected cells that exhibited gelatin degradation.

Previous work has shown that invadopodia are actin-rich structures that contain actin-binding proteins and phosphotyrosine (4, 19). Thus, we investigated whether some of these proteins codistributed with ARF6 in invadapodia of LOX cells. In addition to ARF6, actin, paxillin, and phosphotyrosine (data not shown) also were found in invadopodia (Fig. 2 *C* and *D*). The localization of endogenous ARF6 along with these previously identified components of invadopodia suggested that endogenous ARF6 is a bona fide component of invadopodia and may have a functional role in their formation.

**The GTPase Cycle of ARF6 Regulates Invasion.** To determine the functional significance of the distribution of ARF6 in invadopodia, we examined the effect of disrupting the ARF6 GTPase cycle on cell invasion. For these studies, cells were transfected with HA-tagged expression plasmids encoding the constitutively active, GTPase-deficient mutant of ARF6, ARF6(Q67L), or the dominant negative mutant of ARF6, ARF6(T27N). LOX cells were then seeded on fluorescently labeled, gelatin-coated coverslips and were allowed to invade for 24 h. After fixation, cells were permeablized and immunofluorescently labeled for HA. As previously described for other cell types, ARF6(Q67L), the ARF6-GTP mutant, was diffuse throughout the cell with increased localization at the cell

surface, and in invading cells, similar to endogenous ARF6, we found that ARF6(Q67L) was present also in invadopodia (Fig. 3 *A* and *B*). The invading cells appeared more rounded and ≈3–5% of ARF6(Q67L)-transfected cells created "degradation trails." These trails appeared to be formed as cells first invaded down into the gelatin and then continued to degrade through the matrix while moving horizontally (Fig. 3 *C* and *D*; also see Fig. 7, which is published as supporting information on the PNAS web site). This phenotype was not observed in nontransfected cells, and it suggested a more aggressive invasive phenotype for ARF6(Q67L)-transfected cells. In marked contrast, cells expressing the dominant negative ARF6 mutant, ARF6(T27N), remained spread on the gelatin matrix and did not form invadopodia or degrade gelatin (Fig. 3 *E* and *F*). ARF6(T27N) was localized predominantly to the perinuclear cytoplasm. This effect of the ARF6 mutants on cell-invasion capacity was not restricted to melanoma cells but was also observed in the breast tumor cell line MDA-MB-231 (see Fig. 3*G*). In the latter cell line, expression of ARF6(Q67L) resulted in large degradation patches underneath invading cells. Expression of ARF6(T27N) significantly attenuated invasion relative to nontransfected cells, but this inhibition was not complete, and small degradation spots were observed underneath ARF6(T27N)-expressing cells. Because ARF6 appeared to exert more stringent control on

the invasive potential of LOX cells, subsequent studies were performed by using the LOX cell line.

To quantify the invasion efficiencies of LOX cells expressing ARF6 mutants, the percentage of transfected cells with gelatin degradation underneath them were counted and compared to the percentage of nontransfected cells that were degrading gelatin. We found that both ARF6 mutants had a profound effect on LOX cell invasion. As seen in Fig. 3G, expression of ARF6(Q67L) promoted gelatin degradation by 5-fold compared to mock-transfected cells, whereas expression of ARF6(T27N) almost completely inhibited gelatin degradation and invasion (Fig. 3H). These data indicate a requirement for activated ARF6 in cell invasion.

The structure or number of invadopodia did not appear to be different in cells expressing ARF6-GTP mutant as compared to nontransfected invading cells. It is likely that the rate of turnover of invadopodia is significantly higher in ARF6(Q67L)-expressing cells, leading to a more invasive phenotype. It should be noted that actin foci were also observed at the ventral surface of ARF6(T27N)-expressing cells (see Fig. 8, which is published as supporting information on the PNAS web site). Taken together the above findings suggest that ARF6 activation might serve to control invadopodia formation.

ARF6 Is Required for Invasion Induced by Growth Factors. We investigated whether activated ARF6 might also mediate cell invasiveness induced by a physiologically relevant stimulus. Normal melanocytes require paracrine growth factors from surrounding keratinocytes for proliferation, migration, and survival (20, 21). In contrast, melanoma cells predominantly use autocrine mechanisms and become autonomous (21). Many of the autocrine growth factors up-regulated in melanoma include ligands of receptor tyrosine kinases such as HGF, bFGF (basic fibroblast growth factor), and EGF (epidermal growth factor) as well as G-protein coupled receptor ligands such as α-MSH (α-melanocyte stimulating hormone) (22). We examined the effect of the dominant negative ARF6 mutant on HGF-induced invasion. For these studies, cells transfected with plasmid encoding ARF6(T27N), or those that were mock-transfected, were plated on gelatin and treated with (or without) HGF as described above. As seen in Fig. 4A, HGF treatment increased cell invasiveness but not in the presence of ARF6(T27N). These findings indicate that ARF6 is required for events downstream of growth factor-signaling that lead to melanoma cell invasion.

These findings led us to examine whether the activation of endogenous ARF6 was increased upon treatment with HGF. Using a biochemical ARF6-GTP pull-down assay recently developed in our laboratory (14), we examined the levels of activated endogenous ARF6-GTP in HGF-treated and untreated cells. As shown in Fig. 4B, endogenous ARF6-GTP levels were significantly increased in "stimulated" cells relative to untreated cells. Thus, there appears to be a direct correlation between ARF6 activation and the acquisition of invasive potential.

ARF6 Regulates ERK Activation in LOX Cells. There is now substantial evidence that the activation of the Ras/Raf/MEK/ERK pathway is vital to melanoma cell invasion (23). The constitutive activation of ERK, a member of the MAPK family, has been identified in almost all invasive melanoma tissues and cell lines tested (23, 24). Furthermore, increased levels of phosphorylated ERK have been associated with increased cell motility, matrix metalloproteinase production, and invasion (3). We therefore analyzed the role of ERK in ARF6-regulated melanoma cell invasion. To this end, we first examined the distribution of phosphorylated ERK in cells expressing the GTP- and GDP-bound mutants of ARF6. Using an antibody that specifically recognizes the dually phosphorylated, activated form of ERK, we found that activated ERK localizes to invadopodia along with ARF6 (Fig. 5 A and B). Unexpectedly, we also found that the relative levels of phosphorylated ERK were
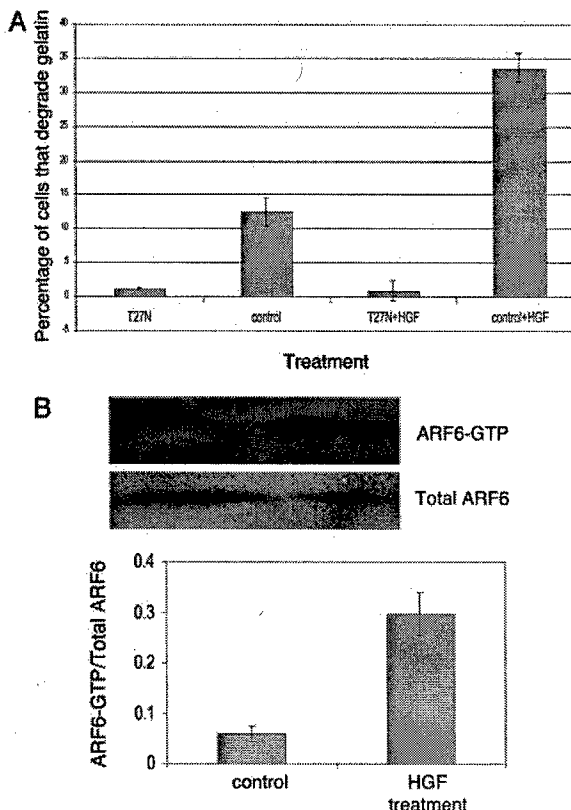
Fig. 4. ARF6 activation is required for and occurs during HGF-induced invasion. (A) LOX cells were transfected with plasmids as indicated. Cells plated on CFDSE-labeled gelatin were treated with (or without) 40 ng/ml HGF for 1 h. The percentage of transfected and nontransfected cells with gelatin degradation underneath them was calculated. (B) LOX cells were seeded on gelatin-coated tissue culture dishes and treated with or without HGF as described above. Equal amounts of cells lysates from each experimental condition were incubated with GST-MT2 beads to analyze the level of endogenous ARF6-GTP by using procedures previously described (14). Bound ARF6-GTP was visualized by Western blot analysis by using an anti-ARF6 mouse monoclonal antibody. The band densities were measured by using the enhanced UltroScan XL Laser Densitometer (Pharmacia) and the ratio of ARF6-GTP to total ARF6 was calculated. A representative immunoblot of three independent experiments is shown.

significantly higher in ARF6(Q67L)-expressing cells, and significantly lower in ARF6(T27N)-cells compared with nontransfected cells (Fig. 5 C–H). We then examined the effect of ARF6 on ERK phosphorylation as well as total ERK levels by using Western blotting procedures. To achieve higher efficiencies of transfection required for the latter set of studies, cells were transfected by using a liposome-based reagent. The latter protocol resulted in 30–40% cell transfection efficiencies. We observed that expression of ARF6(Q67L) augmented ERK activation, whereas the inhibitory effect of ARF6(T27N) on basal levels of ERK activation was not as evident as described above, but likely was masked because of endogenous phospho-ERK in nontransfected cells. However, expression of dominant negative ARF6 significantly inhibited HGF-enhanced ERK activation (Fig. 5I). Expression of ARF6 mutants had no effect on total ERK levels. Taken together, these data suggest a previously uncharacterized role for ARF6 in ERK activation.

Inhibition of ERK Signaling Blocks ARF6(Q67L)-Induced Invasion. Next, we investigated whether inhibiting ERK phosphorylation would prevent ARF6(Q67L)-induced invadopodia formation and gelatin degradation. MEK functions directly upstream of ERK, so inhib-
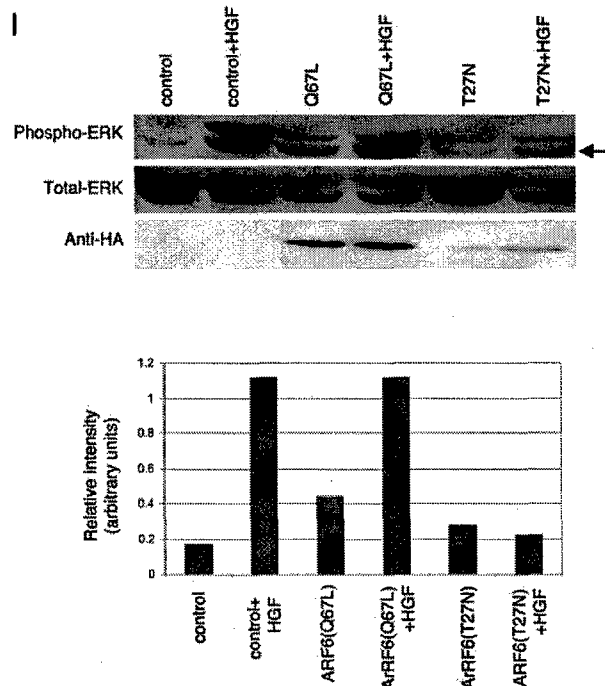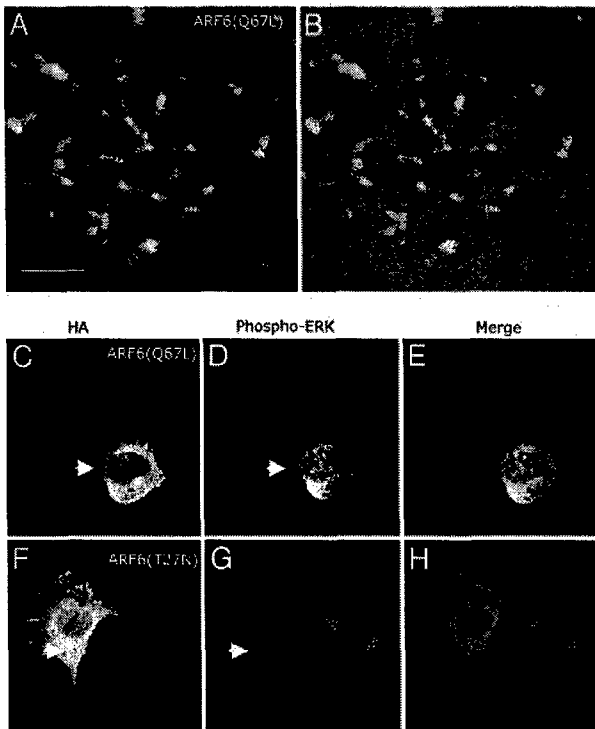
Fig. 5. Activated ARF6 partially colocalizes with activated ERK in invadopodia, and the ARF6 GTPase cycle regulates ERK activation. Cells were transfected as indicated and seeded on CFDSE-labeled gelatin and allowed to invade. Cells were immunofluorescently labeled for HA and/or phosphorylated ERK as indicated. These images were pseudocolored for better visualization of colocalization between ARF6 (red) and phospho-ERK (green). CFDSE-labeled gelatin is pseudo-colored blue. (A and B) Images shown here are single confocal sections at the tips of invadopodia of invading ARF6(Q67L)-expressing cells. A is the same as B except that A does not show gelatin staining. (C–H) These images are confocal sections taken along the cell body to better visualize the differences in phospho-ERK levels. Cells were transfected with ARF6(Q67L)-HA (C–F) or ARF6(T27N)-HA (D–G) and labeled for HA or phospho-ERK as indicated. As seen, ARF6(Q67L)-transfected cells have increased levels of activated ERK (arrows), whereas ARF6(T27N)-transfected cells have decreased levels of activated ERK (arrows) compared with other untransfected cells in the same field. (Bar = 10 μm.) (I) LOX cells transfected with plasmids expressing ARF6(Q67L) or ARF6(T27N) or transfected with empty plasmid as control, were plated on gelatin-coated tissue culture dishes, and treated with or without 40 ng/ml HGF for 30 min and lysed. Equal amounts of cell lysates were resolved by SDS/PAGE followed by probing with antisera directed specifically against total ERK, phospho-ERK, or HA. Representative immunoblots of three independent experiments are shown. The relative intensity of lower phospho-ERK band (arrow) was assessed by densitometric scanning.

iting MEK activation will also inhibit ERK activation (25). Thus, LOX cells were transfected with ARF6(Q67L) or mock-transfected and allowed to invade CFDSE-labeled gelatin in the presence of a 18 μM concentration of the MEK inhibitor PD98059 for 24 h. We found that inactivation of MEK abolished ARF6(Q67L)-induced cell invasion and that, noticeably, the cells exhibited a flattened and spread morphological phenotype similar to cells expressing ARF6(T27N), the dominant negative ARF6 mutant (Fig. 6 A and B). PD98059-treated cells also exhibited actin foci at the ventral surface of cells (data not shown), suggesting that ERK activation occurs downstream of ARF6 to facilitate invadopodia formation from sites at the ventral cell surface. Furthermore, quantitation of invasion efficiencies by scoring the percentage of cells exhibiting gelatin degradation underneath them showed that treatment of PD98059 abolished basal as well ARF6(Q67L)-induced cell invasion (Fig. 6C).

To complement the above investigations, we examined the effect of coexpressing a dominant negative MEK-1 mutant, MEK-1S218A, with ARF6(Q67L), and a constitutively activated MEK-1 mutant, S218/222D, with ARF6(T27N). Dually transfected cells that exhibited gelatin degradation underneath them were scored. As seen in Fig. 6C, coexpression of dominant negative MEK completely abolished the invasive capacity of ARF6(Q67L)-expressing cells. In contrast, coexpression of dominant negative ARF6(T27N) had no effect on the invasive capacity of cells expressing constitutively activated MEK. Taken together, these

studies indicate that ARF6(Q67L) promotes cell invasion at least in part by activating ERK and that ERK activation is essential for melanoma cell invasion.

Discussion

In this study, we have described a critical role for ARF6 in the process of melanoma cell invasion. We have shown that ARF6 regulates invasion in a manner that depends on its GTPase cycle. Sustained activation of ARF6 through the expression of ARF6(Q67L) augmented the invasive potential of the melanoma cell line, LOX, and the expression of a dominant negative ARF6 mutant obliterated cell invasion capacity. In addition to linking ARF6 with the regulation of invasion, this study has also demonstrated a previously unidentified ERK-coupled signaling pathway by which ARF6 exerts its effect on invading cells. Expression of the active form of ARF6 up-regulated the total levels of phosphorylated ERK, whereas expression of the dominant negative mutant of ARF6 down-regulated phospho-ERK levels. Furthermore, we found that ERK activation is essential for ARF6-regulated melanoma invasion.

Although there is accruing evidence that growth factor signaling leading to ERK activation is vital, and even decisive, for the highly metastatic behavior of melanoma, much remains to be understood regarding the molecular events that result in increased ERK activation downstream of growth factor activation during melanoma progression. Activating mutations in N-Ras(Q61L) and
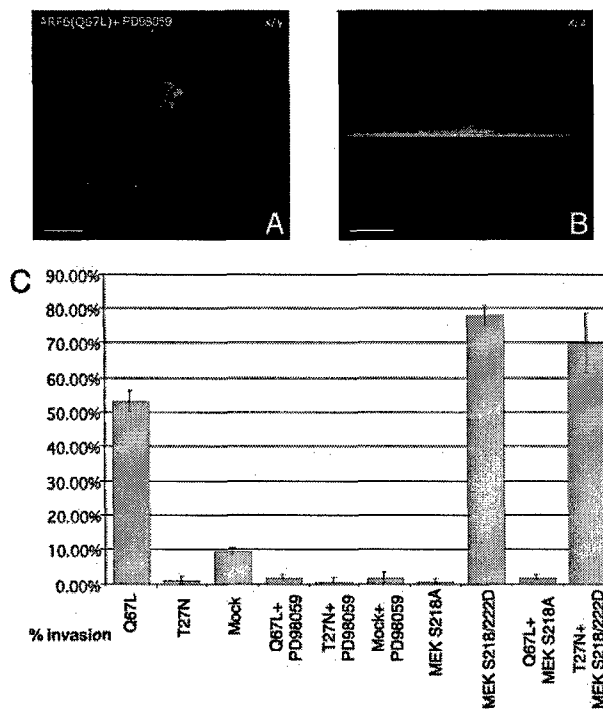
Fig. 6. Inactivation of MEK blocks ARF6-GTP-induced cell invasion. (*A* and *B*) ARF6(Q67L)-transfected cells were seeded on CFDSE-labeled, gelatin-coated coverslips and allowed to invade in the presence of the MEK inhibitor, PD98059. Cells were fixed, permeablized, and immunofluorescently labeled for HA. *A* and *B* are taken along the *x/y* and *x/z* axis respectively. (Bar = 10 μm.) (*C*) LOX cells were singly or dually transfected with plasmids encoding ARF6 and MEK-1 mutants as indicated. Cells were seeded on gelatin and treated with or without PD98059 as indicated. The percentage of single or dually transfected cells exhibiting gelatin degradation underneath them was scored.

B-Raf(V599E) have been found in the majority of melanoma cell lines and tissues tested (23). (The presence of these mutations in the LOX line is not reported.) However, even when the activating mutation in Ras was not detected in some melanoma cell types, it was still constitutively active. Furthermore, inhibitors of growth factor signaling inhibited ERK activation to varying extents in a variety of melanoma cell lines tested (24). Thus, autocrine signaling and B-Raf activation contribute to increased ERK activation to varying degrees in melanoma.

The regulation of ERK activation through ARF6 is a newly characterized signaling pathway and, in light of the above, could potentially be a critical determinant in melanoma progression. There are a number of pathways by which ARF6 activation may regulate ERK signaling. One interesting mechanism by which ARF6 could increase ERK activation is via its regulation of phospholipid metabolism. Previous studies have shown that PA, a product of PLD metabolism, can stimulate ERK activation (26). Because ARF6 activates PLD (8, 10) this is a feasible means by which ARF6 could regulate ERK activation. Second, ARF6 regulation of PIP2 synthesis (27) could affect ERK activation at sites of invadopodia through the recruitment of scaffolding proteins such as MEKK1, which holds Raf, MEK, and ERK together enabling them to activate one another (28). Interestingly in this regard, we observe a significant build up of PIP2 at invadopodia in ARF6(Q67L)-transfected cells (our unpublished observations). ARF6 may also promote ERK activation through interaction with the paxillin kinase linker (PKL), which has an ARF GTPase-activating protein domain and forms a stable trimolecular complex with PAK and PIX (29). PAK, a direct downstream target of Rac1, is capable of activating Raf and stimulating the Raf-MEK-ERK cascade (30, 31). These are just a few avenues that should be explored in future research.

The studies described here, which characterize an important role for ARF6 in the invasion process, further clarify the pathways that regulate tumor cell invasion. The process of melanoma cell invasion is similar to that observed in bone resorption by osteoclasts, invasion by immune cells, and the initial movement of neural crest cells to the skin before they differentiate into melanocytes, as well as invasion by other types of cancer cells. Thus, ARF6 may prove to be important for these invasive processes as well. Also, by identifying a link between ERK signaling and ARF6, this study paves the way for future investigations on the role of ARF6 in other events regulated by ERK, such as the cell cycle, synaptic and neuronal plasticity, and gene expression.

1. Basbaum, C. B. & Werb, Z. (1996) *Curr. Opin. Cell. Biol.* **8**, 731–738.
2. Hernandez-Alcoceba, R., del Peso, L. & Lacal, J. C. (2000) *Cell Mol. Life Sci.* **57**, 65–76.
3. Klemke, R. L., Cai, S., Giannini, A. L., Gallagher, P. J., de Lanerolle, P. & Cheresh, D. A. (1997) *J. Cell Biol.* **137**, 481–492.
4. Bowden, E. T., Barth, M., Thomas, D., Glazer, R. I. & Mueller, S. C. (1999) *Oncogene* **18**, 4440–4449.
5. Chen, W. T. (1996) *Enzyme Protein* **49**, 59–71.
6. Coopman, P. J., Do, M. T., Thompson, E. W. & Mueller, S. C. (1998) *Clin. Cancer Res.* **4**, 507–515.
7. Chen, W. T., Lee, C. C., Goldstein, L., Bernier, S., Liu, C. H., Lin, C. Y., Yeh, Y., Monsky, W. L., Kelly, T., Dai, M., *et al.* (1994) *Breast Cancer Res. Treat.* **31**, 217–226.
8. Chavrier, P. & Goud, B. (1999) *Curr. Opin. Cell Biol.* **11**, 466–475.
9. Palacios, F., Price, L., Schweitzer, J., Collard, J. G. & D'Souza-Schorey, C. (2001) *EMBO J.* **20**, 4973–4986.
10. Santy, L. C. & Casanova, J. E. (2001) *J. Cell Biol.* **154**, 599–610.
11. Monsky, W. L., Lin, C. Y., Aoyama, A., Kelly, T., Akiyama, S. K., Mueller, S. C. & Chen, W. T. (1994) *Cancer Res.* **54**, 5702–5710.
12. Nakahara, H., Mueller, S. C., Nomizu, M., Yamada, Y., Yeh, Y. & Chen, W. T. (1998) *J. Biol. Chem.* **273**, 9–12.
13. Boshans, R. L., Szanto, S., van Aelst, L. & D'Souza-Schorey, C. (2000) *Mol. Cell. Biol.* **20**, 3685–3694.
14. Schweitzer, J. K. & D'Souza-Schorey, C. (2002) *J. Biol. Chem.* **277**, 27210–27216.
15. D'Souza-Schorey, C., van Donselaar, E., Hsu, V. W., Yang, C., Stahl, P. D. & Peters, P. J. (1998) *J. Cell Biol.* **140**, 603–616.
16. Peters, P. J., Gao, M., Gaschet, J., Ambach, A., van Donselaar, E., Traverse, J. F., Bos, E., Wolffe, E. J. & Hsu, V. W. (2001) *Traffic* **2**, 885–895.
17. Aikawa, Y. & Martin, T. F. (2003) *J. Cell Biol.* **162**, 647–659.
18. Radhakrishna, H. & Donaldson, J. G. (1997) *J. Cell Biol.* **139**, 49–61.
19. Mueller, S. C., Yeh, Y. & Chen, W. T. (1992) *J. Cell Biol.* **119**, 1309–1325.
20. Lazar-Molnar, E., Hegyesi, H., Toth, S. & Falus, A. (2000) *Cytokine* **12**, 547–554.
21. Halaban, R. (1996) *Semin. Oncol.* **23**, 673–681.
22. Bogenrieder, T. & Herlyn, M. (2002) *Crit. Rev. Oncol. Hematol.* **44**, 1–15.
23. Smalley, K. S. (2003) *Int. J. Cancer* **104**, 527–532.
24. Satyamoorthy, K., Li, G., Gerrero, M. R., Brose, M. S., Volpe, P., Weber, B. L., Van Belle, P., Elder, D. E. & Herlyn, M. (2003) *Cancer Res.* **63**, 756–759.
25. Cobb, M. H. (1999) *Prog. Biophys. Mol. Biol.* **71**, 479–500.
26. Hong, J. H., Oh, S. O., Lee, M., Kim, Y. R., Kim, D. U., Hur, G. M., Lee, J. H., Lim, K., Hwang, B. D. & Park, S. K. (2001) *Biochem. Biophys. Res. Commun.* **281**, 1337–1342.
27. Honda, A., Nogami, M., Yokozeki, T., Yamazaki, M., Nakamura, H., Watanabe, H., Kawamoto, K., Nakayama, K., Morris, A. J., Frohman, M. A. & Kanaho, Y. (1999) *Cell* **99**, 521–532.
28. Karandikar, M., Xu, S. & Cobb, M. H. (2000) *J. Biol. Chem.* **275**, 40120–40127.
29. Brown, M. C., West, K. A. & Turner, C. E. (2002) *Mol. Biol. Cell* **13**, 1550–1565.
30. Li, W., Chong, H. & Guan, K. L. (2001) *J. Biol. Chem.* **276**, 34728–34737.
31. Zang, M., Hayne, C. & Luo, Z. (2002) *J. Biol. Chem.* **277**, 4395–4405.
32. Hashimoto, S., Onodera, Y., Hashimoto, A., Tanaka, M., Hamaguchi, M., Yamada, A. & Sabe, H. (2004) *Proc. Natl. Acad. Sci. USA* **101**, 6647–6652.

Detection of Plasminogen Fragments in Urine of Patients with Colon Cancer or Breast Cancer

Mary Prorok
Melanie E. DeFord
Rudolph M. Navari, M.D., Ph.D.
Francis J. Castellino, Ph.D.

Abstract

The identification of molecular markers and proteomic patterns in the inception and progression of colon cancer is a major goal in the management of this disease. In the search for sensitive and accurate markers of colon cancer, our initial efforts with cancer patients were hampered by irreproducibility. We have recently redirected our efforts towards the study of transgenic mice (APCMin/+), which develop multiple intestinal adenomas that clinically mimic those observed in patients with familial adenomatous polyposis. In contrast with cancer patients, $APC^{Min/+}$ mice represent highly tractable and contollable models for study. Additionally, a recent comparative study of the transcriptional profile of APCMin/+ intestinal epithelial tissue characterized at normal, adenomatous, and cancerous phases, represents a rich source of potential biomarker candidates. One transcript, cathepsin E (cat E), manifests particularly high relative expression in the epithelium of adenomas and carcinomas versus normal tissue. Using commercially available antibodies to murine cat E, we have confirmed, by immunohistochemistry, the presence of high levels of this protein in the adenomatous and cancerous phenotype. From Western immunoblot analyses, the urine of tumor-bearing mice also appears to contain higher levels of cat E, and fragments thereof. These results preliminarily support the viability of the $APC^{Min/+}$ gene list as a primary reservoir of tumor marker candidates, and authenticate the relationship between transcript abundance and protein levels in transformed tissue. Preliminary immunohistochemical results suggest that increased levels of catE are also present in human colon cancers.

Subject Terms: colon cancer, transgenic mice, APCMin/+, cathepsin

INTRODUCTION

The identification of molecular markers and proteomic patterns in the inception and progression of colon cancer is a major goal in the management of this disease. In the search for sensitive and accurate markers of colon cancer, our initial efforts with cancer patients were hampered by irreproducibility. We have recently redirected our efforts towards the study of $APC^{Min/+}$ mice (heterozygous for a chain-termination mutation in the 15th exon of the APC gene). These animals develop multiple intestinal adenomas that clinically mimic those observed in patients with familial adenomatous polyposis. In contrast with cancer patients, $APC^{Min/+}$ mice represent highly tractable and contollable models for study. Additionally, a recent comparative study of the transcriptional profile of $APC^{Min/+}$ intestinal epithelial tissue characterized at normal, adenomatous, and cancerous phases (Paoni et al., 2003), represents a rich source of potential biomarker candidates. One transcript, cathepsin E (catE), manifests particularly high relative expression in the epithelia of adenomas and carcinomas versus normal tissue. Using commercially available antibodies to murine catE, we have confirmed, by immunohistochemistry, the presence of high levels of this protein in the transfromed phenotype. From Western immunoblot analyses, the urine of tumor-bearing mice also appears to contain higher levels of catE, and fragments thereof. These results preliminarily support the viability of the $APC^{Min/+}$ gene list as a primary reservoir of tumor marker candidates, and authenticate the relationship between transcript abundance and protein levels in transformed tissue. Preliminary immunohistochemical results suggest that increased levels of catE are also present in human colon cancers.

BODY

Three tasks outlined in the original statement of work were as follows: Task 1) detection of urinary kringles in patients with colon cancer and breast cancer; Task 2) establishing the relationship of urinary kringle levels with the type and stage of disease; Task 3) implementing urinary kringles as tumor markers. In short, using Western immunoblot analysis, we observed a high degree of variability in kringle levels in the urine of cancer patients and healthy control subjects alike and were unable to correlate the presence of plasminogen (Pg) and/or Pg fragments (including angiostatin) with any stage of disease in patients with breast or colon cancer. The distinct lack of correlation was also the basis of a publication that came to our attention (Linder-Stragliotto et al., 2002) in which the authors reported a strong dependence of urinary angiostatin concentration in cancer patients with impaired renal function, but no dependence on those patients with normal kidney function. These findings indicate that Pg and Pg fragments hold little clinical promise as reliable tumor markers.

We decided to redirect our efforts towards tumor marker identification using the APC$^{Min/+}$ mouse model. These mice are heterozygous for a chain-termination mutation in the 15th exon of the APC (adenomatous polyposis coli) gene and develop multiple intestinal polyps that are clinically relevant to those detected in patients with familial adenomatous polyposis (Moser et al., 1990). These mice were the recent focus of a publication coauthored by one of us (FJC) on the transcriptional profiling of the intestinal epithelium of APC$^{Min/+}$ mice in the transition from normal to adenomatous to cancerous states (Paoni et al., 2003). The availability of these data, coupled our ready access to APC$^{Min/+}$ mice (colonies are housed and maintained in the Keck Center for Transgene Research at the University of Notre Dame) render these animals as highly attractive models for biomarker investigation in intestinal cancers relevant to the human experience. We have therefore reformulated the hypotheses of this funded work as follows: *1) transcripts with high expression in adenomas and carcinomas versus normal intestinal tissue will likely (but not necessarily) correlate at the translational (protein) level; 2) confirmed higher levels of these proteins in the intestines may reflect higher levels in plasma, urine or feces-- criteria for clinically viable tumor markers.* Examination of the transcript list has yielded several genes that are differentially expressed in normal and dysplastic tissue in APC$^{Min/+}$ mice. Particularly striking is cathepsin E (catE), an intracellular aspartic protease involved in the degradation of proteins important to cellular proliferation and tissue homeostasis (Tsukuba et al., 2000). When compared with normal epithelial cells, catE displays a 125- and 106-fold increase in mRNA levels in adenomas and carcinomas, respectively.

In testing the first hypothesis, i.e., if catE protein levels in adenomas and carcinomas reflect transcript upregulation, we performed immunohistochemistry on numerous tissue sections from wild-type (n = 21) and APC$^{Min/+}$ (n = 33) mice. Areas corresponding to dysplasia were confirmed by a veterinary pathologist (Dr. Mark Suckow, University of Notre Dame), who was not informed of genotype prior to inspection of the samples. For all tissue sections examined, wild-type intestinal epithelium and normal tissue from the APC$^{Min/+}$ mice displayed faint background immunostaining, while sections corresponding to the adenomatous and cancerous lesions in the APC$^{Min/+}$ mice, *in all cases*, displayed intense, often dramatic, staining. Representative immunohistochemical analyses are shown in Fig. 1. These data confirm the presence of high catE protein levels in dysplasic regions of APC$^{Min/+}$ mice and are, at a qualitative level, consistent with catE transcript abundance as determined from the gene profiling data.
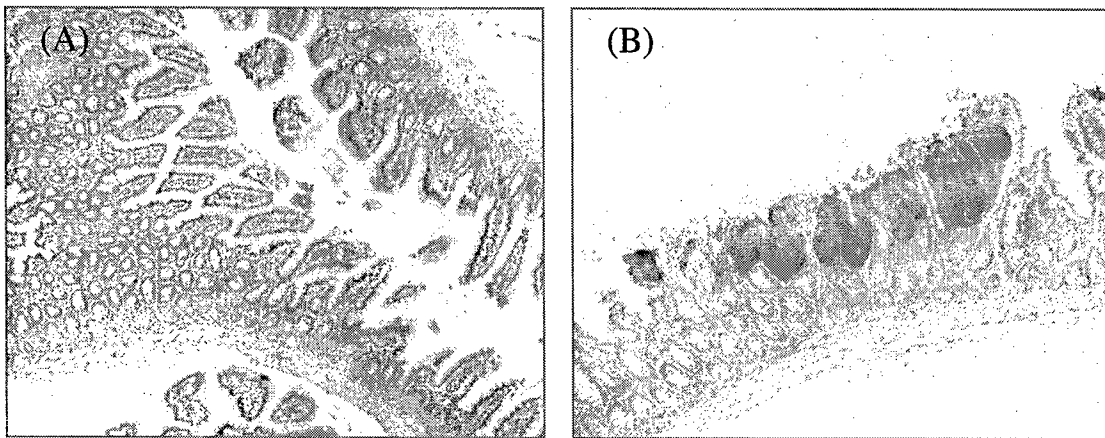
Fig. 1. Immunohistochemical analyses of intestinal tissue from a (A) wild-type and (B) APC$^{Min/+}$ mouse. Mice were sacrificed after 90 days and segments of intestine were fixed in formalin and paraffin-embedded. Sections (4 μm) were incubated overnight with a polyclonal antibody to catE (goat anti-mouse, R & D Systems, Inc., Minneapolis, MN). Visualization was accomplished with the DakoCytomation (Carpinteria, CA) PAP system.

After establishing that elevated levels of catE are present in adenomas and carcinomas of APC$^{Min/+}$ mice, we next examined whether this phenomenon might translate into an increase in catE and/or catE fragments in urine. A representative Western immunoblot of urine samples from wild-type and APC$^{Min/+}$ mice, developed with a polyclonal antibody to murine catE, is shown in Fig. 2. Bands corresponding to the dimeric (108 & 86 kDa) and monomeric (46 kDa) forms of catE were observed in the urine of both wild-type and APC$^{Min/+}$ 90-day old mice. Qualitative inspection of this and other blots indicated a marked increase in the intensity of the 46 kDa band in the APC$^{Min/+}$ urine specimens, compared to samples from wild-type animals.
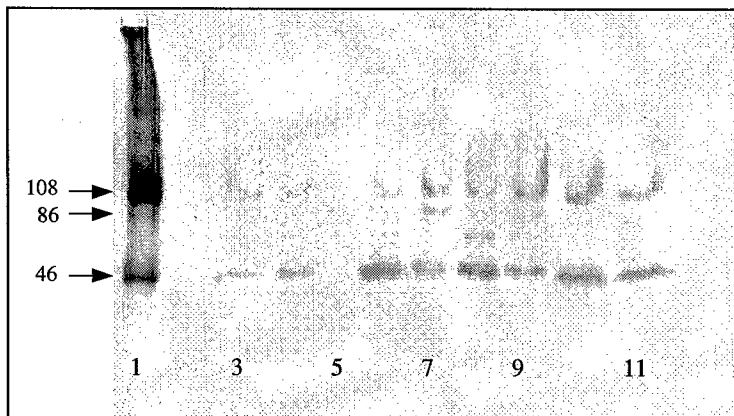

Fig. 2. Detection of urinary catE by Western immunoblot analysis following SDS-PAGE of urine samples from 90-day old wild-type (lanes 3 and 4) and APC$^{Min/+}$ mice (lanes 6-11). Membranes were developed with the same polyclonal antibody to catE employed in the immunohistochemical studies. Recombinant murine catE was loaded in lane 1. The indicated molecular weights (kDa) of the various forms of catE were previously determined from separate SDS-PAGE analysis of the recombinant protein run in tandem with ProSieve protein markers (Cambrex, East Rutherford, NJ).

Densitometric analysis for the quantification of monomeric catE band intensities revealed a statistically significant (p = 0.0012) increase in the amount of monomeric catE present in APC$^{Min/+}$ (n = 33) *versus* wild-type (n = 21) urine (Fig. 3A). No significant differences in monomeric catE concentrations were observed between females and males in either the wild-type or APC$^{Min/+}$ group. A similar analysis was conducted on 60-day old mice and revealed comparable levels of catE, irrespective of genotype. (Fig 3B). Because the tumor counts in 60-day old APC$^{Min/+}$ mice are approximately 50% of that routinely found in 90-day old mice (Suckow, et al., 2004), we conclude that the increase in urinary catE observed in 90-day old APC$^{Min/+}$ mice is directly attributable to an increase in tumor proliferation, rather than an inherent consequence of the APC$^{Min/+}$ genotype.
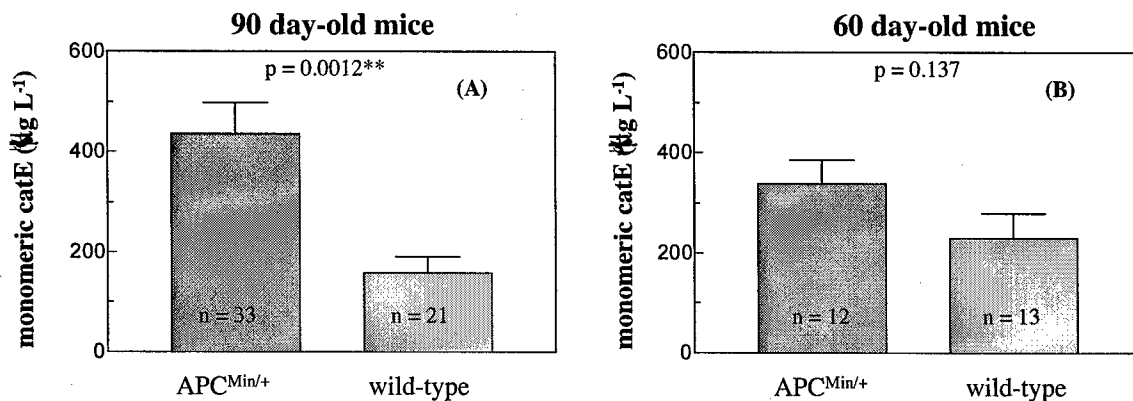

Fig. 3. Results of NIH Image analysis of the 46 kDa anti-catE positive protein bands from Western blots of APC$^{Min/+}$ and wild-type mouse urine. **A.** Mean urine concentrations (± SEM) for 90-day old APC$^{Min/+}$ and wild-type mice; **B.** Mean urine concentrations (± SEM) for 60-day old APC$^{Min/+}$ and wild-type mice.

To determine whether human intestinal cancers display increased catE levels that parallel those observed with APC$^{Min/+}$ mice, we initiated a study of tumor specimens excised from patients diagnosed with colorectal cancer. (A collaboration with the Northern Indiana Cancer Research Consortium; normal and colonic tumor tissue specimens were obtained from patients who underwent elective surgical resections following diagnoses of colon cancer.) Our preliminary assessment revealed that 10 of the 21 individual patient specimens probed for immunoreactivity to anti-catE were moderately to strongly catE-positive. A representative section is shown in Fig. 4. Stained areas present pathologic features similar to those seen in the catE-positive APC$^{Min/+}$ mice sections, including abnormal mucosal architecture, crowding, prominent cellular atypia, and elongated nuclei. These immunohistochemical analyses suggests that catE may represent a reliable biological marker in the diagnosis and prognosis of the human disease.
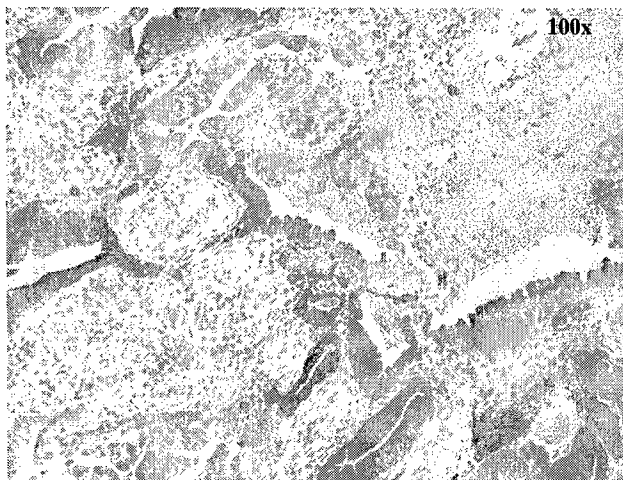
Fig. 4. Immunohistochemical analysis of a section of submucosa from an excised human colonic tumor (invasive malignant glandular neoplasm). Staining was carried out with a polyclonal antibody to recombinant human catE. Stained areas are consistent with marked dysplasia. Areas of normal morphology do not exhibit appreciable staining.

KEY RESEARCH ACCOMPLISHMENTS

The presence of increased catE in the dysplasic tissue of $APC^{Min/+}$ mice was confirmed by immunohistochemistry and is consistent with the relative mRNA levels determined from transcriptional profiling.

Immunoblot inspection and densitometric analyses of the urine of $APC^{Min/+}$ and wild-type mice indicates a statistically significant increase of catE fragments in transgenic mouse urine. These data suggest that catE may be a reliable urinary marker of tumor progression.

Preliminary immunohistochemical analyses suggests that catE may represent a reliable biological marker in the diagnosis and prognosis of the human disease.

REPORTABLE OUTCOMES

Carlo A. Perrina, Melanie E. DeFord, Francis J. Castellino, Rudolph M. Navari, and Mary Prorok "Biomarker Discovery in the Urine of Subjects with Colon Cancer" Poster Presentation, Walther Cancer Center Retreat, August 2003, Indianapolis, IN.

Lizette Busquets, Melanie E. DeFord, Francis J. Castellino, Rudolph M. Navari, Mark Suckow and Mary Prorok "Cathepsin E is a Specific Marker of Dysplasia in $APC^{Min/+}$ Mouse Intestine." Poster Presentation, Walther Cancer Institute Scientific Retreat, August 2004, University of Notre Dame, Notre Dame, IN.

Lizette Busquets, Melanie E. DeFord, Francis J. Castellino, Rudolph M. Navari, Mark Suckow and Mary Prorok "Cathepsin E is a Specific Marker of Dysplasia in APC$^{Min/+}$ Mouse Intestine" Submitted.

CONCLUSIONS

The availability of the gene expression profile of normal, adenomatous, and cancerous intestinal tissue of APC$^{Min/+}$ mice represents a rich source of potential biomarker candidates. We have identified one gene from the list, catE, which displays greatly increased mRNA levels in dysplasic tissue versus normal epithelia. Immunohistochemistry has confirmed the presence of high catE protein levels in adenomas and carcinomas. Increased levels of catE in the urine of diseased animals has been quantitatively confirmed and is statistically valid. Lastly, positive catE staining in human colon tumors suggest the possibility that catE may be a clinically useful biomarker in the diagnosis of human colon cancers.

Our immediate goals are to examine the urine and sera of colon cancer patients to determine the feasibility of catE as a biomarker of human disease. Development of ELISA-based methodology for catE screening in urine and sera is underway.

REFERENCES

Linder-Stragliotto, C., Strander, H., Munck-Wikland, E., and Sten-Linder, M. (2002) Low levels of endostatin in the urine from patients with malignant disease. *Tumor Biol.* **23**, 222-227.

Moser, A. R., Pitot, H.C., and Dove W.F. (1990) A dominant mutation that predisposes to multiple intestinal neoplasia in the mouse. *Science* **247**, 322-324.

Paoni, N. F., Feldman, M. W., Gutierrez, L. S., Ploplis, V. A., and Castellino, F. J. (2003) Transcriptional profiling of the transition from normal intestinal epithelia to adenomas and carcinomas in the APC$^{Min/+}$ mouse. *Physiol. Genomics* **15**, 228-235.

Suckow, M.A., Gutierrez, L.S., Risatti, C.A., Wolter, W.R., Taylor, R.E., Pollard, M., Navari, R.M., Castellino, F.J., and Paoni, N.F. (2004) The anti-ischemia agent ranolazine promotes the development of intestinal tumors in APC$^{(min/+)}$ mice. *Canc. Lett.* **209**, 165-169.

Tsukuba T., Okamoto,K., Yasuda, Y., Morikawa, W., Nakanishi, H., and Yamamoto, K. (2000) New functional aspects of cathepsin D and cathepsin E. *Mol. Cells* **10**, 601-611.

Project 5: Death Receptors as Mediators of Cell Death in Ovarian Granulosa Cells

Rudolph M. Navari, M.D., Ph.D.
Alan L. Johnson, Ph.D.

Abstract

Tumor Necrosis Factor-Related Apoptosis Inducing Ligand (TRAIL) is a naturally occurring cytokine that exhibits selective death-iducing effects on a variety of cancerous, but not normal, cell types, Given the paucity of information regarding the actions of TRAIL within the ovary, studies were conducted to characterize the biological actions of TRAIl in primary cultured granulose cells, human ovarian cancer epithelial cells, and human complement of intracellular adaptor and effector proteins reportedly responsible for mediating extrinsically initiated cell death, TRAIL treatment does not reduce cell viability. By contrast, TRAIL treatment of the human granulose tumor cell line, COV434, induces a small but significant reduction in cell viability after 24 h of culture. Importantly, combinatorial treatment of COV434 cells with cisplatin plus TRAIL produces a synergistic reduction in cell viability compared to either treatment alone. Furthermore, inhibition of protein synthesis (with cycloheximde) or inhibition of the protein kinase B/Akt cell survival pathway (with LY294006) promotes a similar synergistic action on TRAIL-induced apoptosis. Accordingly, we hypothesize that at least one short-term action of cisplatin is to interfere with cell survival signaling pathway(s) and the transcription/translation of cellular anti-apoptotic proteins.

Subject Terms: TRAIL, ovarian cancer, granulos cell tumors, apoptosis

DEATH RECEPTORS AS MEDIATORS OF CELL DEATH IN OVARIAN GRANULOSA CELLS

INTRODUCTION

Death Receptors (DRs) comprise a select receptor subset from the Tumor Necrosis Factor Receptor Superfamily (TNFRSF). Such receptors are recognized as important and specific mediators of programmed cell death (apoptosis) in a variety of cell types, and have been implicated in the pathogenesis of a wide variety of diseases ranging from osteoporosis to cancers. Significantly, activation of select DRs (e.g., DR4 and DR5) via the DR ligand, Tumor Necrosis Factor-Related Apoptosis Inducing Ligand (TRAIL), has been proposed for use in the clinical treatment of a variety of human cancers, including ovarian cancers. The potential for TRAIL treatment is derived from studies indicating that TRAIL is selective in killing cancerous, but not normal, cells. However, there is currently insufficient information relative to the efficacy and cellular mechanisms of action for this adjuvant treatment in ovarian cancers (especially granulosa cell tumors), or regarding the potential for nonspecific, adverse effects of TRAIL on the pool of undifferentiated ovarian follicles during the course of treatment for non-ovarian cancers. Consequences of the latter inevitably impair or preclude the future reproductive potential of the patient.

Ovarian granulosa cell tumors occur most frequently in juvenile and peri-/post-menopausal women, and are often diagnosed early because tumor-derived estrogen production is commonly presented by abnormal vaginal bleeding. Such tumors are most commonly treated by surgical excision, while advanced cases may be effectively treated with cisplatin-based therapeutics. Nevertheless, the survival rate following diagnosis at Stage III-IV is only 30% and the reocurrence rate after 10 and 20 years is significant (Fuller and Chu, 2004). Currently utilized chemotherapeutic agents induce cell death via an 'intrinsic' signaling pathway involving DNA damage or generation of reactive oxygen species, mitochondrial perturbations and eventual caspase activation. By comparison, TRAIL promotes apoptotic cell death via a receptor-mediated 'extrinsic' pathway that can directly activate caspase activity plus amplify caspase activation via the intrinsic mitochondrial pathway (for a review of extrinsic pathway signaling, see Özören and El-Deiry, 2003). Accordingly, combinatorial treatments that promote both extrinsic and intrinsic cell death pathways could provide a more effective initial treatment regime to maximize tumor reduction and minimize recurrent tumor development.

We have continued studies in primary granulosa cell cultures to establish mechanisms by which resistance to TRAIL-induced cell death is afforded. Such information will be useful

towards addressing the real potential for the development of
TRAIL-resistance in granulosa tumor cells. We have now
characterized in normal granulosa cells the expression of the
intracellular signaling proteins reportedly required for TRAIL-
induced apoptosis. Importantly, we have also begun to evaluate
cellular pathways by which TRAIL promotes apoptosis in the
unique human granulosa tumor cell lines, COV434 and KGN. These
studies represent the first to not only evaluate TRAIL
sensitivity in granulosa tumor cell lines, but also to directly
compare cellular mechanisms resulting in sensitivity/resistance
to TRAIL treatment in normal versus cancerous granulosa cells.

RESEARCH ACCOMPLISHMENTS (Year 2)

1. Normal Ovarian Follicle Granulosa Cells. Results from the
first year of studies determined that TRAIL treatment did not
decrease cell viability in primary cultured, normal granulosa
cells. These results are consistent with data from a variety of
non-ovarian cell types in which normal cells are resistant to
TRAIL-induced cell death. We next asked whether normal, primary
cultured granulosa cells lacked expression of one or more
critical components of the TRAIL intracellular signaling
pathway. We have previously documented the expression and
activity within normal granulosa cells of TRAIL (Johnson et al.,
unpublished), the TRAIL receptor (TVB; Bridgham and Johnson,
2002), and caspases-8, -9 and -3 (Johnson and Bridgham, 2002).
We have now confirmed mRNA expression for the TRAIL-Receptor
adaptor proteins, FADD, FLIP and RIP, and the cytosolic effector
protein, Bid (mRNA and protein), in freshly collected and
primary cultured hen granulosa cells (Fig. 1).
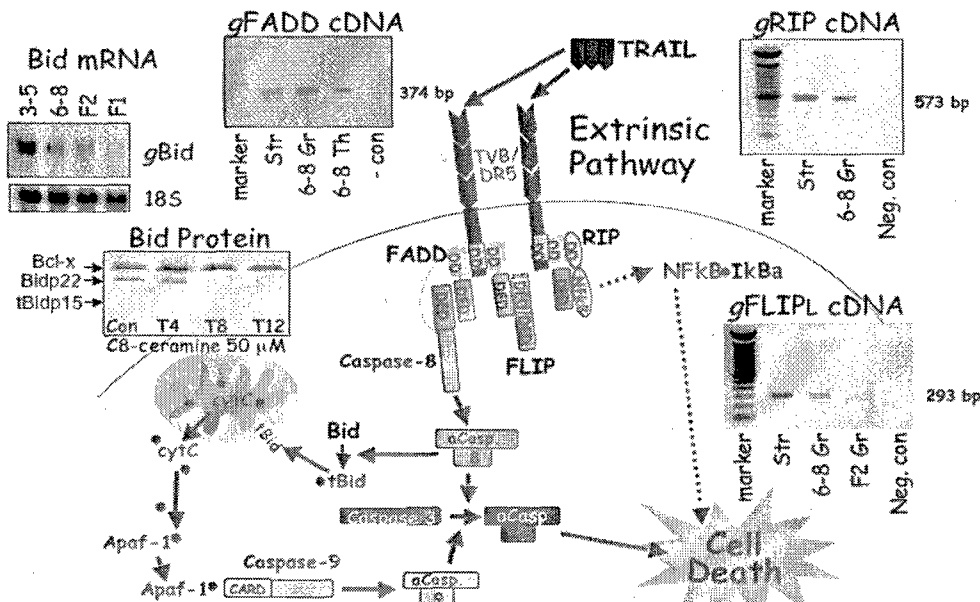
Figure 1. Receptor adaptor and effector proteins mediating or modulating the extrinsic
cell death pathway in normal hen granulosa cells. Str, ovarian stromal tissue; Gr,
granulosa cells, Theca, follicle theca tissue; 3-5,6-8,F2, F1, follicle size.

Johnson, A.L.

Accordingly, the inability of TRAIL to induce apoptotic cell death in normal granulosa cells cannot be simply attributed to the absence of a functional intracellular signaling pathway. Rather, we hypothesize that cell survival signaling pathways, particularly by protein kinase B/Akt (see Johnson *et al.*, 2001) normally provide resistance to TRAIL-induced cell death via the induced expression of FLIP and/or RIP. Studies to test this hypothesis are currently ongoing.

2. TRAIL responsiveness in the unique human granulosa tumor cell lines, COV434 and KGN. We have recently aquired in our laboratory the human granulosa tumor cell lines, COV434 (Zhang *et al.*, 2000) and KGN (Nishi et al., 2001). These two cell lines represent ideal model systems for comparison to normal granulosa cells primarily because, like normal cells, they express a functional FSH receptor and are steroidogenically competent. This latter aspect is of importance because a unique feature of granulosa cell tumors, *in situ*, is their capacity to produce estrogens (plus to a lesser extent, progestins and androgens). There is currently no published information available pertaining to either the sensitivity of established granulosa tumor cell lines to conventional chemotherapeutics (e.g., cisplatin) or to TRAIL treatment. Culture of COV434 cells with cisplatin (5 to 100 µM) induced cell death in a dose-dependent fashion (a maximal reduction in viability to 45% after only 24 h of culture; Fig 2). TRAIL treatment (100 ng/ml) also induced cell death after a 24 h culture, but the viability of cells was reduced by only 12% (P<0.05 versus control cultured cells). Importantly, however, the combination of cisplatin (at 25 µM) plus TRAIL treatment produced greater than an additive (synergistic) effect on reducing cell viability. A synergistic effect on cell killing was also observed with TRAIL treatment in combination with cycloheximide and the protein kinase B/Akt inhibitor, LY294006. Significantly, neither cycloheximide nor LY294006 reduced cell viability via significant caspase activation (as indicated by the relative absence of oligonucleosome formation [Fig. 2] or poly (ADP-ribose) polymerase (PARP) cleavage [Fig. 3]). By contrast, the combination of TRAIL treatment with either cycloheximide or LY294006 resulted in pronounced caspase activation (indicated by oligonucleosome formation) and subsequent apoptotic cell death. Taken collectively, these results suggest that preventing expression of a labile anti-apoptotic protein induced via a cell survival signaling pathway can provide for enhanced treatment efficacy by enhancing granulosa tumor cell apoptosis.

Studies during this one-year no-cost extension period have been initiated to evaluate TRAIL-induced cell death in the KGN cell line.

Johnson, A.L.

95
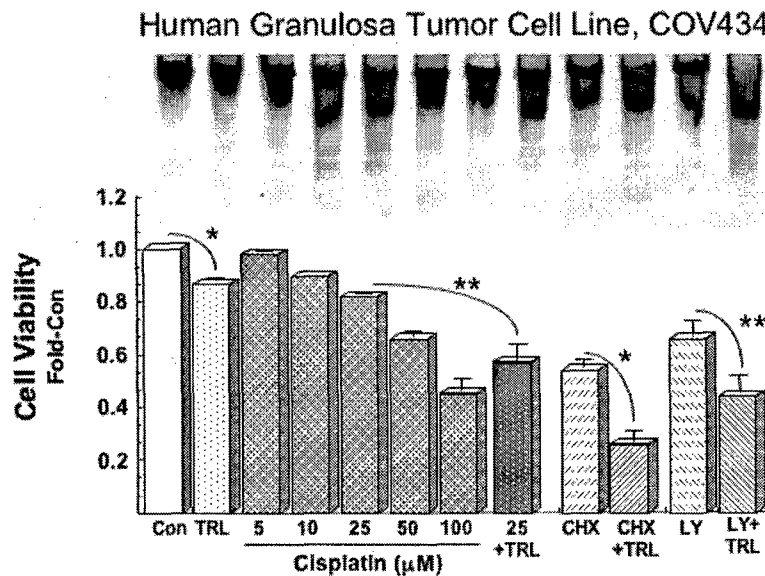
Figure 2. TRAIL (TRL) and cisplatin-induced cell death in the human granulosa tumor cell line, COV434 after a 24 h culture. Top panel: oligonucleosome formation (indicative of apoptotic cell death). Bottom panel: cell viability assay (Promega CellTiter 96 assay) showing a more than additive effect of TRL treatment when combined with cisplatin (25 μM), cycloheximide (CHX; 1 μg/ml) or the protein kinase B/Akt cell survival pathway inhibitor, LY294006 (LY; 50 μM). * denotes P<0.05 versus Control; ** denotes additive effect of TRL when used in a combinatorial treatment (P<0.05).

3. TRAIL responsiveness in the human ovarian surface epithelial caner cell line, PA-1.

We have previously determined (reported following the first year of funding) that the human surface epithelial cancer cell line, PA-1, is TRAIL-responsive. Furthermore, co-treatment with the protein synthesis inhibitor, cycloheximide, synergistically enhances TRAIL-induced cell death. We now report that, like COV434 cells, both cisplatin and the cell survival pathway inhibitor, LY294002, also synergistically promote TRAIL-induced caspase activity (as reflected by PARP cleavage; Fig. 3) and subsequent apoptotic cell death (cell viability data not shown). Cellular mechanisms to explain this synergistic effect of combinatorial treatment have been initiated.
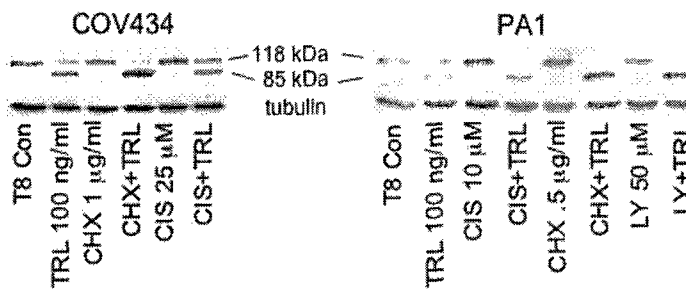

Figure 3. Poly (ADP-ribose) polymerase (PARP) cleavage in COV434 human granulosa tumor cells and PA1 human cancerous ovarian surface epithelial cells. PARP cleavage represents an indicator of caspase activation in response to TRAIL (TRL) treatment in the absence versus presence of cisplatin (CIS), cycloheximide (CHX) or the cell survival signaling pathway inhibitor, LY294002 (LY). Levels of tubulin are provided as evidence of specificity of caspase activity and equal loading of protein.

Johnson, A.L.

KEY RESEARCH ACCOMPLISHMENTS
- It has been demonstrated that normal ovarian granulosa cells express the complement of receptor adaptor and intracellular effector proteins required for a functional extrinsic cell death pathway. Nevertheless, such normal cells are resistant to TRAIL-induced cell death. Identification of cellular mechanisms providing such resistance will aid in the understanding of TRAIL-resistant forms of cancers (e.g. as reported last year for the ovarian surface epithelial cancer cell line, SK-OV3).
- The acquisition of two unique human granulosa tumor cell lines will enable us to elucidate cellular mechanisms that provide for TRAIL-sensitivity in tumor granulosa cells as compared to TRAIL-resistance in normal granulosa cells.
- The COV434 and KGN human granulosa cell lines will also enable us to identify the cellular mechanisms by which chemotherapeutics that typically promote cell death via the intrinsic cell death pathway (such as cisplatin), can enhance the effectiveness of TRAIL to significantly enhance apoptotic cell death via recruitment of the extrinsic cell death pathway.

REPORTABLE OUTCOMES
GenBank Submissions

AY112660: *Gallus gallus* BH3 interacting domain death agonist, Bid, complete cds. We have also produced a Bid-specific polyclonal antiserum against the recombinant Bid protein.

AY251406: *Gallus gallus* decoy receptor 3 (DcR3) mRNA, partial cds

AY251407: *Gallus gallus* osteoprotegrin (OPG) mRNA, partial cds

AY251408: *Gallus gallus* TNFRSF23 v.1

AY251409: *Gallus gallus* TNFRSF23 v.2

CONCLUSIONS
While normal, primary cultured hen granulosa cells express the complement of intracellular adaptor and effector proteins reportedly responsible for mediating extrinsically initiated cell death, TRAIL treatment for 24 h does not reduce cell viability. The cell survival pathways and intracellular mechanisms that confer such resistance in normal cells are currently under investigation. By contrast, TRAIL treatment of the human granulosa tumor cell line, COV434, induces a small but significant reduction in cell viability after 24 h of culture. Importantly, combinatorial treatment of COV434 cells with

Johnson, A.L.

cisplatin plus TRAIL produces a synergistic reduction in cell viability compared to either treatment alone. Furthermore, inhibition of protein synthesis (with cycloheximide) or inhibition of the protein kinase B/Akt cell survival pathway (with LY294006) promotes a similar synergistic action on TRAIL induced apoptosis. Accordingly, we are currently testing the hypothesis that at least one short-term action of cisplatin is to interfere with cell survival signaling pathway(s) and the transcription/translation of cellular anti-apoptotic proteins.

REFERENCES

Bridgham J and Johnson, AL (2002) Avian TVB (DR5-like) death receptor expression in hen ovarian follicles. Biochem. Biophys. Res Comm. 291: 226-232.

Fuller, Chu (2004) Signalling pathways in the molecular pathogenesis of ovarian granulosa cell tumours. Trends Endocrinol Metab. 15: 122-8.

Johnson AL and Bridgham JT (2002) Caspase expression and activity associated with follicle atresia in the vertebrate ovary. Reproduction 124 (1): 19-27.

Johnson AL, Bridgham JT, Swenson JA (2001) Activation of the AKT / Protein kinase B signaling pathway is associated with granulosa cell survival. Biol. Reprod. 64:1566-1574.

Nishi Y, Yanase T, Mu Y, Oba K, Ichino I, Saito M, Nomura M, Mukasa C, Okabe T, Goto K, Takayanagi R, Kashimura Y, Haji M (2001) Establishment and characterization of a steroidogenic human granulosa-like tumor cell line, KGN, that expresses functional follicle-stimulating hormone receptor. Endocrinology. 142:437-45.

Ozoren, N and El-Deiry, WS. Cell surface death receptor signaling in normal and cancer cells. Seminars in Cancer Biology 13 (2003) 135-147.

Zhang H, Vollmer M, De Geyter M, Litzistorf Y, Ladewig A, Durrenberger M, Guggenheim R, Miny P, Holzgreve W, De Geyter C. (2000) Characterization of an immortalized human granulosa cell line (COV434). Mol Hum Reprod. 6:146-53.

Appendices
None

The Role of Unregulated Centrosome Reproduction in the Generation of Aneuploidy, Genomic Instability, and Cancer

Edward H. Hinchcliffe, Ph.D.

Abstract

The reproduction, or duplication of the centrosome is a critical event in the cell's preparation for mitosis, because the pair of daughter centrosomes defines the two poles of the mitotic spindle. Thus, centrosome duplication must be limited to once per cell cycle to ensure the strict bipolarity of cell division. Previous work has demonstrated that when arrested in S-phase transformed cells will undergo multiple rounds of centrosome duplication without coordinate cell cycle progression (a process termed "centrosome amplification"). Our recent work has revealed that the centrosome in G1-arrested cells undergoes a single round of duplication. However, the centrosome in these cells cannot duplicate again without entering into S-phase. Based on these observations, we propose a model for how centrosome duplication is normally coordinated with the cell cycle: centrosome duplication normally occurs prior to S-phase, but requires the transition into S-phase for a "licensing" event necessary for duplication to occur in the next division cycle. Centrosome amplification is an abnormal phenotype that occurs when the cell is "stuck" in S-phase, and consists of centrosome duplication plus the re-acquisition of reproductive capacity (i.e. "licensing") in the same cell cycle stage. This suggests that there is a "re-replication block" that prevents centrosome amplification.

Subject Terms: cell cycle, centrosome, mitosis

A. Introduction: We are investigating mechanisms that coordinate the reproduction of the centrosome with progression of the cell cycle in mammalian cells. We are testing the hypothesis centrosome duplication occurs during G_1 and then acquires reproductive capacity during S-phase. This is important, because certain transformed cell types can assemble multiple centrosomes (possibly during S-phase arrest) and this can contribute to aneuploidy and genomic instability. Using cells stably transfected with GFP-tagged centrosome components - combined with 4-D multimode, live-cell videomicroscopy – we are analyzing the cycles of centrosome amplification in living S-phase arrested cells. Finally, we will directly test whether or not centrosome amplification during S-phase arrest is prevented by p53 activity.

B. Body: We have made the following progress towards our Aims:

Task 1. Characterize centrosome duplication in mammalian cultured cells by immunofluorescence microscopy, flow cytometry, and _in vitro_ kinase assays.

We have analyzed centrosome duplication in CHO cells arrested in S-phase using a variety of pharmacological agents. First, we measured the cycle of centrosome reproduction in CHO cells arrested with aphidicolin. Cells were continuously incubated in 10mg/ml aphidicolin for 72 hrs. Coverslips, containing S-phase arrested cells were removed at 12 hr. intervals over the 72 hr. incubation, fixed, and immunolabeled with antibodies against γ-tubulin (detects pericentriolar material, and used to count centrosome number). The number of γ-tubulin foci in these cells was counted and these data are shown in Table 1. We find that centrosome number increases over the 72 hr. arrest.
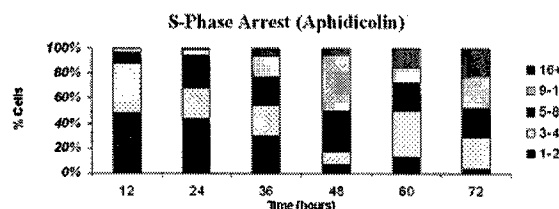

Table 1. Centrosome number increases during S-phase arrest. The total number of centrosomes per cell was counted for 400 cells per time point (taken every 12 hrs.).

Next, we tested whether or not the cycles of centrosome amplification becomes altered by treating cells with different S-phase agents. We incubated CHO cells in aphidicolin (which arrests S-phase by inhibiting the activity of DNA polymerase α), hydroxyurea (which prevents elongation of replicating DNA), and thymidine (which down-regulates uridine synthesis). Cells were treated with these agents for 72 hrs. Coverslips containing these cells were fixed every 24 hrs, immunolabeled with antibodies to γ-tubulin and centrosome number counted. There does not appear to be any difference between the different agents used to arrest the cell cycle, suggesting that there is no difference in the ability of early S-phase vs. later S-phase to influence centrosome duplication.
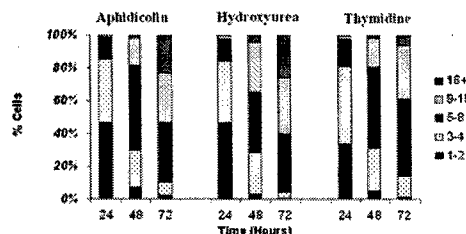
Table 2. Centrosome number increases during S-phase arrest, irrespective of drug used. The total number of centrosomes per cell was counted for 400 cells per time point (taken every 24 hrs.).

Next, we tested the idea that repeated centrosome duplication during S-phase arrest requires the presence of soluble serum growth factors. We arrested cells in S-phase with aphidicolin for 12 hrs. to ensure all cells entered into S-phase. Then we removed the serum from the media (but maintained the aphidicolin. These cells were fixed at 24 hr. intervals, and processed for immunofluorescence as above.
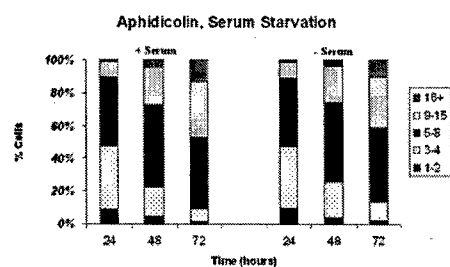

Table 3. Centrosome number increases during S-phase arrest in the absence of soluble growth factors. The total number of centrosomes per cell was counted for 400 cells per time point (taken every 24 hrs.). Cells were treated with aphidicolin in the presence or absence of serum (growth factors).

Finally, we investigated whether or not centrosome duplication requires the presence of an intact microtubule network. For this, we arrest cells in S-phase with aphidicolin for 12 hrs, then add aphidicolin *plus* colcemid (which depolymerizes the microtubule network) to the cells. The cells are kept in aphidicolin/colcemid for 72 hrs total, and coverslips are removed at 24 hr intervals for immunofluorescence with anti γ-tubulin antibodies. The results are shown in table 4.
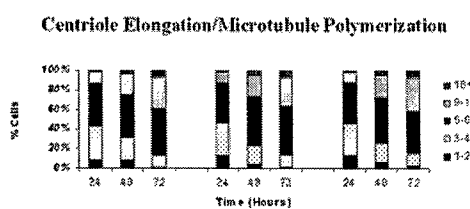

Table 4. Centrosome number increases during S-phase arrest in the absence of microtubules. Cells are treated with aphidicolin and colcemid (to depolymerize microtubules). The total number of centrosomes per cell was counted for 400 cells per time point (taken every 24 hrs.). First set of graphs shows cells w/o colcemid. Second set is centrosome number in cells treated with aphidicolin and colcemid. Third set of graphs shows centrosome number in cells in which the colcemid has been washed out for four hours.

Task 2. Analyze centrosome duplication in living cells by time-lapse multi-mode videomicroscopy.

The key construct for our work is the generation of a mammalian somatic cell line stably expressing centrin coupled to green fluorescent protein (GFP). This cell line is crucial to our making progress on the grant. We have successfully generated this cell

line. We prepared centrin plasmid and transfected CHO-K1 (Chinese hamster ovary epithelial) cells with this construct. After subjecting the transfected cells to antibiotic selection, individual colonies were isolated by pipeting and limited dilution to 72 primary colonies. These colonies were screened by fluorescence microscopy to identify colonies derived from single cells that express low but detectable levels of centrin -GFP. We subjected the cells to three rounds of selection and screening: out of 72 initial colonies we identified 2 colonies that expressed ideal levels of centrin -GFP and work for our experiments.

We selected one colony for further study (and have stored the second colony in LN_2). We analyzed the behavior of these cells (termed CHO-A8) by time-lapse video microscopy. Cells were cultured in imaging chambers and imaged with fluorescence microscopy. We followed small colonies for >60 hrs. These cells continued to undergo cycles of division for the duration of our observations.

Figure 1 shows centriole number in centrin-GFP cells, fixed and immunolabelled with antibodies to γ-tubulin (detects the pericentriolar material).
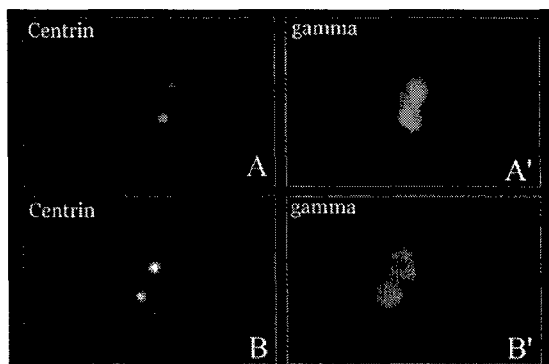

Figure 1. Centrioles tagged with centrin-GFP. In the unduplicated centrosome, there are two centrioles, each surrounded by a cloud of γ-tubulin (A, A'). In the duplicated centrosome, there are four centrioles (centrin-GFP dots). Only the mature centrioles have a cloud of g-tubulin (B, B').

Having generated these cells, we are in the process of working out the imaging conditions to examine centrosome duplication in vivo.

Task 3. Test whether or not inactivation of the p53 tumor suppressor protein leads to centrosome amplification.

We are currently obtaining the necessary molecular reagents for these experiments, and anticipate making rapid progress on this task during the second year of the grant, as originally proposed.

C. Key Research Accomplishments:

1. Measured cycles of centrosome duplication during S-phase arrest.

2. Determined impact of DNA synthesis inhibitory agents on ability of the centrosome to undergo repreated cycle of duplication.

3. Demonstrated that centrosome re-duplication during S-phase arrest does not require the presence of soluble growth factors.

4. Demonstrated that centrosome re-duplication during S-phase arrest does not require the presence of a microtubule network.

5. Generated a CHO cell line that constitutively expresses tektin-GFP.

D. Reportable Outcomes:

1. Invited seminar: Dept. of Biology, Univ. of Indiana, Bloomington, IN.

2. Invited Speaker: *Minisymposium*, Chicago Cytoskeleton Meeting, Northwestern University, Chicago, IL.

3. Funded grant: Mechanisms of Centrosome Reproduction in Animal Cells. National Institutes of General Medical Sciences

4. Developed CHO cells, which constitutively express Tektin-GFP.

E. Conclusions: We find that centrosome duplication occurs in a slow and uncoordinated fashion during prolonged S-phase arrest. The ability of the centrosome to duplicate multiple times is not affected by the pharmacological agent used. In addition, repeated centrosome duplication does not require growth factors, once the cell cycle has been arrested in S-phase. Finally, we can uncouple the duplication of the centrosome from the elongation of centriole microtubules, using aphidicolin and colcemid. This should allow us to characterize early centriole intermediates in the absence of triplet microtubules.

F. References: NA

G. Appendix: NA.